UNIVERSITY OF CALIFORNIA SAN DIEGO

Cancer Regulation Through Splice Modulation

A dissertation submitted in partial satisfaction of the requirements for the degree
Doctor of Philosophy

in

Chemistry

by

Kelsey Ann Trieger

Committee in charge:

Professor Michael Burkart, Chair
Professor Adam Engler
Professor Thomas Hermann
Professor Tadeusz Molinski
Professor Navtej Toor

2021

This dissertation of Kelsey Ann Trieger is approved, and it is acceptable in quality and form for publication on microfilm and electronically.

University of California San Diego

2021

DEDICATION

To my husband, family and friends who supported me during my time in graduate school.

EPIGRAPH

If I have seen further, it is by standing on the shoulders of giants.

— Isaac Newton

TABLE OF CONTENTS

LIST OF ABBREVIATIONS

Acute myeloid leukemia	AML
Aurora kinase	AURK
Exon skipping	ES
Intron retention	IR
Mode of action	MOA
Nonsense-mediated decay	NMD
PHD finger protein 5a	PHF5A
Polo-like kinase 1	PLK-1
Precursor messenger RNA	pre-mRNA
Quantitative reverse transcriptase polymer chain reaction	qPCR
Reverse transcriptase polymerase chain reaction	RT-PCR
Ribonucleic acid	RNA
RNA sequencing	RNAseq
Small nuclear ribonucleoprotein	snRNP
Small nuclear RNA	snRNA
Splicing factor 3b 1	SF3B1
Structure-activity relationship	SAR
Splice modulator	SPLM

LIST OF FIGURES

LIST OF TABLES

ACKNOWLEDGEMENTS

I would like to thank my advisor and mentor, Professor Michael Burkart, for his support throughout my years in graduate school. Mike has always encouraged me to follow my research in whatever direction it flows, allowing me to develop into a fully independent researcher with a broad skill set and problem-solving capabilities.

I would like to also thank my committee members, Professor Thomas Hermann, Professor Ted Molinski, Professor Navtej Toor, and Professor Adam Engler. All their feedback and comments were essential and helpful in my research progress. Moreover, I would like to thank my collaborators, Professor Catriona Jamieson and Professor Jeffrey Rinehart, for constructive feedback and discussions throughout my research progress.

I thank current and former members of the Burkart lab for all of their support and friendship throughout my time in graduate school. The welcoming environment of the Burkart lab is what encouraged me to join, and I have been fortunate enough to develop many long-term friendships with my lab mates over the years. Among my favorite memories are our coffee runs, lab lunches, and 6123 birthday outings. I thank all of you for making my graduate school experience an enjoyable and memorable one.

I am thankful for my close friends who have supported me throughout my years in graduate school. You have celebrated with me in the good times, and lent an ear and a hug in challenging times. I would especially like to thank Elsa Felgar for coffee shop sessions, walks on the beach, traveling adventures, and too much wine.

I would like to express a huge thank you to my family for their love and support. You have always encouraged me to be the best I can be and follow my passions. I would not be where I am today without you.

Finally, I would like to thank my husband, Greg Trieger, for his endless love and support. You have cooked me dinner when I've come home late overwhelmed with work, celebrated my successes with me with flowers and outings on the town, talked through the challenges I have faced and offered advice, served as a mentor to me, and even passed my cells in lab. I don't know where I would be without you, and I will be forever thankful for the role you played in shaping my experience as a researcher and person.

I appreciate my collaborators allowing me to use the following publications in my dissertation:

Chapter 1, in part, is a reprint of the material as it appears: Leon, B, Kashyap, M.K., Chan, W.C., Krug, K.A., Castro, J.E., La Clair, J.J., Burkart, M.D. "A Challenging Pie to Splice: Drugging the Spliceosome" *Angew. Chem. Int. Ed.* **2017** *56* (40), 12052-12063. The dissertation author is a co-author of this manuscript.

Chapter 2, in full, is a reprint of the material as it appears: Trieger, K.A., La Clair, J.J., Burkart, M.D. "Splice Modulation Synergizes Cell Cycle Inhibition" *ACS Chem. Biol.* **2020** 15 (3), 669-674. The dissertation author is the primary co-author of this manuscript.

Chapter 3, in part, is material being prepared for submission under the title "Stereochemical Attenuation of Splice Modulation." The dissertation author is the primary co-author of this manuscript.

VITA

2021	Doctor of Philosophy, Chemistry, University of California San Diego
2018	Master of Science, University of California San Diego
2016	Bachelor of Science, University of California San Diego

PUBLICATIONS

Trieger, K.A. Chan, W.C., La Clair, J. J., Burkart, M. D. Stereochemical Attenuation of Splice Modulation. *In preparation.*

Trieger, K.A., La Clair, J.J., Burkart, M.D. Splice Modulation Synergizes Cell Cycle Inhibition. *ACS Chem. Biol.* **2020** *15* (3), 669-674.

Chan, W.C., La Clair, J.J., Leon, B., Trieger, K.A., Slagt, M.Q., Verhaar, M.T., Bachera, D.U., Rispens, M.T., Hogman, R.M., de Boer, V. L., van der Hulst, R., Bus, R., Hiemstra, P., Neville, M.L., Mandla, K.A., Figueroa, J.S., Jamieson, C., Burkart, M.D. Scalable Synthesis of 17S-FD-895 Expands the Structural Understanding of Splice Modulatory Activity. *Cell Rep. Phys. Sci.* **2020**, *1 (12).*

Xie, Y., Krug, K. A., Kalaj, M., McCallum, N.C., Siwicka, Z., Wang, Z., Gianneschi, N.C., Burkart, M.D., Rinehart, J.D. Peroxidase-Like Reactivity at Iron-Chelation Sites in a Mesoporous Synthetic Melanin. *CCS Chem.* **2020** *2*, 1483-1490.

Chan, W.C.*, León, B.*, Krug, K.A.*, Patel, A.*, La Clair, J.J., Burkart, M.D. Daedal Facets of Splice Modulator Optimization. *ACS Med. Chem. Lett.* **2018** *9 (11)*, 1070–1072. (*authors contributed equally)

Xie, Y., Wang, J., Wang, Z., Krug, K.A., Rinehart, J.D. Perfluorocarbon-Loaded Polydopamine Nanoparticles as Ultrasound Contrast Agents. *Nanoscale* **2018** 10 (26), 12813–12819.

Leon, B., Kashyap, M.K., Chan, W.C., Krug, K.A., Castro, J.E., La Clair, J.J., Burkart, M.D. "A Challenging Pie to Splice: Drugging the Spliceosome" *Angew. Chem. Int. Ed.* **2017** *56* (40), 12052-12063.

ABSTRACT OF DISSERTATION

Cancer Regulation Through Splice Modulation

by

Kelsey Ann Trieger

Doctor of Philosophy in Chemistry

University of California San Diego, 2021

Professor Michael D. Burkart, Chair

RNA splicing plays a central role in cell regulation, development, and disease progression, but the complexity of this macromolecular assembly process has left RNA splicing underexplored in cancer. In recent years, it has become clear that alternative RNA splicing becomes mis-regulated in and plays a role in the progression of a wide range of cancers. Therefore, drugs that regulate RNA splicing could serve as powerful therapeutics for cancer. Splice modulators (SPLMs) are a class of chemotherapeutics that regulate aberrant splicing profiles in tumors, thereby inducing tumor cell apoptosis. SPLMs interfere with the overused splicing machinery that cancer cells become dependent upon for expansion, thereby

limiting the tumor's ability to produce proteins necessary for growth and survival. Understanding the relationship between splicing and cancer progression will allow for expansion of our therapeutic arsenal in tackling cancer.

In my graduate studies, I evaluated splice modulator regulation of the cell cycle genes Aurora kinase (AURK) and Polo-like kinase 1 (PLK-1). Next, I leveraged the SPLM FD-895's regulation of the cell cycle to develop a splicing-based combination therapy capable of targeting a wide range of tumor types. This co-dosing approach relied on use of the splice modulator FD-895 to reduce cell cycle RNA, followed by treatment with a cell cycle protein inhibitor to further reduce cell cycle protein expression. This combination therapy was found to be effective against a range of tumor types, including cervical, ovarian, and colorectal tumor cell lines, indicating that this approach has wide therapeutic applications. These studies suggest the potential to engage small molecule SPLM pretreatment as a therapeutic tool to edit the levels of therapeutically targeted proteins by mis-splicing their RNAs. SPLM combination therapy may be particularly useful for enhancing clinical agents that suffer from off-target effects or dose-limiting toxicity and could therefore allow for previously abandoned lead molecules (therapeutics) to re-enter the clinic.

Next, I synthesized analogs of the splice modulator FD-895 to investigate structure-activity relationships (SARs) for this class of compound. It has been found that structural differences from one SPLM to another lead to significant changes in splicing activity based on SPLM orientation within the spliceosome binding pocket and contact with the incipient premature messenger RNA (pre-mRNA). To this end, we synthesized a panel of splice-modulating analogs of the natural product FD-895. I then used these analogs to explore the role of drug structure in potency, gene selectivity, and splicing activity. I found that

epimerization of stereocenters in the side chain or macrolide core typically led to a loss in cytotoxic activity. However, I also found that some analogs had unique splicing selectivity profiles, indicating that cytotoxic potency does not necessarily correlate with splicing selectivity. Instead, a more complex relationship exists, accounting for SPLM fit in the SF3B1•PHF5A pocket and SPLM interactions with pre-mRNA. Overall, these findings indicate that SPLM structure could be tailored to target specific oncogenes, allowing for tumor-specific targeting, opening the door for future studies on a personalized-medicine approach using splice-modulating chemotherapeutics.

Chapter 1. A Challenging Pie to Splice: Drugging the Spliceosome

Section 1.1 Introduction

Life operates through the orchestrated translation of the four-digit genetic code into a 20 amino acid code to give proteins. During this process, DNA, the storage oligonucleotide, passes its information on through conversion into RNA, which in turn serves as an intermediary for the translation of a gene into a protein. To match the needs of longer-lived eukaryotes, this process has an additional stage of information processing. Here, the transcribed gene product mRNA undergoes splicing, a reorganization process that allows the cell and organism to rapidly alter the gene product in response to temporal or environmental challenges. Beginning in the 1970s,[1] understanding the complex mechanisms of RNA splicing has become a vital new avenue for chemical biological studies. While the bulk of splicing studies have been conducted in genetics and RNA biology laboratories, the discovery of spliceosome-targeting natural products in 2007[2] opened the door to chemists.

Section 1.2 The Chemistry of Splice Modulation

Access to splice modulators (SPLMs) has evolved from the early stages of natural product isolation[3—5] to the current state of medicinal chemistry optimization and high-fidelity total synthesis.[6—17] To date, the most established set of SPLMs share a common mode of action (MOA), targeting the SF3b multiprotein component within the U2 small nuclear ribonucleoprotein (snRNP) of the spliceosome.[2] This molecular class is broken down into three families that share a common motif comprised of two functional moieties united through a central diene. Over the

last decade, total synthesis has played a key role in structural determination, material access, medicinal chemistry optimization, and the facilitation of clinical trials.

Structures of Splice Modulators

To date, the most established SPLMs arise from three distinct families of polyketide natural products. The first family is comprised of 12-membered macrolides 1−−3 (Figure 1.1).[3] The second family contains a pyran ring linked to a comparable side chain, as illustrated by 4−−5 (Figure 1.1).[4]

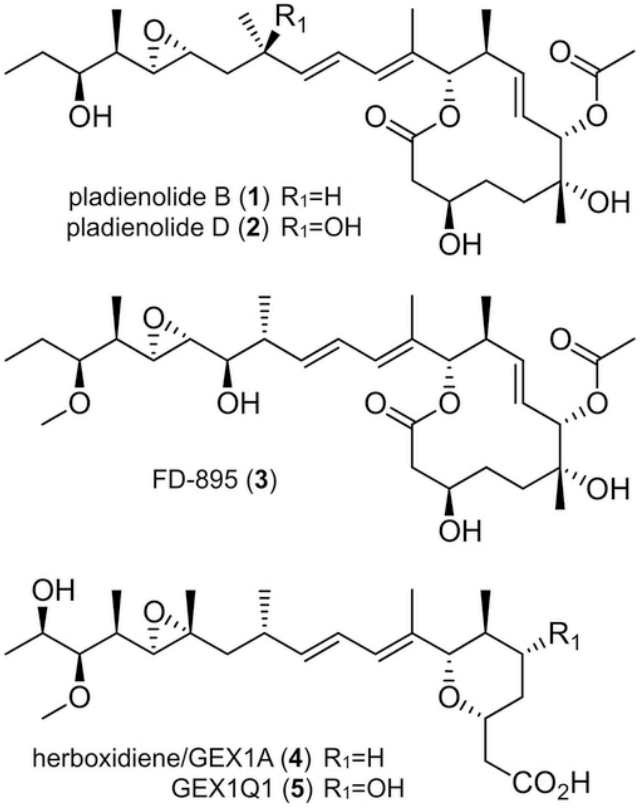

Figure 1.1 Structures of selected examples of the 12-membered macrolide and 6-membered cyclic ether families of polyketide SPLMs.

The third family is composed of four discrete chiral fragments: two pyran rings joined by a diene moiety and an acyclic side chain linked to the central pyran via an α,β-unsaturated amide

bond. Examples of this family include 6−−8 (Figure 1.2).[5] Overall, each of polyketides 1−−8 contains 2−−3 rings, 9−−11 chiral centers, and various reactive groups (epoxide and/or α,β-unsaturated amide), to which their potent activity has in part been attributed.

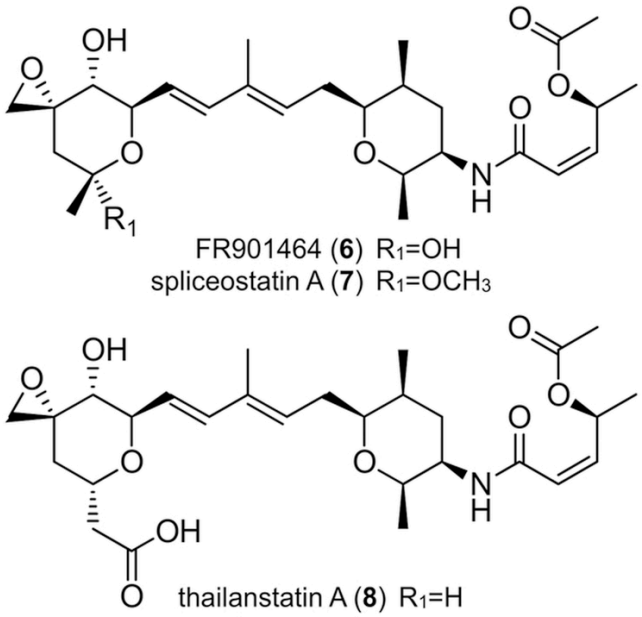

Figure 1.2 Structures of members of a third family of polyketide SPLMs.

Synthetic Challenges and Solutions

Synthetic strategies toward these three families of SPLMs primarily dissect the molecule into 2−−3 components. In the 12-membered macrolide class (Figure 1.3), the routes developed by Kotake and co-workers from Eisai Co.[6] and the Burkart,[7] Maier,[8] Ghosh,[9] and Chandrasekhar groups,[10] derive the macrolide core using ring-closing metathesis. The core is then attached to the respective side chains using either a Julia--Kocienski olefination (blue, (Figure 3 a,c) or Stille coupling (blue, (Figure 1.3b).

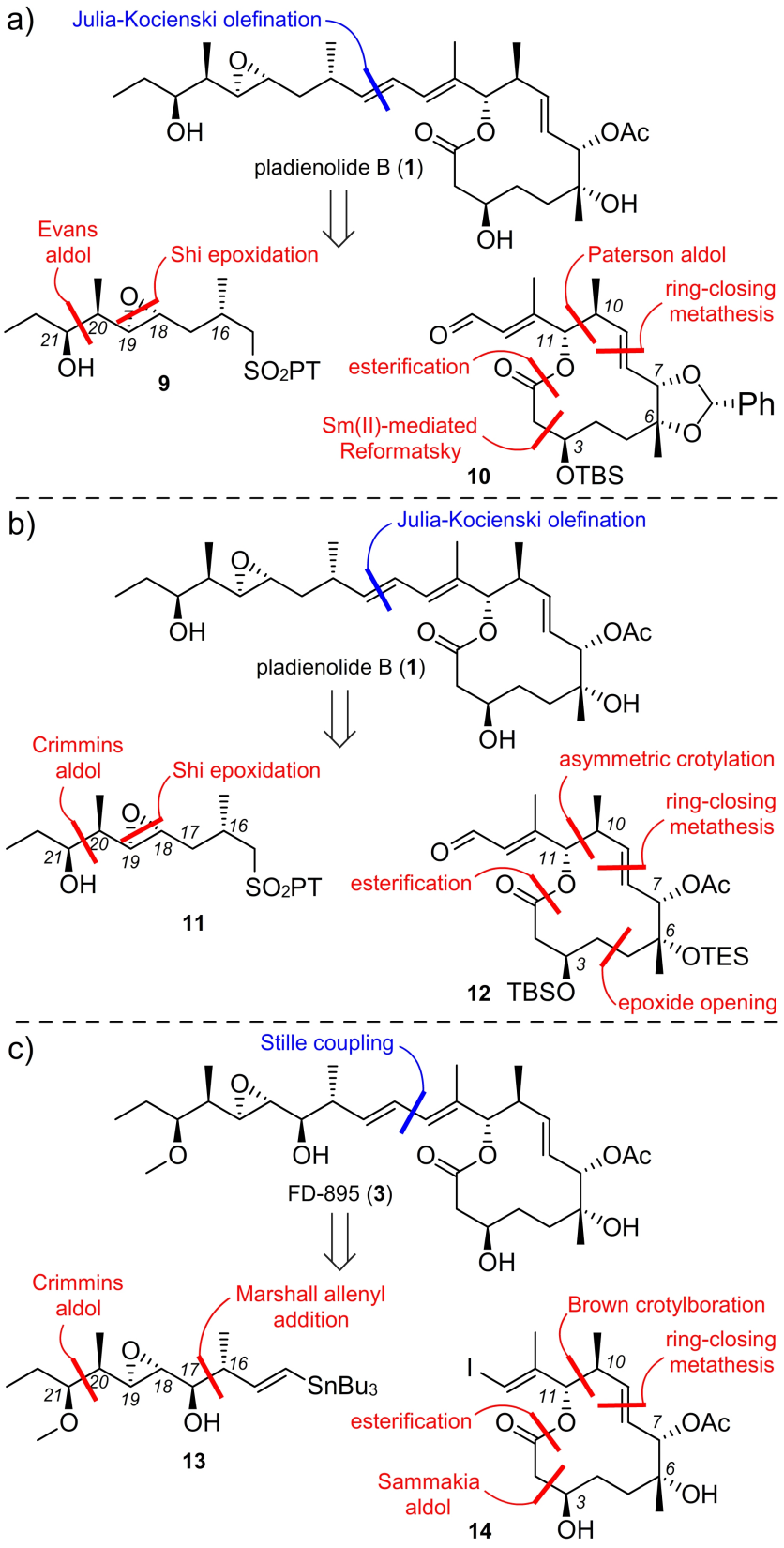

Figure 1.3 Synthetic disconnections implemented in the total syntheses of a--b) pladienolide B (**1**) or c) FD-895 (**3**). Bond disconnections for component coupling steps (blue) and key steps in component syntheses (red) are shown.

In the Eisai Co. synthesis of pladienolide B (1), core 10 was assembled by using a SmII-type Reformatsky reaction to create the C(3) carbinol and a Paterson aldol reaction to install the C(10)C(11) stereodiad (Figure 1.3 a).[6] The C(6)C(7) centers were created early on through Sharpless dihydroxylation. The synthesis of side chain 9 was conducted using an Evans aldol to install the C(20)C(21) stereodiad followed by Shi epoxidation at C(18)C(19). In the Ghosh route to 1 (Figure 1.3 b), C(20)C(21) in component 11 was set using a Crimmins aldol.[9] This was followed by the implementation of a Shi epoxidation to set C(18)C(19). Core 12 was assembled by an epoxide ring opening to afford the C(4)C(5) diad and a subsequent asymmetric crotylation to install the C(10)C(11) stereocenters. Esterification, followed by ring-closing metathesis, completed the synthesis of 12.

In our studies on 3 (Figure 1.3 c),[7] the C(3) center was installed in core 14 using a Sammakia aldol on material that contained the C(6)C(7) stereodiad. This diad was prepared by a Brown allylboration followed by 2-methoxyethoxymethyl (MEM) ether directed installation of the methyl group at C(6). The C(10)C(11) centers were prepared using a Brown crotylboration. In this route (Figure 1.3 c), component 13 was constructed using a Crimmins aldol to install the C(20)C(21) stereodiad, a Sharpless epoxidation to install C(18)C(19) and a Marshall allenyl addition to create the C(16)C(17) diad. The use of Marshall allenyl stannane chemistry was advantageous, since it allowed access to all four of the C(16)C(17) diastereomers, a feature for which the structure--activity relationship (SAR) was not previously investigated.

A number of groups, including the Koide,[11] Webb,[12] Ghosh-Jurica,[13] Hoveyda,[14] Alvarez-Valcárcel,[15] and Nicolaou[17] groups, as well as Koehn and co-workers,[16] have explored the second and third families (Figure 1.4). In the first example, Webb used a Julia--Kocienski olefination strategy to complete the backbone of 4 ((Figure 1.4 a, blue), with the

C(12)C(13) epoxide being added in the last step.[12] Alternatively, the Koide group's synthesis of 6 illustrated the use of olefin cross-metathesis to bring together both fragments ((Figure 1.4 b, blue).[11] The third approach was demonstrated by the Nicolaou group's synthesis of 8, which involved the use of a Suzuki coupling to unite the two olefins of the internal diene.[17]

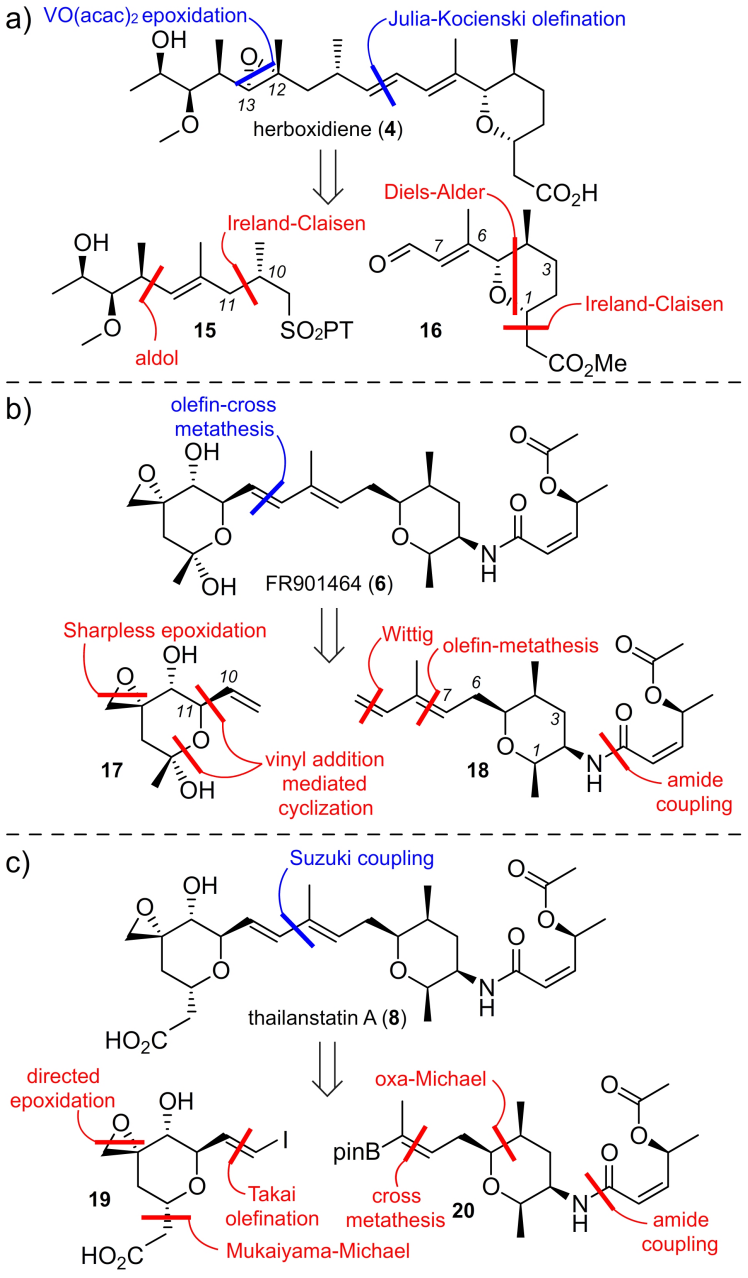

Figure 1.4 Synthetic disconnections implemented in the total syntheses of a) herboxidiene (**4**), b) FR901464 (**6**), and c) thailanstatin A (**8**). Bond disconnections for component coupling steps (blue) and key steps in component syntheses (red) are shown.

A detailed evaluation of the three synthetic approaches in Figure 1.4 illustrates several of the key transformations required to complete the respective component syntheses. In the first example Figure 1.4 a),[12] core 16 was prepared through an Ireland--Claisen rearrangement to functionalize C(1) with an ester. Next, a PCC-mediated allylic alcohol transposition followed by oxidation gave the distal aldehyde in 16. Side chain 15 was assembled through the use of an aldol reaction to produce the C(13)C(14) connection. Next, an Ireland-- Claisen rearrangement was used to orient all of the carbon atoms correctly, and this fragment was completed by using a Mitsunobu reaction. While the routes developed to date are viable for small-scale syntheses, future efforts in the application of new carbon--carbon bond forming reactions are needed to provide effective routes to enable gram-scale access to these materials, as demonstrated by the Hoveyda laboratory.[14]

In the Koide group's synthesis of 6 ((Figure 1.4 b,[11] component 17 was prepared through a vinyl addition-mediated cyclization of an epoxy aldehyde. The synthesis of the second component 18 began with an amide coupling at C(2), which was followed by a Wittig olefination. The components were then coupled through olefin-cross metathesis at C(9)C(10). The diene was achieved through use of a Wittig olefination.

In the final example (Figure 1.4 c), Nicolaou and co-workers prepared the pyran of 20 through an oxa-Michael reaction, followed by an amide coupling and cross-metathesis.[17] Fragment 19 is prepared by a Mukaiyama--Michael addition that adds the acyl group. Next, a Takai olefination yields a vinyl iodide, which is completed by an epoxidation mediated by VO(acac)2.

Medicinal Chemistry Optimization

To date there is limited structural information regarding the binding site of SPLMs on SF3b, with suggestions of a tentative binding region obtained only through structure comparisons from mutational studies.[18] Despite the lack of structural data, detailed SARs of the three major families of SPLMs have been determined.[9] Of particular note is work in which four isomers of FD-895 were synthesized. Upon screening in HCT-116 cells, improved activity and stability was shown for 17S-FD-895 (23).[7] Along with ongoing synthetic modification, these efforts have provided a detailed SAR map of the 12-membered macrolide family (Figure 1.5 a).

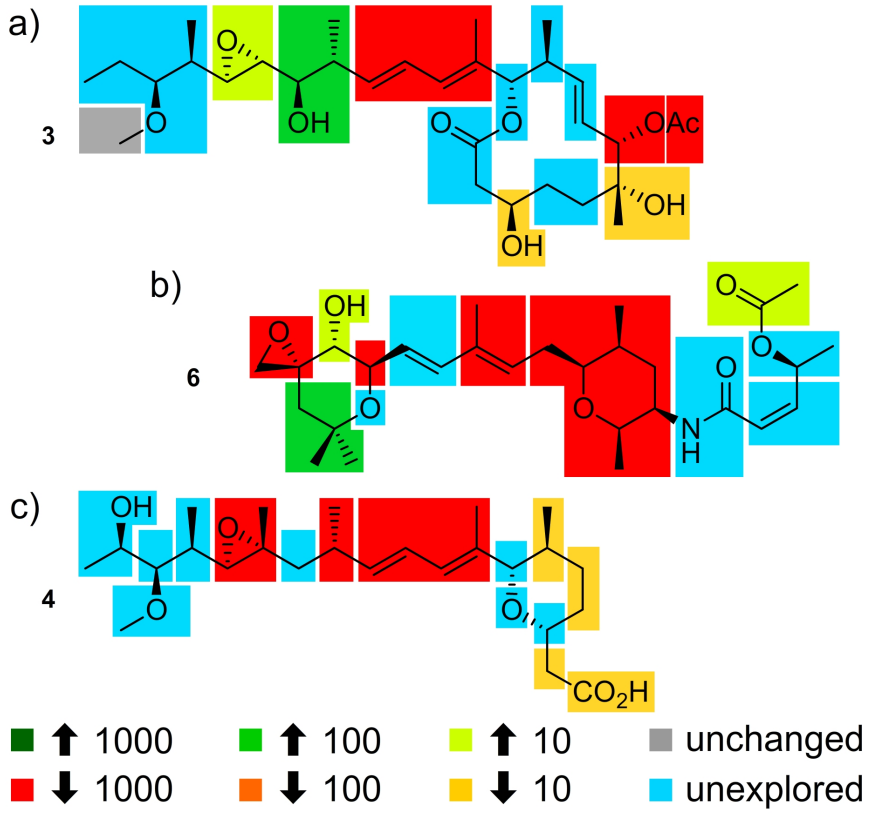

Figure 1.5 Structure--activity relationships (SARs) identified through synthetic and semisynthetic studies. These maps were developed using data published up to January 2017 and represent findings from in vitro cytotoxicity assays, not direct comparisons of the effect on RNA splicing. Data has been presented to show the optimal analogues for each position, as given by fold increase (up arrow) or decrease (down arrow) in activity. Unchanged denotes substitutions that have been shown to have little effect, while unexplored represents regions that lack sufficient data for assignment.

Furthermore, comparable SAR maps are also available for the second and third families, as shown for 6 (Figure 1.5 b) and 4 Figure 1.5 c), respectively.[19] One of the problems with the development of accurate SAR maps arises from the use of different cytotoxicity assays, cell lines, and culture conditions (therein making it difficult to compare the current data). Moreover, many of the activity reports do not provide splicing-modulation data using techniques such as RNAseq, reverse transcriptase polymerase chain reaction (RT-PCR), or quantitative reverse transcriptase polymer chain reaction (qRT-PCR). The lack of this data has further complicated the establishment of detailed SAR studies. That aside, the SAR maps in Figure 1.5 reveal that few, if any, structural modifications within these natural products lead to analogues with increased activity.

Ongoing Translational Efforts

Compounds targeting SF3b have entered clinical trials with various degrees of success (Figure 1.6). E7107 (21), a derivative of 1, successfully altered RNA splicing in solid tumors in phase I clinical trials; however, the trials were halted due to severe toxicity.[20] Studies from H3 Biomedicine have provided detailed evaluation of 6-deoxypladienolide B (22).[21] More recently this team has translated a new candidate into Phase I clinical trials. Other compounds showing promise include 17S-FD-895 (23) and its corresponding cyclopropane 24,[22] which have recently demonstrated viable in vivo efficacy for acute myeloid leukemia (AML) by mediating stem cell maintenance.[23]

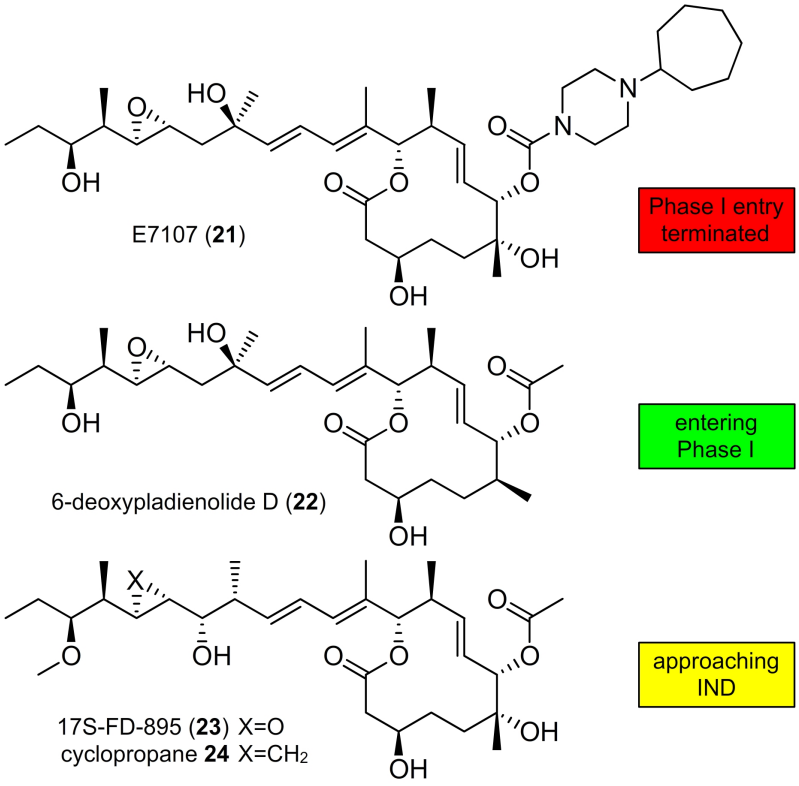

Figure 1.6 Structure of the first clinical entry, E7107 (**21**), which entered Phase 1 clinical trials for patients with solid tumors. The next-generation analogues 6-deoxypladienolide D (H3B-8800, **22**), 17*S*-FD-895 (**23**), and cyclopropane **24** are currently being examined for clinical translation for hematologic malignancies. IND=investigational new drug application.

In addition to derivatives of natural products, a new generation of synthetic derivatives are currently under investigation. One of the key observations in this field was the identification of two consensus motifs within these families (Figures 1.1).[24] This was validated by the preparation of the pladienolide--herboxidiene hybrid 25 Figure 1.7). While 25 displayed reduced activity, it demonstrated that structural simplification could facilitate SAR studies.

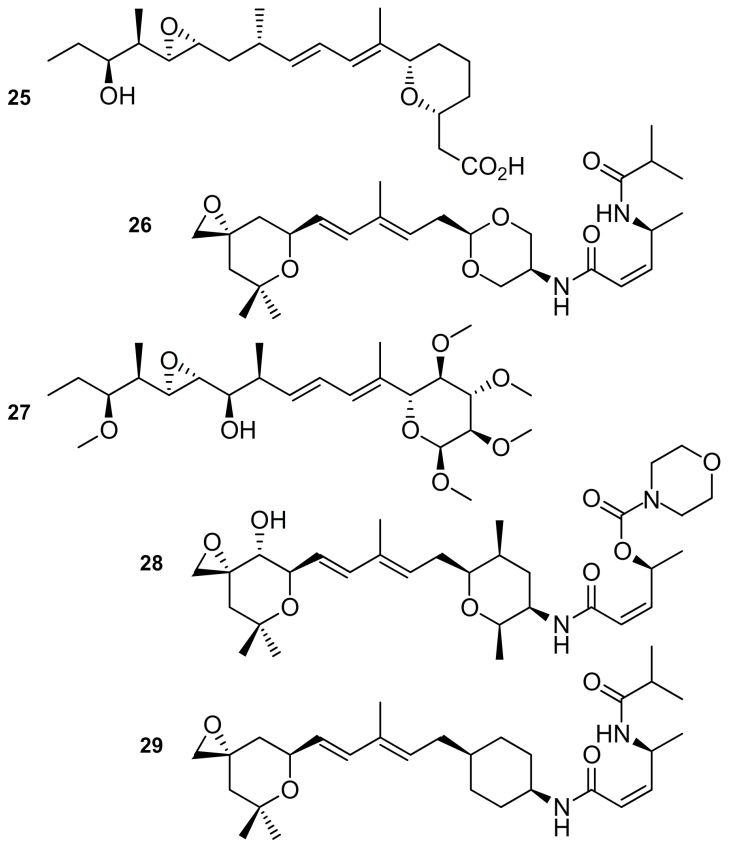

Figure 1.7 Exemplary structures of synthetic analogues of natural products developed from the SAR profiles. These include analogues that offer increased stability (**27** or **29**), provide improved synthetic access (**25**—**29)**, or serve as fusions between the pladienolide and herboxidiene families (**25**).

Recent studies have continued to search for a consensus motif that contains the minimum atoms necessary to elicit activity (Figure 1.7). Subsequent efforts in the Webb laboratory have led to the development of 26,[25] an analogue that demonstrated viable activity in cell and animal models. Further explorations have also led to complete replacements of core units, including the development of carbohydrate-based analogues such as 27,[26] meayamycin B (28),[27] or cyclohexyl-derived analogue 29.[15] While the activity of these analogues may not be comparable to their respective natural products, the improved stability in these materials, as demonstrated by 27 and 29, provide a solid foundation for next-generation advances (Figure 1.7).

Section 1.3 Selectivity in Splice Modulation

RNA splicing is a complex multistep process that is carried out by a large macromolecular machine called the spliceosome,[28] a ribonucleoprotein (RNP) particle containing five RNAs and more than 100 associated proteins.[29] During its action, the spliceosome forms a series of complexes, each of which serves to conduct a discrete step required to excise an intron, a nucleotide sequence within a gene that is removed during RNA splicing, from the pre-mRNA.[30] As illustrated in Figure 1.8, the process proceeds through the transesterification of an intron to form a lariat (step 1), followed by cleavage of the lariat and release (step 2) to provide the fully intact mRNA for translation into protein (Figure 1.8). Unsurprisingly, modulation of this process by a small molecule is extremely complex, and hence prediction of selectivity becomes increasingly complicated. Recent studies have identified some of the variables that need to be considered when evaluating a SPLM.

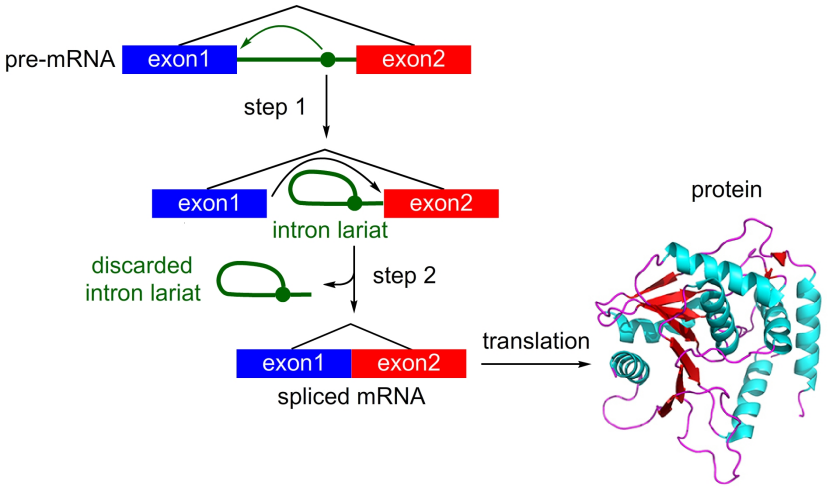

Figure 1.8 Overview of the splicing process, depicting the conversion of pre-mRNA into spliced mRNA followed by translation into a functional protein.

Cell Selectivity

RNA splicing has been targeted in solid tumors and hematologic malignancies by using SPLMs designed to modulate the action of the SF3b complex in the spliceosome. Among the 12-

membered macrolide family, 1 has been the most explored.[31] Screening in the NCI-60 cell line indicated potent activity in a unique set of cells, including NCI-H522 (nonsmall-cell lung cancer) and NCI-H460 (large-cell lung carcinoma) cells.[2b] Pladienolide B (1) and 6 induced in vitro cytotoxicity in A549 (lung adenocarcinoma) cells and showed in vivo efficacy in tumor xenograft models. In addition, meayamycin B (28) and 1 inhibited tumor growth in xenografts derived from HCT-116 (colon carcinoma) cells.[32] While NCI screening has been used to calibrate the activity of these compounds in tumor cell lines, early studies have indicated that many of these materials demonstrate remarkable efficacy in tumor cells over normal cells, with selectivity indices of 3−−4 orders of magnitude often observed, thus providing a wide therapeutic window for treatment.[33]

In addition to altering the normal splicing process, SPLMs also modulate splicing to deliver a gene product with differential functions to cells. One clear example involves the MCL1 and BCL-x family of genes, which in cancerous cells typically modulate alternative splicing from anti-apoptotic MCL1L (long) to pro-apoptotic MCL1S (short) upon SPLM treatment. [34, 35] In addition, SPLMs can modulate post-translational modifications, as demonstrated by recent studies illustrating that pladienolide B (1) can modulate the level of phosphorylation of SF3B1 at Thr 313.[35]

Mechanistic Selectivity

SPLMs produce different types of alternative splicing (AS) events when compared to normal constitutive splicing (Figure 1.9).[36] Exon skipping (ES)[37] and intron retention (IR)[38] are the most common AS events observed in SPLM-treated cells both in vitro and in vivo. Several of the best studied compounds, including pladienolide B (1), FD-895 (3), meayamycin B (28), FR901464 (6), and spliceostatin (7), have been characterized according to their ability to induce

IR events by using a combination of RNAseq and RT/qRT-PCR analyses.[34, 39] Other efforts have identified detailed maps of ES events.[12, 40] While both approaches are viable, there is a need to move toward a detailed characterization of both IR and ES events in combination with other less common forms of AS, such as mutually-exclusive splicing (Figure 1.9).[41]

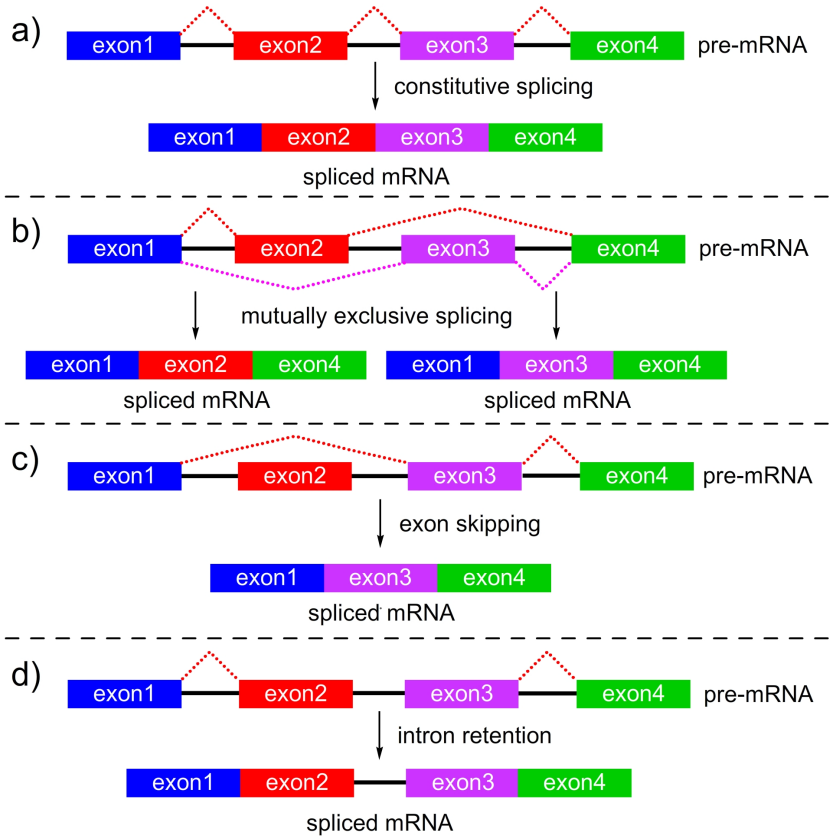

Figure 1.9 Different modes of RNA splicing. a) Constitutive splicing is most common, where, as part of the normal processing of transcription, the spliceosome removes intronic (non-coding) portions of pre-mRNA. b) In diseased or abnormal cells, other pathways, such as aberrant splicing machinery could, lead to mutually exclusive splicing. c) Exon skipping or d) intron retention can also occur as part of normal splicing or in malignant cells treated with SPLMs.

Gene Selectivity

To date, RNAseq data (Figure 1.10 a) has provided a wealth of information about gene selectivity. The use of these data, along with that from qRT-PCR and RT-PCR analysis, has revealed two key findings.

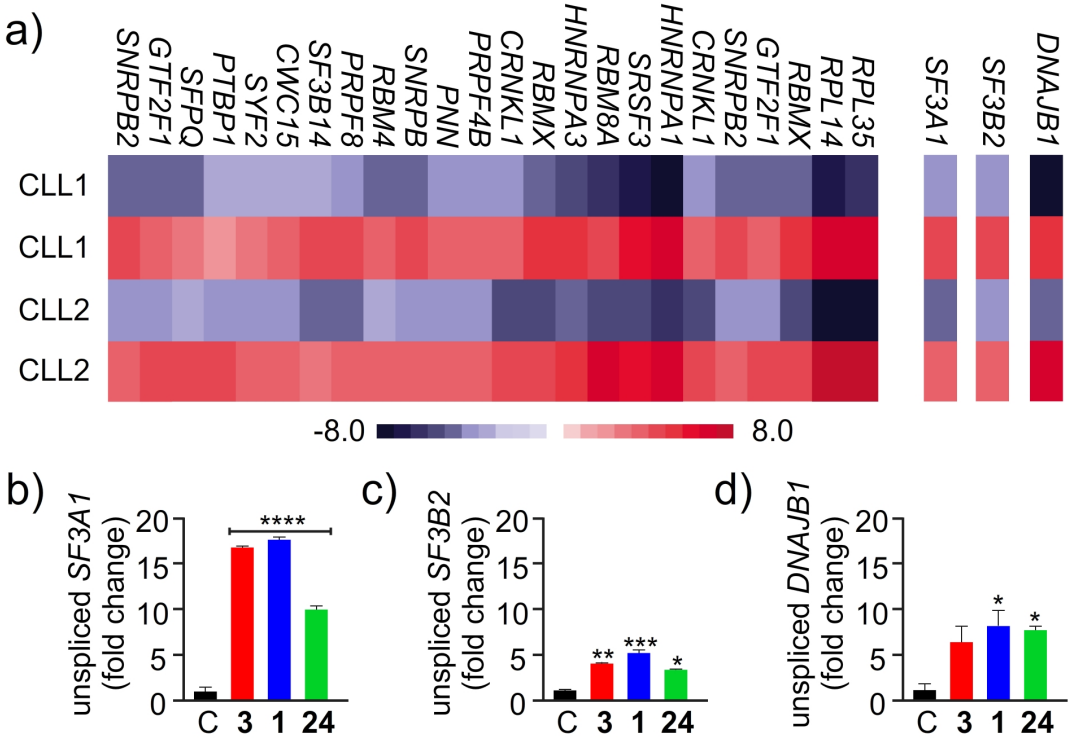

Figure 1.10 a) Examples of gene selectivity identified by RNAseq analysis. b) Examples of gene selectivity identified by qRT-PCR analysis. Three selected genes (*SF3A1*, *SF3B2*, and *DNAJB1*) are shown as representative examples. The level of splicing in these genes was not identical for FD-895 (**3**), pladienolide B (**1**), and cyclopropane **24**, as shown in (b--d), respectively.

First, current data suggest that the different SF3b-targeting SPLMs do not necessarily target the same genes.[35] As shown in Figure 1.10 a, the levels of IR in CLL-B cells treated with 3 clearly differ for each gene. While this in part reflects the level of gene expression and splicing ongoing for each gene, the relative levels of the splicing in untreated cells (blue) versus treated cells (red) do not correlate. This indicates a complicated interplay between the splicing of specific genes and the efficacy of 3 in inducing IR within a specific gene.

Second, early evidence indicates that different structural features within a SPLM can alter its gene selectivity. As shown in Figure 1.10 b--d, the relative levels of splicing are different for SF3A1, SF3B2, and DNAJB1.[35] While complete analyses of all AS events upon drug treatment

has yet to be reported for any SPLM, current studies are now providing compelling evidence that trends arise within genes from similar families, thus suggesting that gene- or gene-family-selective SPLM development could be possible.[41]

Intron/Exon Selectivity

The complexity of SPLM selectivity is not limited to the mode of splicing (Section 3.2) or gene specificity (Section 3.3), but is also reflected at the level of specific intron/exon pairs within a gene transcript. While not fully charted, SPLM activity is not required to have comparable efficacy for the removal of each intron within a gene. As shown in Figure 1.11, it is possible that a given SPLM may have a different rate of activity for inducing IR of one intron (intron2) versus that for another (intron3). While efforts are underway to explore this level of selectivity, the fact that multiple mechanisms exist at each intron further complicates this analysis. Each human gene contains on average 7.8 introns,[42] which adds further complexity to this problem. Recent evidence indicates that small and GC-rich introns are more prone to undergo IR/ES events.[43] Understanding the rules that guide this selectivity is not only fundamental to gauge the activity of a given SPLM, but also essential for understanding the underlying nature of the selectivity.

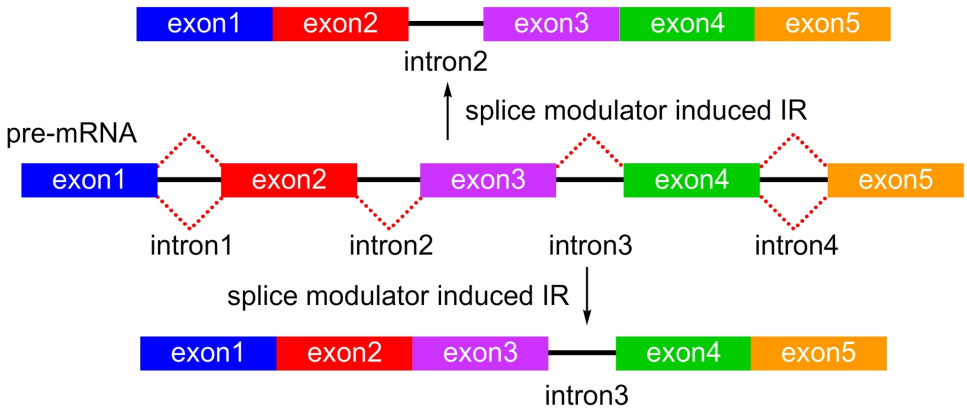

Figure 1.11 A schematic representation of intron/exon selectivity. In this example, two different IR products bearing either intron2 (top) or intron3 (bottom) can arise from the same pre-mRNA.

Downstream Protein Selectivity

While there is a good understanding of how to mark and identify SPLMs at the mRNA level, as well as a conceptual understanding of how these events terminate or alter protein synthesis, following these events at an analytical level will require significant additional study. Our current knowledge arises predominantly from the study of genes that are regulated by AS, such as commonly observed in MCL1.[34, 35] As shown in Figure 1.12, the SPLMs 1, 3, and 24 result in a shift from the long mRNA and translation of the MCL1 longer isoform 1, which inhibits apoptosis, to the short mRNA and corresponding MCL1 shorter isoform 2, which induces apoptosis.

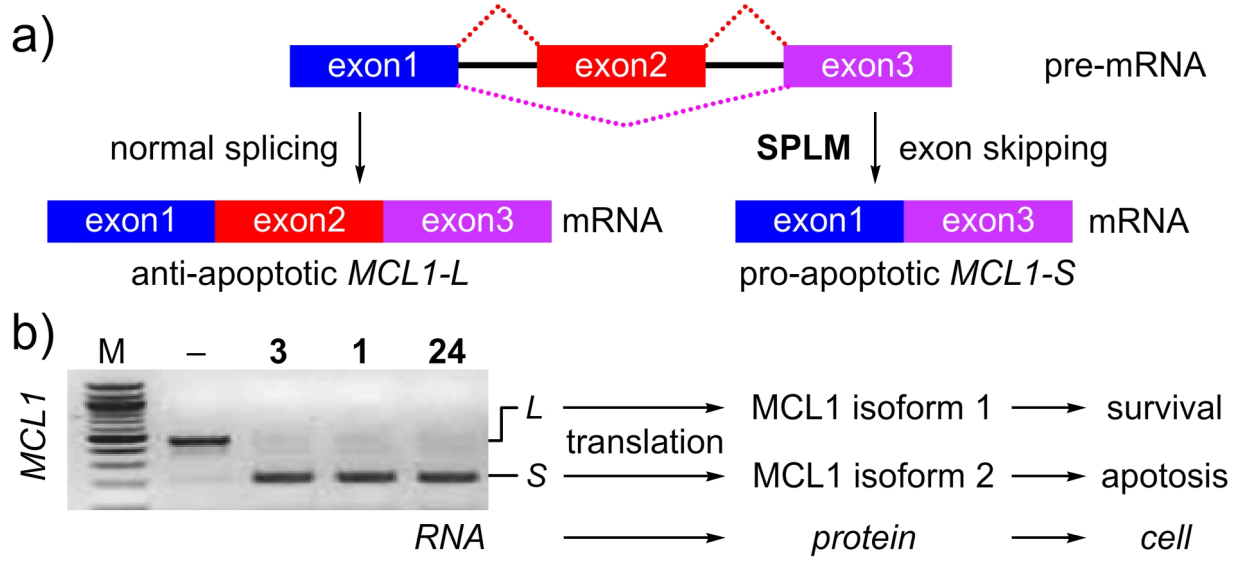

Figure 1.12 Example of splicing selectivity at the protein level. a) Mechanism of splicing modulation in *MCL1*. b) *MCL1* splicing in mantel cell lymphoma (MCL-B) cells after treatment with control (<M->) or 100 nm **1**, **3**, or **24** for 4 h. The levels of spliced (*S*) and unspliced (*L*) transcripts were evaluated by RT-PCR analysis. Without splicing modulation, *MCL1* undergoes normal splicing leaving the longer form. Treatment with **1**, **3**, or **24** results in exon skipping as noted by the formation of the shorter form.

While these effects can corroborate the potent antitumor activity of SPLMs, new tools are needed to analytically evaluate SPLM activity on genes that are prone to alternative splicing, such

as MCL-1 described above. Furthermore, there is a vital need to understand the regulatory systems that lie between the formation of a spliced mRNA and its ultimately translated protein product.

Attenuation through Feedback

The elegance and complexity of splicing modulation, however, does not end there. Recent data have indicated that mRNAs encoding the protein components of the spliceosome are among the most common families of genes to undergo splicing modulation during the action of a SPLM.[35] Remarkably, RNAseq analysis along with RT-PCR Figure 1.13 a) and qRTPCR (Figure 1.13 b) indicate that SF3B1, the gene associated with the protein target of 1, 3, and 24, is one of the most commonly observed splicing-modified genes in cells treated with 1, 3, and 24 (Figure 1.13 a,b). This in turn results in a reduction in the levels of both SF3B1 and phosphorylated SF3B1 (pSF3B1; (Figure 1.13 c).[35] Overall, the feedback between missplicing of SF3B1 RNA through IR and loss of protein leads to even more compromised spliceosomes through the formation of a splice-altered U2 snRNP (Figure 1.13 d). While not yet established, it is likely that this splice-altered U2 snRNP also induces further modulation of splicing events.

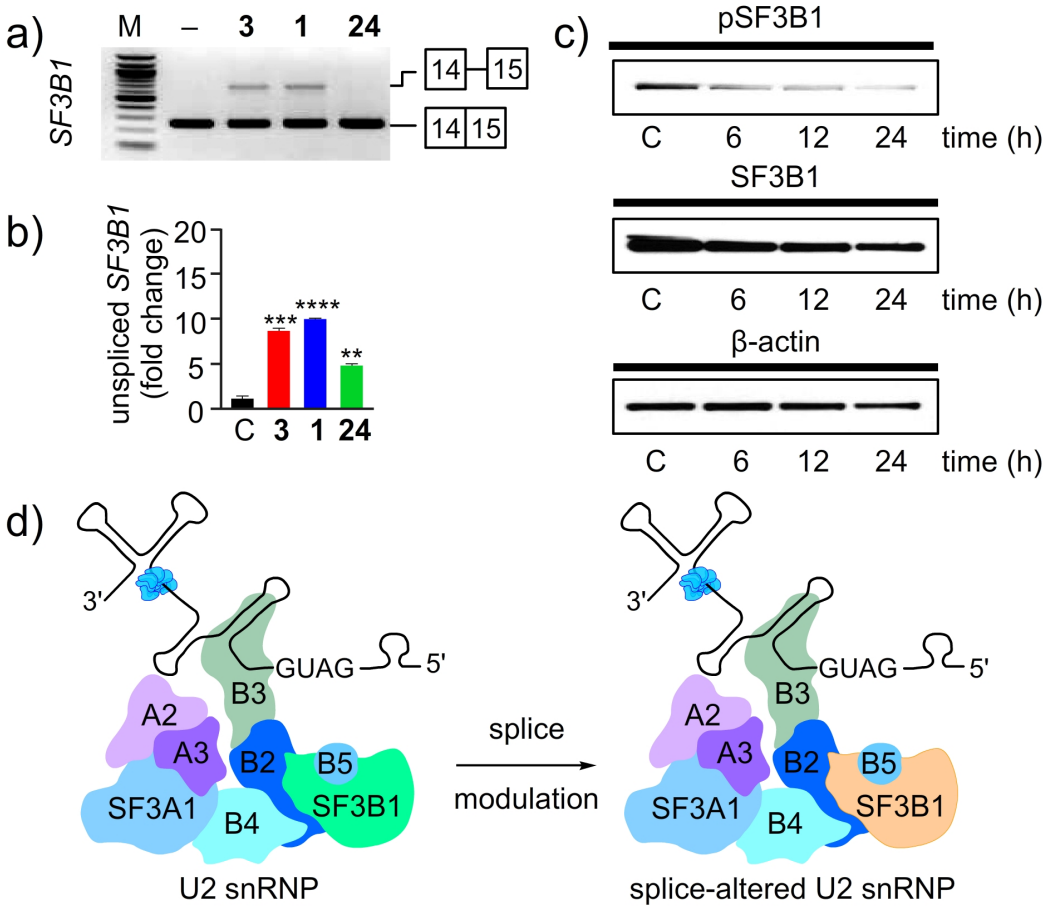

Figure 1.13 Feedback in splicing modulation. a) RT-PCR and b) qRT-PCR analysis of MCL-B cells treated with 100 nm **1**, **3**, or **24**, or a DMSO control for 4 h. c) Pladienolide B (**1**) regulates the level of SF3B1 phosphorylation. JeKo-1 cells were treated with 100 nm **1** for 6 h, 12 h or 24 h. Untreated cells grown for 24 h were used as a control (C). d) Schematic representation of the feedback modulation of SF3B1. Inhibition of SF3B1 (green) results in IR in *SF3B1* and leads to a reduction in the amount of SF3B1 protein (orange) within the U2 snRNP. The net effect is a reduction in SF3B1 levels and the formation of a compromised splice-altered U2 snRNP.

Section 1.4 Chemical Biology of Splice Modulation

In addition to the issues of selectivity, understanding the fine details of SPLM activity must be addressed by chemical biology. Our discussion will highlight two critical features relating to the application of SPLMs, namely, the unique effects of timing and dose.

Timing in Splice Modulation

Until recently, the bulk of splicing studies were conducted using unsynchronized cells. Here, the observed effects at both the RNA and protein levels represent an average over different states of the cell cycle. Recent evidence, however, indicates that synchronization is key to providing a detailed link between splicing modulations at the RNA and protein levels and their effects on the cell. In one study, the presentation of 24 during a brief window in the G1 phase of the cell cycle (Figure 1.14 a) induced an effect that resulted in IR in PLK1 (Figure 1.14 b). While little PLK1 protein was expressed during G1 (Figure 1.14 d), the levels of PLK1 prior to mitosis were reduced in cells treated briefly with 24 several hours before passing from G2 to M. In this study, the direct interrogations of the temporal properties of splicing modulation were evaluated by using PLK1 as a marker of mitotic entry.

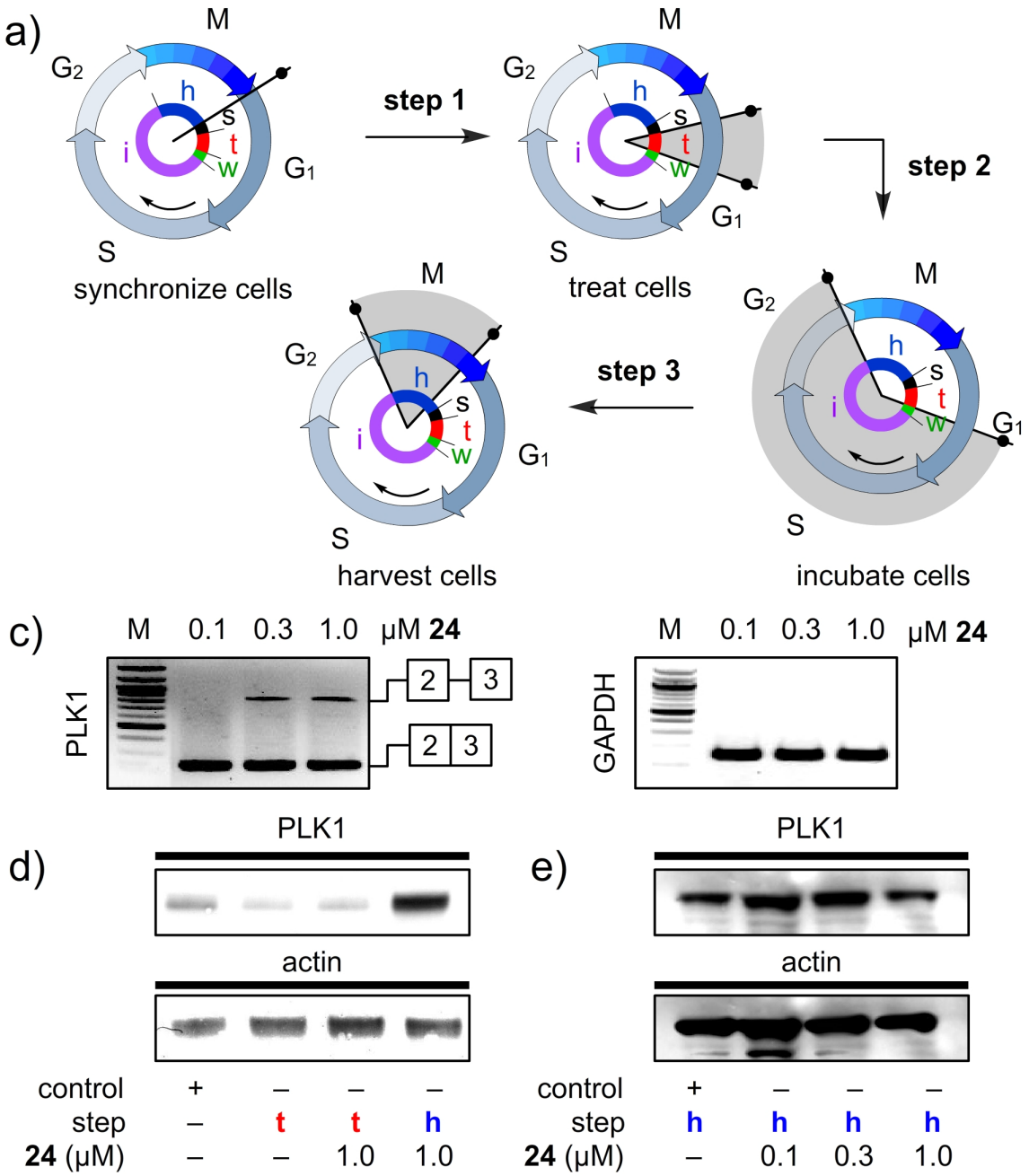

Figure 1.14 A study on timing in splicing modulation. a) Clock diagrams denote the experimental timing as given by: Step 1: synchronized JeKo-1 cells were treated 1 h after release from starvation (start, s) with 24. Step 2: after incubation (treatment, t, red), the media was removed, the cells were washed with media lacking 24 and the cells were cultured (incubation, i, purple) for an additional 12 h without 24. Step 3: the cells were collected (harvest, h, blue) and evaluated. b) RT-PCR analysis was used to evaluate the levels of PLK1 in JeKo-1 cells treated (t) with **24**, washed, and harvested (h). IR was observed for PLK1 after treatment with **24**. c) Western blot analyses of lysates from cells treated with **24** and collected either after treatment (t) or at harvest (h). PLK1 expression arises as cells enter the G_2/M transition during harvest and not at G_1 during treatment. This blot confirms the increase in protein at the state of harvest (h), thus indicating that the cells were at G_2/M. d) Western blot analyses of cells treated with **24** and collected at harvest (h). This blot confirms a dose-dependent reduction in the levels of PLK1 protein in cells exposed to **24** relative to controls. See Ref. [15] for further details.

Mechanistic Action of Splice Modulation

In 2007, it was shown that the molecular probes 1, 2 (Figure 1.1) and(7 (Figure 1.2) target the SF3b complex within the U2 subunit of the spliceosome.[2] This data was soon validated by the observation that pladienolide-resistant clones contained a mutation at Arg 1074 (R1074H) in SF3B1, thus suggesting that this residue is critical for activity.[44] While ongoing studies suggest that all three families of natural products share a common binding site within SF3b, a lack of kinetic and structural data currently prevents this validation.[18]

In addition to the SF3b complex, there is a vast array of different proteins, protein--protein complexes, and protein--RNA complexes in the spliceosome that could be targeted. Like many macromolecular machines, the spliceosome undergoes a complex, timed, mechanical process that serves to loop an intron from within two exons and then clip it.[45] The current understanding of this process has been highlighted schematically in Figure 1.15.

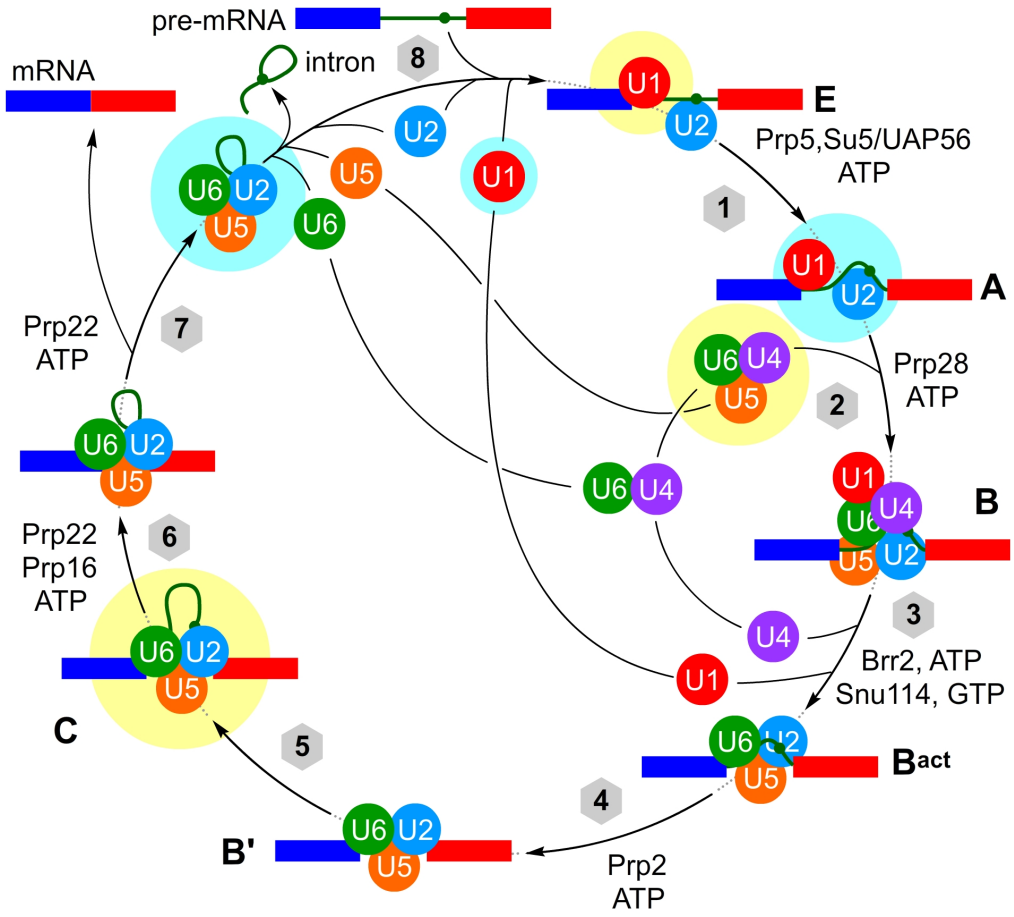

Figure 1.15 The mechanism of splicing, depicting complexes A, B, B^{act}, B', C, and E. A detailed structural understanding of each of the eight steps in this process is slowly being revealed using a combination of cryo-EM and X-ray crystallography with recent human or yeast structures, as noted by highlighting in yellow (human) and cyan (yeast).

Structural Understanding of Splicing

As shown in Figure 1.15, splicing begins with the formation of complexes E and A, which are composed of the U1 and U2 snRNP and mRNA. Action of the U4/U5/U6 tri-snRNP results in the formation of the precatalytic spliceosome, complex B, which in turn is activated to complex Bact through loss of the U1 and U4 snRNPs. The catalytically activated complex B' then performs the first splicing step, cutting the intron, and the resulting complex C completes the process by fusing the two exons and removing the intron lariat. SPLMs may interrupt many of these steps.

One of the most impressive recent advances has been the development of detailed structures of specific spliceosome complexes using a combination of cryo-EM[46] and X-ray crystallography.[47] Cryo-EM has proven particularly useful to tease out the organization of the snRNPs within each complex and illustrate the structural rearrangements within each snRNP. While outside the scope of this review, structures of spliceosome complexes that include the U1 snRNP, [48] complex A, [49] the U4/U5/U6 complex, [50] complex C,[51] and the post-spliceosome complex[52] are beginning to reveal the mechanistic motions within this machine.

Recently teams led by Pena and Srinivasan elucidated the structure of the SF3b complex. [18] Using protein--protein crosslinking, they were able not only to elucidate the structure of the HEAT superhelix but also to determine its contacts with SF3b130, SF3b10, and SF3b14B and its proximity to p14 and U2AF6. Using this data, they utilized established pladienolide-resistance mutations to gain a first glimpse of the possible binding pocket for SPLMs (cyan circle, (Figure 1.16).

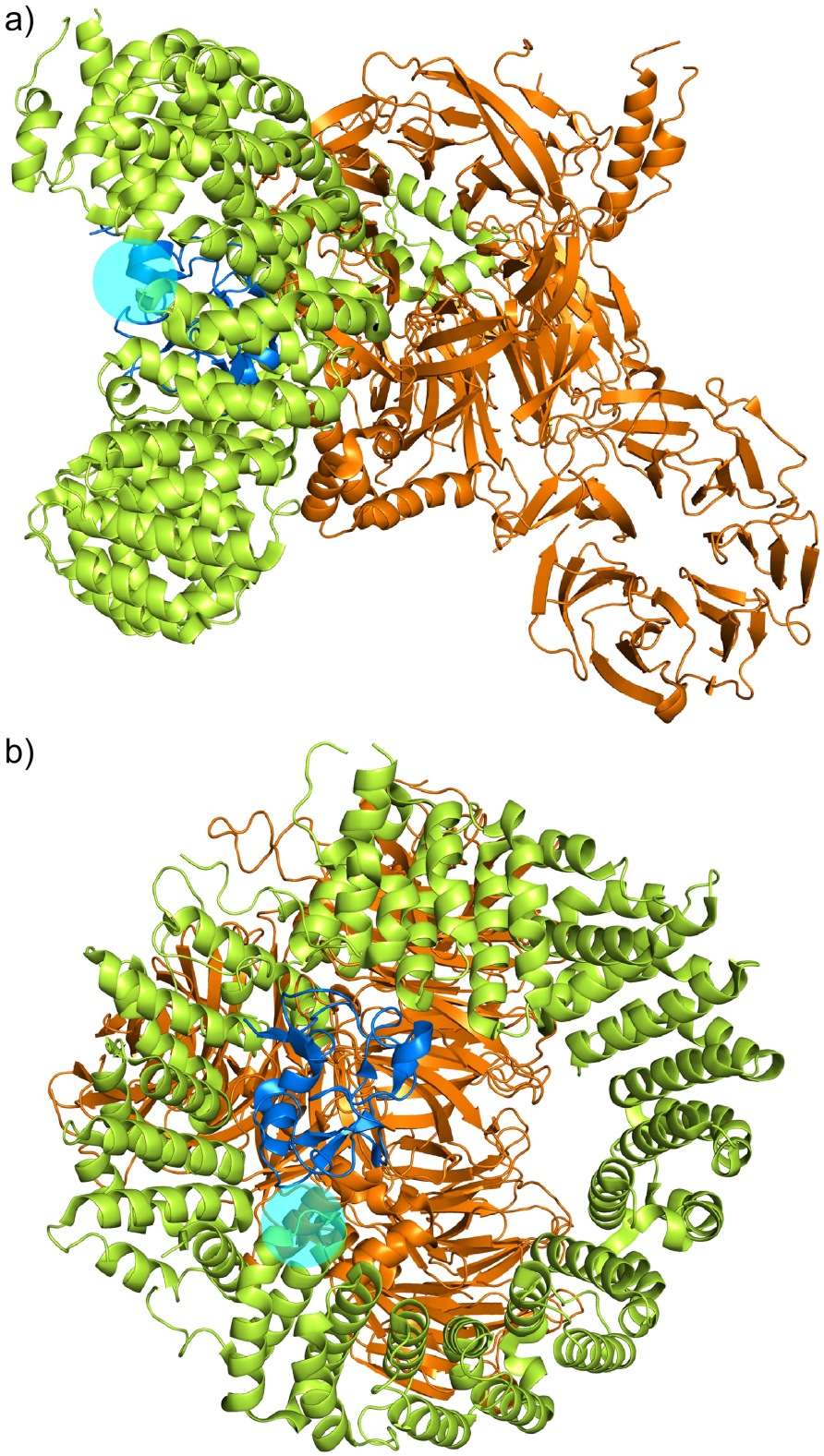

Figure 1.16 Structure of the human SF3b core complex with a cyan sphere showing the position of the R1074 mutation found in cells resistant to pladienolide B (**1**). Two views are provided: a) front view, b) rotation 90° into the page.

Alternate Avenues for Modulation through Chemical Biology

While this review has focused predominantly on SF3b-targeting inhibitors, efforts are now underway to discover new motifs that target different complexes and their associated snRNPs, as well as post-translational events associated with splicing. These materials include a variety of natural products, their derivatives, as well as synthetic leads (Figure 1.17). One of these leads is the CDC2-like kinase (CLK) inhibitor 30, which has been suggested to target the splicing factor SRSF4.[53] Additional studies have also identified SPLM activity in a variety of kinase inhibitors, such as the CLK1-targeting compound 31,[54] the PRP4 inhibitor 32,[55] and the potent CLK1-binding compound 33.[56] In addition, there are number of other leads for which the detailed modes of splicing modulation have not fully been established, including the inhibitor of spliceosome assembly 34,[57] 35,[58] 36,[58] and N-palmitoyl-L-leucine.[59] Other leads such as isoginkgetin (37), which inhibits precatalytic spliceosome complex B formation by blocking the binding of U4/U5/U6 trisnRNP,[60] are already demonstrating that a variety of steps of the splicing process can be effectively modulated. Further examples, including the use of SRPK1 inhibitors, have shown remarkable in vivo utility for regulating neovascularization in tumor tissues by modulating VEGF splicing.[61]

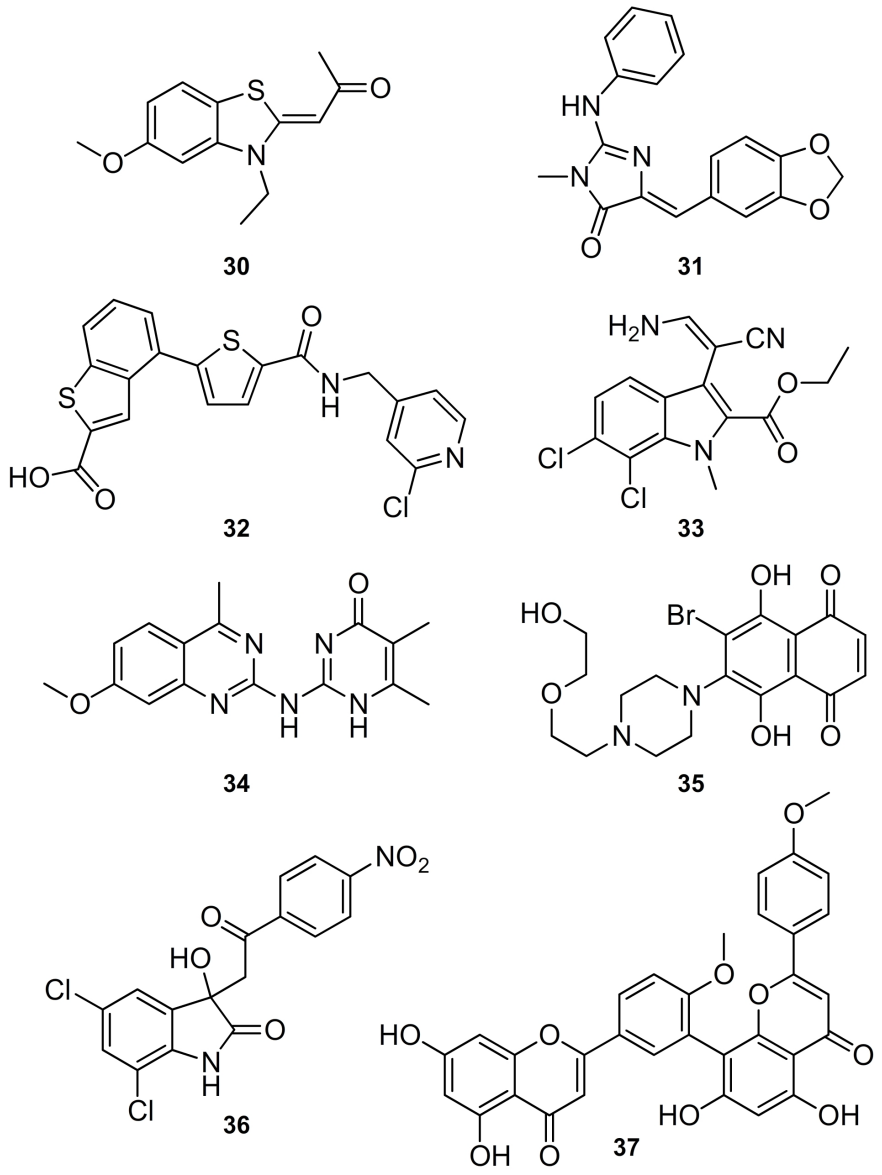

Figure 1.17 Structures of SPLMs that do not target SF3b. These include TG003 (**30**), leucettine L41 (**31**), the PRP4 inhibitor **32**, KH-CB20 (**33**), madrasin (**34**), NSC659999 (**35**), NSC635326 (**36**), and isoginkgetin (**37**).

Section 1.5 Conclusion

The advance of SPLMs brings tremendous therapeutic potential. First, it offers a new set of tools for the clinic, with immediate applications to cancer therapy. Recent evidence also supports the use of SPLMs to regulate the formation of stem cells, thus suggesting that they may

also serve as future tools to guide tissue reprogramming. Second, SPLMs provide a new set of tools for basic biological studies.

Two main hurdles remain in the development of SPLM-based drugs. The first focuses on properly adapting the SF3b-targeting SPLMs for clinical use. Second, there is a need to develop a uniform standard (using defined cell lines with full RNA-seq characterization) to accurately evaluate SPLM activity and RNA splicing to provide a detailed map of molecular features that lead to distinct splicing patterns. While not always carefully identified in the literature, many of the natural product SPLMs and associated analogues used lack sufficient pharmacological stability and associated pharmacological properties for clinical applications. While initial evidence indicates that this may have contributed to problems with the clinical application of E7107 (21), further studies are needed to effectively evaluate activities in patients and develop SPLMs with reduced potential for side or off-target effects. Although a series of studies have produced materials with increased stability,[22, 53] often these compounds are significantly less effective at modulating RNA splicing.[24—28] As illustrated in the current SAR maps (Figure 1.5),[19] only a small number of analogues, such as 23 (Figure 1.6), have been identified that offer enhanced activity over their natural product counterparts.

While first discovered as natural products, it has become increasingly clear that synthetic chemistry will play an integral part in translating splicing modulators to clinical applications. This, along with studies that advance a more detailed mechanistic understanding of the splicing process[35, 62] at both the single-gene and genome-wide levels, are key to advancing SPLMs into the clinic.[63]

Acknowledgements: Chapter 1, in full, is a reprint of the material as it appears: León, B., Kashyap, M. K., Chan, W. C., Krug, K. A., Castro, J. E., La Clair, J. J., Burkart, M. D. *"*A

Challenging Pie to Splice: Drugging the Spliceosome" *Angewandte. Chemie International Edition* 2017, *56* (40). The dissertation author is the fourth author of this manuscript.

Section 1.6 References

(1) a. Matera AG, Wang Z, Nat. Rev. Mol. Cell Biol. 2014, 15, 108.; [PubMed: 24452469] bPapasaikas P, Valcárcel J, Trends Biochem. Sci. 2016, 41, 33. [PubMed: 26682498]

(2) a. Kaida D.,Motoyoshi H, Tashiro E, Nojima T, Hagiwara M, Ishigami K, Watanabe H, Kitahara T, Yoshida T, Nakajima H, Tani T, Horinouchi S, Yoshida M, Nat. Chem. Biol. 2007, 3, 576.; [PubMed: 17643111] bKotake Y., Sagane K, Owa T, Mimori-Kiyosue Y, Shimizu H, Uesugi M, Ishihama Y, Iwata M, Mizui Y, Nat. Chem. Biol. 2007, 3, 570. [PubMed: 17643112]

(3) a. Sakai T., Sameshima T, Matsufuji M, Kawamura N, Dobashi K, Mizui Y, J. Antibiot. 2004, 57, 173.; [PubMed: 15152802] bSeki-Asano M., Okazaki T, Yamagishi M, Sakai N, Takayama Y, Hanada K, Morimoto S, Takatsuki A, Mizoue K, J. Antibiot. 1994, 47, 1395. [PubMed: 7844034]

(4) a. Isaac BG., Ayer SW, Elliott RC, Stonard RJ, J. Org. Chem. 1992, 57, 7220.;bSakai Y, Yoshida T, Ochiai K, Uosaki Y, Saitoh Y, Tanaka F, Akiyama T, Akinaga S, Mizukami T, J. Antibiot. 2002, 55, 855. [PubMed: 12523818]

(5) a. Nakajima H, Sato B, Fujita T, Takase S, Terano H, Okuhara M, J. Antibiot. 1996, 49, 1196.; [PubMed: 9031664] bLiu X, Biswas S, Berg MG, Antapli CM, Xie F, Wang Q, Tang MC, Tang GL, Zhang L, Dreyfuss G, Cheng YQ, J. Nat. Prod. 2013, 76, 685. [PubMed: 23517093]

(6) Kanada RM, Itoh D, Nagai M, Niijima J, Asai N, Mizui Y, Abe S, Kotake Y, Angew. Chem. Int. Ed. 2007, 46, 4350;Angew. Chem 2007, 119, 4428.

(7) Villa R, Mandel AL, Jones BD, La Clair JJ, Burkart MD, Org. Lett. 2012, 14, 5396. [PubMed: 23072504]

(8) Müller S, Mayer T, Sasse F, Maier M, Org. Lett. 2011, 13, 3940. [PubMed: 21707025]

(9) Ghosh AK, Anderson DD, Org. Lett. 2012, 14, 4730. [PubMed: 22954141]

(10) Kumar V, Chandrasekhar S, Org. Lett. 2013, 15, 3610. [PubMed: 23822896]

(11) Pham D, Koide K, Nat. Prod. Rep. 2016, 33, 637. [PubMed: 26812544]

(12) Lagisetti C, Yermolina MV, Sharma LK, Palacios G, Prigaro BJ, Webb TR, ACS Chem. Biol. 2014, 9, 643. [PubMed: 24377313]

(13) a. Ghosh AK, Ma N, Effenberger KA, Jurica MS, Org. Lett. 2014, 16, 3154−−3157.; [PubMed: 24869489] b. Ghosh AK, Li J, Org. Lett. 2011, 13, 66. [PubMed: 21126066]

(14) Meng F, McGrath KP, Hoveyda AH, Nature 2014, 513, 367. [PubMed: 25230659]

(15) Makowski K, Vigevani L, Alberico F, Valcárcel J, Álvarez M, ACS Chem. Biol. 2017, 12, 163. [PubMed: 28103691]

(16) Eustáquio AS, Chang LP, Steele GL, O'Donnell CJ, Koehn FE, Metab. Eng. 2016, 33, 67. [PubMed: 26620532]

(17) Nicolaou KC, Rhoades D, Lamani M, Pattanayak MR, Kumar SM, J. Am. Chem. Soc. 2016, 138, 7532. [PubMed: 27266914]

(18) a. Cretu C, Schmitzová J, Ponce-Salvatierra A, Dybkov O, De Laurentiis EI, Sharma K, Will CL, Urlaub H, Lührmann R, Pena V, Mol. Cell 2016, 64, 307.; [PubMed: 27720643] bRakesh R, Joseph AP, Bhaskara RM, Srinivasan N, RNA Biol. 2016, 13, 1025. [PubMed: 27618338]

(19) a. Effenberger KA, Urabe VK, Jurica MS, Wiley Interdiscip. Rev. RNA 2017, 8, e1381.;bEffenberger KA, Urabe VK, Prichard BE, Ghosh AK, Jurica MS, RNA 2016, 22, 350. [PubMed: 26742993]

(20) a. Folco EG, Coil KE, Reed R, Genes Dev. 2011, 25, 440.; [PubMed: 21363962] bEskens FALM, Ramos FJ, Burger H, O'Brien JP, Piera A, De Jonge MJA, Mizui Y, Wiemer EAC, Carreras MJ, Baselga J, Taberno J, Clin. Cancer Res. 2013, 19, 6296. [PubMed: 23983259]

(21) Arai K, Buonamici S, Chan B, Corson L, Endo A, Gerard B, Hao MH, Karr C, Kira K, Lee L, Liu X, Lowe JT, Luo T, Marcaurelle LA, Mizui Y, Nevalainen M, O'Shea MW, Park ES, Perino SA, Prajapati S, Shan M, Smith PG, Tivitmahaisoon P, Wang JY, Warmuth M, Wu KM, Yu L, Zhang H, Zheng GZ, Keaney GF, Org. Lett. 2014, 16, 5560. [PubMed: 25376106]

(22) Villa R, Kashyap MK, Kumar D, Kipps TJ, Castro JE, La Clair JJ, Burkart MD, J. Med. Chem. 2013, 56, 6576. [PubMed: 23919277]

(23) Crews LA, Balaian L, Delos Santos NP, Leu HS, Court AC, Lazzari E, Sadarangani A, Zipeto MA, La Clair JJ, Villa R, Kulidjian A, Storb R, Morris SR, Ball ED, Burkart MD, Jamieson CH, Cell Stem Cell 2016, 19, 599. [PubMed: 27570067]

(24) Lagisetti C, Pourpak A, Jiang Q, Cui X, Goronga T, Morris SW, Webb TR, J. Med. Chem. 2008, 51, 6220. [PubMed: 18788726]

(25) Lagisetti C, Palacios G, Goronga T, Freeman B, Caufield W, Webb TR, J. Med. Chem. 2013, 56, 10033. [PubMed: 24325474]

(26) Dhar S, La Clair JJ, León B, Hammons JC, Yu Z, Kashyap MK, Castro JE, Burkart MD, J. Am. Chem. Soc. 2016, 138, 5063. [PubMed: 27058259]

(27) Albert BJ, Sivaramakrishnan A, Naka T, Czaicki NL, Koide K, J. Am. Chem. Soc. 2007, 129, 2648. [PubMed: 17279752]

(28) Sahebi M, Hanafi MM, van Wijnen AJ, Azizi P, Abiri R, Ashkani S, Taheri S, Gene 2016, 587, 107. [PubMed: 27154819]

(29) a. Lee Y., Rio DC, Annu. Rev. Biochem. 2015, 84, 291.; [PubMed: 25784052] bWahl MC, Will CL, Lührmann R, Cell 2009, 136, 701. [PubMed: 19239890]

(30) a. Van Der Feltz C, Anthony K, Brilot A, Pomeranz Krummel DA, Biochemistry 2012, 51, 3321.; [PubMed: 22471593] bWill CL, Lührmann R, Cold Spring Harbor Perspect. Biol 2011, 3, a003707.

(31) Kotake Y, Kaida D, Mizui Y, Yoshida M, Tanpakushitsu Kakusan Koso 2008, 53, 28. [PubMed: 18186300]

(32) Albert BJ, McPherson PA, O'Brien K, Czaicki NL, Destefino V, Osman S, Li M, Day BW, Grabowski PJ, Moore MJ, Vogt A, Koide K, Mol. Cancer Ther. 2009, 8, 2308. [PubMed: 19671752]

(33) a. Lagisetti C, Pourpak A, Goronga T, Jiang Q, Cui X, Hyle J, Lahti JM, Morris SW, Webb TR, J. Med. Chem. 2009, 52, 6979.; [PubMed: 19877647] bKashyap MK, Kumar D, Villa R, La Clair JJ, Benner C, Sasik R, Jones H, Ghia EM, Rassenti LZ, Kipps TJ, Burkart MD, Castro JE, Haematologica 2015, 100, 945. [PubMed: 25862704]

(34) a. Bae J, Leo CP, Hsu SY, Hsueh AJW, J. Biol. Chem. 2000, 275, 25255.; [PubMed: 10837489] bKim JH, Sim SH, Ha HJ, Ko JJ, Lee K, Bae J, FEBS Lett. 2009, 583, 2758.; [PubMed: 19683529] cGao Y, Koide K, ACS Chem. Biol. 2013, 8, 895. [PubMed: 23485022]

(35) Kumar D, Kashyap MK, La Clair JJ, Villa R, Spaanderman I, Chien S, Rassenti LZ, Kipps TJ, Burkart MD, Castro JE, ACS Chem. Biol. 2016, 11, 2716. [PubMed: 27499047]

(36) a. Breitbart RE, Andreadis A, Nadal-Ginard B, Annu. Rev. Biochem. 1987, 56, 467.; [PubMed: 3304142] bChen M, Manley JL, Nat. Rev. Mol. Cell Biol. 2009, 10, 741. [PubMed: 19773805]

(37) Watakabe A, Tanaka K, Shimura Y, Genes Dev. 1993, 7, 407. [PubMed: 8449402]

(38) Kozak M, Cell Biol J. 1988, 107, 1.

(39) Corrionero A, Miñana B, Valcárcel J, Genes Dev. 2011, 25, 445. [PubMed: 21363963]

(40) Hasegawa M, Miura T, Kuzuya K, Inoue A, Won Ki S, Horinouchi S, Yoshida T, Kunoh T, Koseki K, Mino K, Sasaki R, Yoshida M, Mizukami T, ACS Chem. Biol. 2011, 6, 229. [PubMed: 21138297]

(41) Convertini P, Shen M, Potter PM, Palacios G, Lagisetti C, de la Grange P, Horbinski C, FondufeMittendorf YN, Webb TR, Stamm S, Nucleic Acids Res. 2014, 42, 4947. [PubMed: 24623796]

(42) Sakharkar MK, Chow VTK, Kangueane P, In Silico Biol. 2004, 4, 387. [PubMed: 15217358]

(43) Galante PAF, Sakabe NJ, Kirschbaum-Slager N, de Souza SJ, RNA 2004, 10, 757. [PubMed: 15100430]

(44) Yokoi A, Kotake Y, Takahashi K, Kadowaki T, Matsumoto Y, Minoshima Y, Sugi NH, Sagane K, Hamaguchi M, Iwata M, Mizui Y, FEBS J 2011, 278, 4870. [PubMed: 21981285]

(45) a. Patel AA, Steitz JA, Nat. Rev. Mol. Cell Biol. 2003, 4, 960.; [PubMed: 14685174] bNoren CJ, Wang J, Perler FB, Angew. Chem. Int. Ed. 2000, 39, 450;Angew. Chem 2000, 112, 458.;bPaulus H, Annu. Rev. Biochem. 2000, 69, 447. [PubMed: 10966466]

(46) a. Stark H, Lührmann R, Annu. Rev. Biophys. Biomol. Struct. 2006, 35, 435.; [PubMed: 16689644] bValadkhan S, Jaladat Y, Proteomics 2010, 10, 4128.; [PubMed: 21080498] cFica SM, Oubridge C, Galej WP, Wilkinson ME, Bai XC, Newman AJ, Nagai K, Nature 2017, 524, 337.;dBertram K, Agafonov DE, Liu WT, Dybkov O, Will CL, Hartmuth K, Urlaub H, Kastner B, Stark H, Lührmann R, Nature 2017, 524, 318.;eGalej WP, Wilkinson ME, Fica SM, Oubridge C, Newman AJ, Nagai K, Nature 2016, 537, 197. [PubMed: 27459055]

(47) a. Sperling J, Azubel M, Sperling R, Structure 2008, 16, 1605.; [PubMed: 19000813] bKorneta I, Magnus M, Bujnicki JM, Nucleic Acids Res. 2012, 40, 7046.; [PubMed: 22573172] cvan Roon AM, Oubridge C, Obayashi E, Sposito B, Newman AJ, Séraphin B, Nagai K, RNA 2017, 23, 968. [PubMed: 28348170]

(48) a. Kondo Y, Oubridge C, van Roon A-MM, Nagai K, eLife 2015, 4, 4986.;bPomeranz Krummel DA, Oubridge C, Leung AKW, Li J, Nagai K, Nature 2009, 458, 475. [PubMed: 19325628]

(49) Behzadnia N, Golas MM, Hartmuth K, Sander B, Kastner B, Deckert J, Dube P, Will CL, Urlaub H, Stark H, Lührmann H, EMBO J. 2007, 26, 1737. [PubMed: 17332742]

(50) Nguyen THD, Galej WP, Bai X, Savva CG, Newman AJ, Scheres SHW, Nagai K, Nature 2015, 523, 47. [PubMed: 26106855]

(51) Golas MM, Sander B, Bessonov S, Grote M, Wolf E, Kastner B, Stark H, Lührmann R, Mol. Cell 2010, 40, 927. [PubMed: 21172658]

(52) Nguyen THD, Galej WP, Fica SM, Lin P-C, Newman AJ, Nagai K, Curr. Opin. Struct. Biol. 2016, 36, 48. [PubMed: 26803803]

(53) Nishida A, Kataoka N, Takeshima Y, Yagi M, Awano H, Ota M, Itoh K, Hagiwara M, Matsuo M, Nat. Commun. 2011, 2, 308. [PubMed: 21556062]

(54) Tahtouh T, Elkins JM, Filippakopoulos P, Soundararajan M, Burgy G, Durieu E, Cochet C, Schmid RS, Lo DC, Delhommel F, Oberholzer AE, Pearl LH, Carreaux F, Bazureau JP, Knapp S, Meijer L, J. Med. Chem. 2012, 55, 9312. [PubMed: 22998443]

(55) Gao Q, Mechin I, Kothari N, Guo Z, Deng G, Haas K, McManus J, Hoffmann D, Wang A, Wiederschain D, Rocnik J, Czechtizky W, Chen X, McLean L, Arlt H, Harper D, Liu F, Majid T, Patel V, Lengauer C, Garcia-Echeverria C, Zhang B, Cheng H, Dorsch M, Huang SM, J. Biol. Chem. 2013, 288, 30125. [PubMed: 24003220]

(56) Fedorov O, Huber K, Eisenreich A, Filippakopoulos P, King O, Bullock AN, Szklarczyk D, Jensen LJ, Fabbro D, Trappe J, Rauch U, Bracher F, Knapp S, Chem. Biol. 2011, 18, 67. [PubMed: 21276940]

(57) Pawellek A, McElroy S, Samatov T, Mitchell L, Woodland A, Ryder U, Gray D, Lührmann R, Lamond AI, J. Biol. Chem. 2014, 289, 34683. [PubMed: 25281741]

(58) Effenberger KA, Perriman RJ, Bray WM, Lokey RS, Ares M, Jurica MS, Biomol J. Screening 2013, 18, 1110.

(59) Effenberger KA, James RC, Urabe VK, Dickey BJ, Linington RG, Jurica MS, J. Biol. Chem. 2015, 290, 27524. [PubMed: 26408199]

(60) O'Brien K, Matlin AJ, Lowell AM, Moore MJ, J. Biol. Chem. 2008, 283, 33147. [PubMed: 18826947]

(61) Nowak DG, Amin EM, Rennel ES, Hoareau-Aveilla C, Gammons M, Damodoran G, Hagiwara M, Harper SJ, Woolard J, Ladomery MR, Bates DO, J. Biol. Chem. 2010, 285, 5532. [PubMed: 19906640]

(62) a. Boswell SA, Snavely A, Landry HM, Churchman LS, Gray JM, Springer M, Nat. Chem. Biol. 2017, 501.; [PubMed: 28263964] bCarrocci TJ, Zoerner DM, Paulson JC, Hoskins AA, Nucleic Acids Res. 2017, 45, 4837; [PubMed: 28062854] cLiu B, Abdel-Wahab O, eLife 2017, 6, e25996; [PubMed: 28304277] dJenkins JL, Kielkopf CL, Trends Genet. 2017, 33, 336. [PubMed: 28372848]

Chapter 2. Splice Modulation Synergizes Cell Cycle Inhibition

Section 2.1 Introduction

Splicing is an essential eukaryotic biological process that is frequently mis-regulated in cancer.1 Since their discovery in the early 1990s, splice-modulating polyketide natural products FD-8952 (1a, Figure 2.1), pladienolide B3 (1b, Figure S2.1), or herboxidiene4 (1c, Figure S2.1), and FR9014645 (1d, Figure S2.1), have been proposed as new anticancer therapeutics and used to investigate the impact of spliceosome inhibition in healthy or tumor cells.6,7 These SPLMs share a common mode of action (MOA) by targeting the splicing factor 3b (SF3B) unit of the human spliceosome, leading to splicing inhibition and changes in alternative splicing patterns.8–10 Many tumors depend on aberrant use of splicing machinery for expansion and metastasis, but interruption of splicing by SPLMs limits the expression of genes necessary for tumor survival, ultimately resulting in apoptotic cell death. 11 Because SPLMs regulate the splicing of several genes that are overexpressed in cancer, they have been identified for their potential in anti-cancer therapy.6,12–14 To date two SPLMs have entered the clinic, including the most recent entrance of H3B-880015 (1f, Figure S2.1) for acute myeloid leukemia (AML), and E-710716 (1e, Figure S2.1) against solid tumors. Recent efforts in medicinal chemistry, RNA biology, and structural biology have allowed for better understanding of SPLM activity and enhanced pharmaceutical access to SPLMs.17,18

Despite recent progress towards the development of anticancer chemotherapeutics, desensitization, chemoresistance, and patient relapse remain challenges in the field. Advances in combination therapy indicate that splice modulators could serve as a potential way to overcome these issues. For instance, studies led by Mistelli suggest that splicing modulation can be used to combat vemurafenib-resistance.19 More recently, studies led by Yamano have shown that

FR901464 (1d, Figure S2.1), the natural product precursor to spliceostatin A, synergistically improved efficacy of the PARP1 inhibitor olaparib.20 These studies suggest that splice modulatory combination therapy may offer a new approach to target many of the challenges associated protein-targeting chemotherapeutics.

To date, SPLMs have been found to interfere with the splicing of specific RNAs6 by targeting the branch point adenosine binding pocket defined by the PHF5A-SF3b complex,21 ultimately down-regulating expression of encoded proteins. The timing of this effect was demonstrated by examining the splice modulation of cell cycle regulatory proteins.22,23 We reasoned that that SPLMs could likewise sensitize tumor cells to cell cycle inhibitors, leading to synergistic anti-tumor effects (Figure 2.1). Here we describe these synergy studies to determine whether pre-treatment of cancer cells with SPLMs followed by administration of established kinase inhibitors could play a role in enhancing chemotherapeutics.

Section 2.2 Results and Discussion

Over the last decade, our laboratory has been exploring the multi-level effects of SPLMs upon the normal course of splicing.6 We have found that SPLMs regulate splicing at two levels: directly, through interactions with SF3b subunit within the spliceosome;17,18 and indirectly, by altering the expression of spliceosomal proteins, which in turn modifies the splicing of subsequent transcripts.22 As SPLMs such as FD-895 (1a, Figure 2.1) target the splicing process and result in aberrant splicing within tumor cells, we suspected that pretreatment of cells with 1a could decrease the expression of cell cycle RNA, thereby decreasing cellular levels of a target protein for a specific inhibitor. Cell cycle RNA is only expressed at certain times in the cell cycle, such as the onset of mitosis, so FD-895 (1a) can be applied at this time for optimal regulation of cell cycle RNA.

Therefore, tumor cells pretreated with 1a would be more sensitive to inhibitors of a targeted protein, as its levels would be reduced by mis-splicing of its precursor RNA. In this way we hoped to achieve reduction of target protein levels, ultimately enhancing the efficacy of tumor cell death (Figure 2.1).

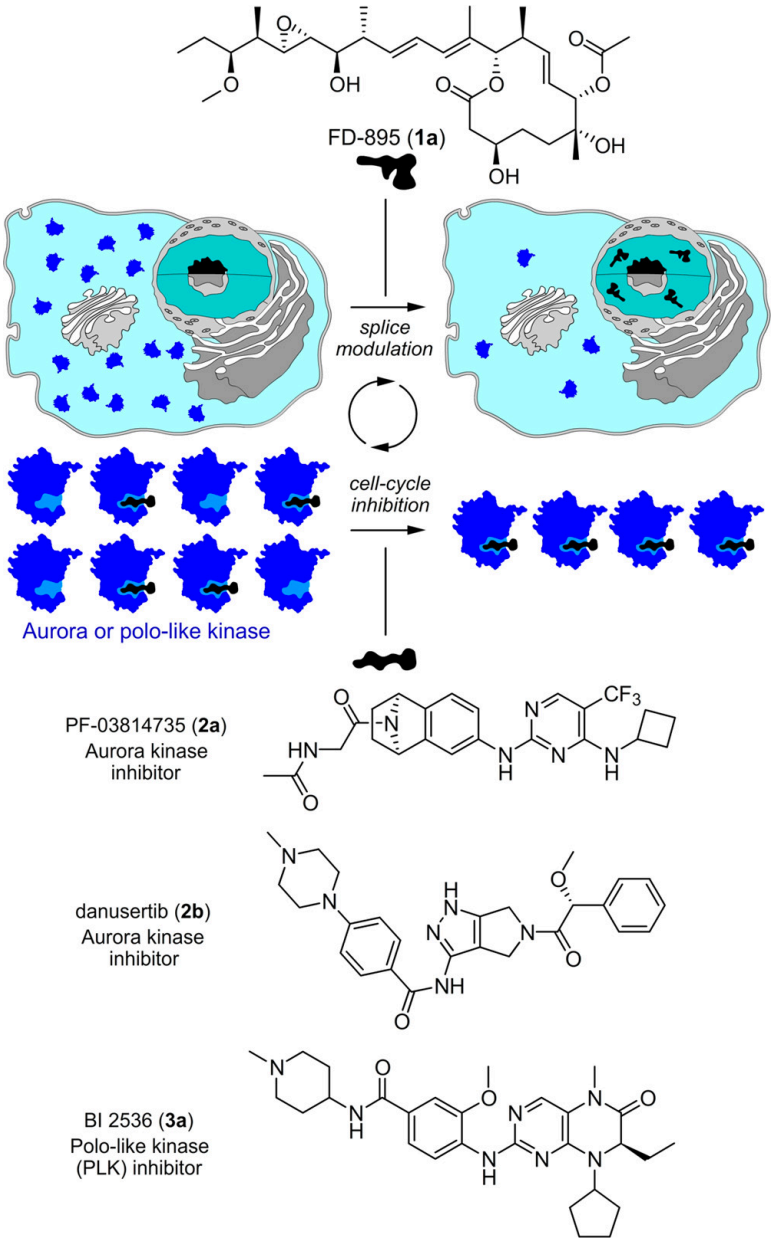

Figure 2.1 Concept of splice synergy of cell cycle inhibitors. Pretreatment of tumor cells with a SPLM such as FD-895 (1a) induces alternate splicing of a RNA associated with a cell cycle response. Rendered unproductive, the resulting mis-spliced RNA is no longer translated into protein leading to net loss in the levels of the given cell cycle regulatory protein. Ultimately, this results in a synergistic enhancement of inhibitors of that cell cycle protein, as demonstrated by AURK inhibitors 2a, 2b or a PLK-1 inhibitor 3a.

Using cell cycle regulation as a model, we sought to evaluate the effect of FD-895 (1a) treatment on the expression of critical cell cycle regulators (Figure 2.1). Using RNA-seq data previously collected on cancer cells treated with FD-895,6 we identified the oncogenic kinases aurora kinase A (AURKA), aurora kinase B (AURKB) and polo-like kinase 1 (PLK-1) as likely targets for SPLM modulation.24 These proteins are established chemotherapeutic targets. AURKA and AURKB regulate chromatin segregation during cell division. PLK-1 promotes centrosome development while activating the anaphase-promoting complex. A schematic representation of their role in the cell cycle has been provided in Supporting Figure S2.2. Despite much progress towards the development of cell cycle-inhibiting chemotherapeutics, the concentrations required for in vivo efficacy often lead to off-target activity.

We screened the cytotoxicity of FD-895 (1a) alone or in combination with the AURK inhibitors danusertib (2a) 27 or PF-03814735 (2b). 28 Consistent with the literature, the GI50 values were observed at 0.8±0.1 nM for 1a29 (Figure 2.2a,d), 4.3±0.4 μM for 2a27 (Figure 2.2a), and 2.1±0.2 μM for 2b28 (Figure 2.2d) in HCT-116 colorectal carcinoma cells. Comparable activities were observed in Caov3 ovarian adenocarcinoma or HeLa cervical adenocarcinoma cells with GI50 values at 2.0±0.1 nM for 1a (Caov3, Figure 2.2b), 3.7±0.4 nM for 1a (HeLa, Figure 2.2c), 5.5±0.5 μM for 2a (Caov3, Figure 2.2b), 10.1±1.0 μM for 2a (HeLa, Figure 2.2c), 6.0±0.6 μM for 2b (Caov3, Figure 2.2e) and 19.5±2.0 μM for 2b (HeLa, Figure 2.2f). Pre-treatment of either cell line with 1 nM 1a or 5 nM 1a was found to significantly decrease the associated GI50 values for each inhibitor (Figure 2.2a-f). Treatments with 1 nM 1a led to reductions up to 10-fold reduction in cell cycle inhibitor GI50 values, whereas 5 nM 1a led to reduction by up to 90,000-fold. At 1 nM 1a, the combination of 1a and the AURK inhibitors 2a and 2b was found to be

antagonistic. Interestingly, in cells treated with 5 nM 1a, the combination was synergistic for both 2a and 2b. Similar trends were observed for combination treatment in Caov3 (Figure 2.2b,e) and HeLa (Figure 2.2c,f) cells, indicating that this effect was not cell line specific.

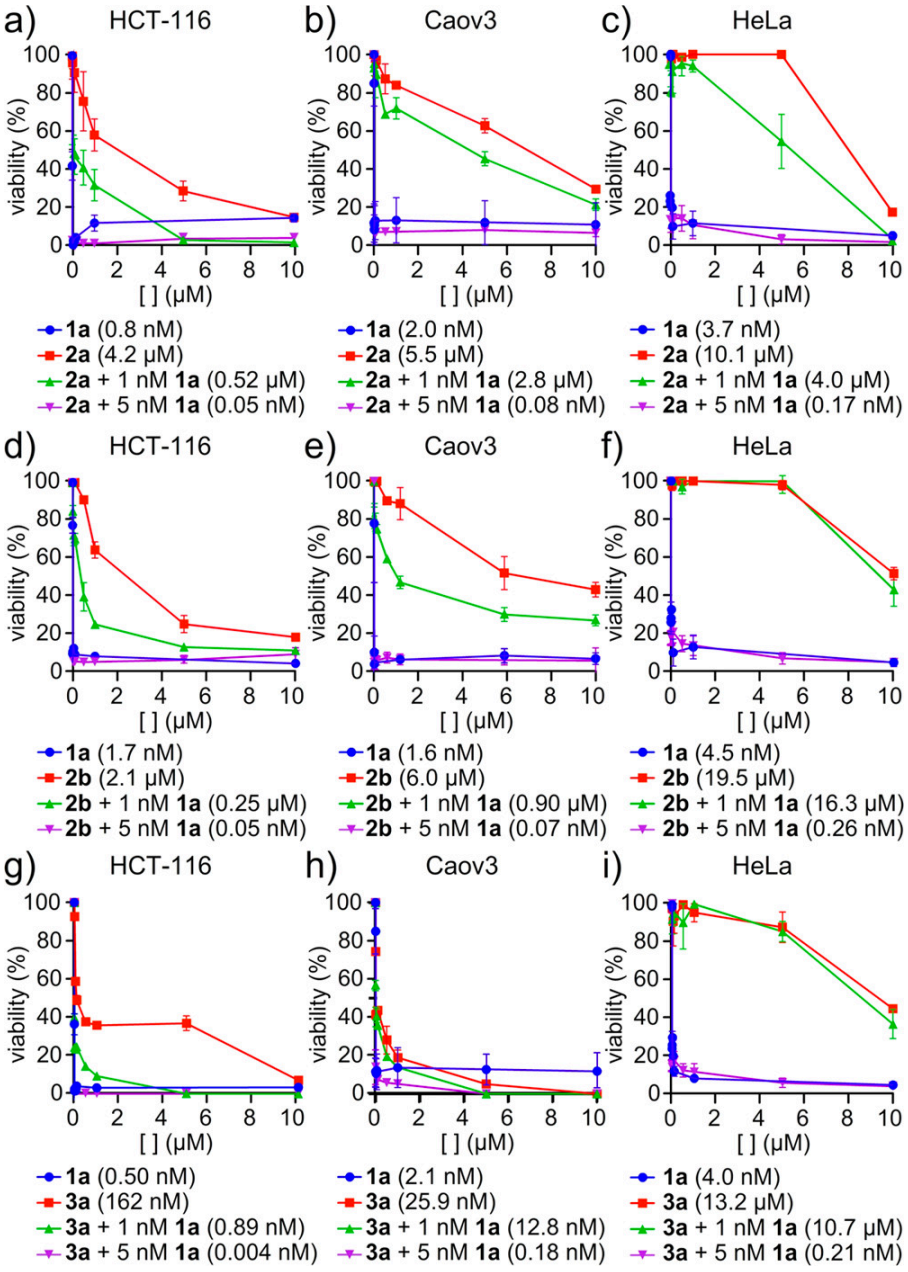

Figure 2.2 Synergistic reduction in tumor cell viability. HCT-116, HeLa, or Caov3 cells were treated with FD-895 (**1a**) for 24 h, washed with PBS to remove **1a**, and then treated with cell cycle inhibitors: (a–c) PF-03814735 (**2a**), (d–f) danusertib (**2b**), or (g–i) BI 2536 (**3a**) for 72 h. Analysis of tumor cell viability showed that pretreatment with 1 nM **1a** led to an antagonistic reduction in cell viability, whereas treatment with 5 nM **1a** led to synergistic reductions in cell viability. Experiments were conducted in triplicate with GI_{50} values reported for each experiment. Statistical analyses and confidence limits are provided in Tables S2 and S3.

We then explored the effects of 1a in combination with the PLK-1 inhibitor BI 2536 (3a) (Figure 2.2g-i). In accordance with the literature, the GI50 values were 0.5 ± 0.1 nM for 1a28 and 160 ± 50 nM for 3a30 in HCT-116 cells. Comparable activities were observed in Coav3 or HeLa cells with GI50 values were observed at 2.0±0.2 nM for 1a (Caov3, Figure 2.2h), 4.0±0.4 nM for 1a (HeLa, Figure 2.2i), 25.9±3 nM for 3a (Caov3, Figure 2.2h), and 13.2±1 μM for 3a (HeLa, Figure 2.2i). Pre-treatment of either cell line with 1 nM 1a or 5 nM 1a was found to decrease the associated GI50 values for 3a (Figure 2.2g-i); 1 nM 1a led to reductions in cell cycle inhibitor GI50 values by a factor of up to 200-fold, whereas 5 nM 1a led to reduction by a factor of up to 60,000-fold. At 1 nM 1a, the combination of 1a and 3a was found to be antagonistic, but at the slightly higher concentration of 5 nM 1a, this combination was synergistic for 3a. Once again, similar trends were observed in HeLa and Caov3 cell lines.

To further investigate the synergistic relationship between 1a and the AURK inhibitors, we investigated the effects of FD-895 (1a) treatment on AURK gene expression at the RNA and AURK protein level. We treated HCT-116 cells with 1a and found that nanomolar concentrations could diminish the levels of AURKA (Figure 2.3a) and AURKB (Figure 2.3b). As depicted in Figure 2.3, SPLM 1a was found to decrease the expression of AURKA (Figure 2.3d) and AURKB (Figure 2.3e), inducing exon skipping in AURKA and AURKB (Figure S2.3), likely introducing a premature termination codon (PTC) and leading to nonsense mediated decay (NMD). These reductions in AURKA and AURKB also translated to decreases in AURKA and AURKB protein (Figure 2.3c,d).

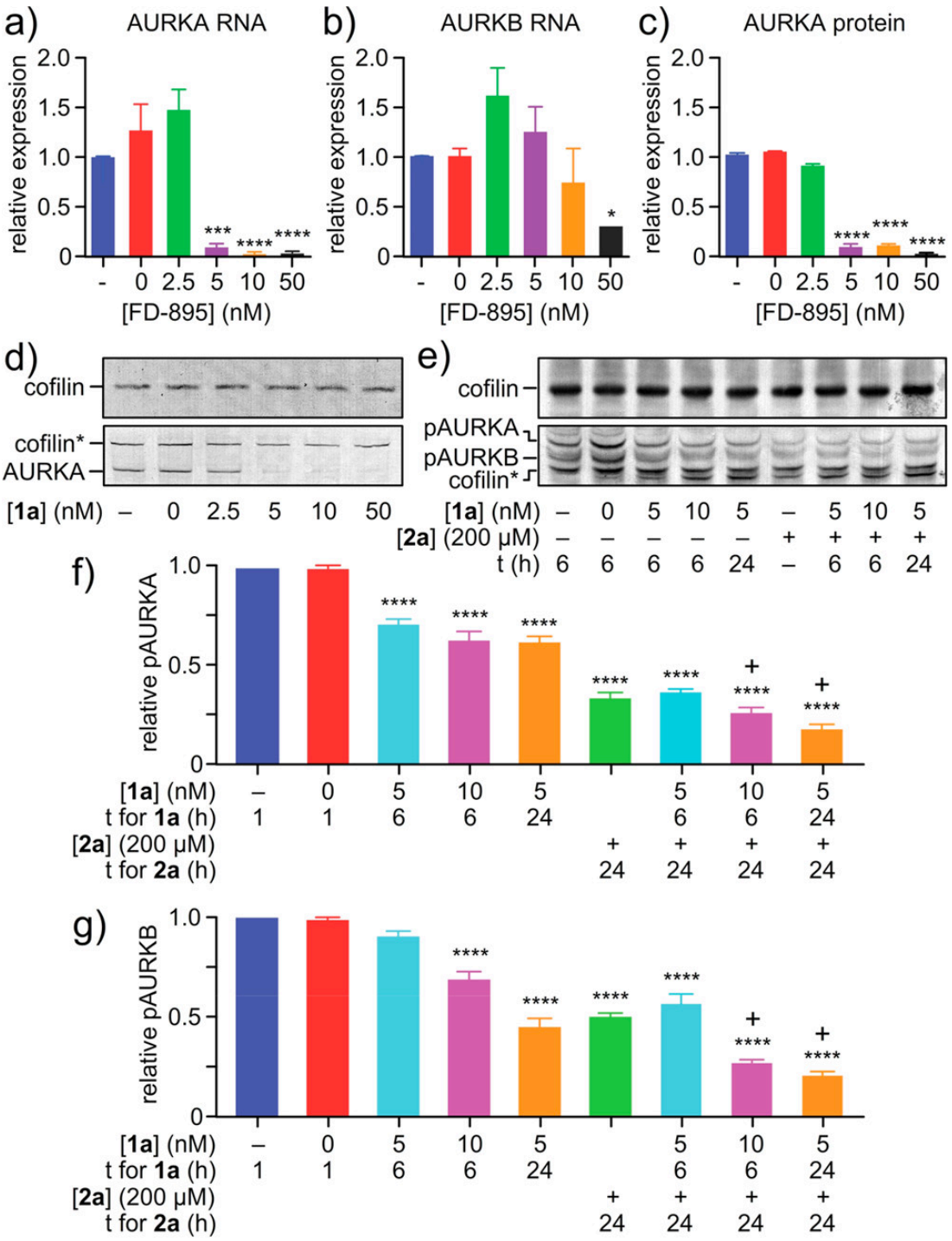

Figure 2.3 Demonstration of synergistic splice modulation of AURKA and AURKB. HCT-116 cells were treated with SPLM **1a** for 24 h and then expression of (a) *AURKA* RNA, (b) *AURKB* RNA, or (c, d) AURKA protein was analyzed. (e–g) For combination studies, synchronized HCT-116 cells were treated with 5 nM or 10 nM **1a** for 6 or 24 h, 200 nM **2a** for 24 h, or a combination of **1a** and **2a**. Treatment efficacy was assessed by visualizing pAURKA and pAURKB levels by western blotting. pAURK values were expressed relative to the reference gene cofilin. The "+" sign above bars indicates synergy. Experiments were conducted in biological triplicate. Statistics were calculated using a standard one-way ANVOA; *p*-values were represented so that * signifies $p < 0.05$, ** signifies $p < 0.01$, *** signifies $p < 0.001$, and **** signifies $p < 0.0001$.

This observation was not limited to AURK alone. Similarly, SPLM 1a diminished PLK-1 RNA levels (Figure 2.4a). Previous studies have found that 1a induces utilization of an alternative 5' splice site, introducing a PTC and leading to nonsense mediated decay (NMD) of PLK-1. 22 Complete loss of PLK-1 was observed at treatments ≥ 20 nM 1a. As evident in Figure 4d, comparable results were also observed in phosphorylated PLK-1 where treatments ≥ 20 nM 1a demonstrated complete loss of PLK-1. Interestingly, treatment with ≤ 10 nM 1a resulted in an increase in PLK-1 protein (clearly evident at 2.5 nM in Figure 2.4b,c), presumably through feedback regulation. However, cells treated with ≥20 nM 1a underwent a loss in PLK-1 expression as expected from modulated splicing of its incipient PLK-1. We were able to confirm that this decreases in PLK-1 correlated with a reduction in PLK-1 protein (Figure 2.4e).

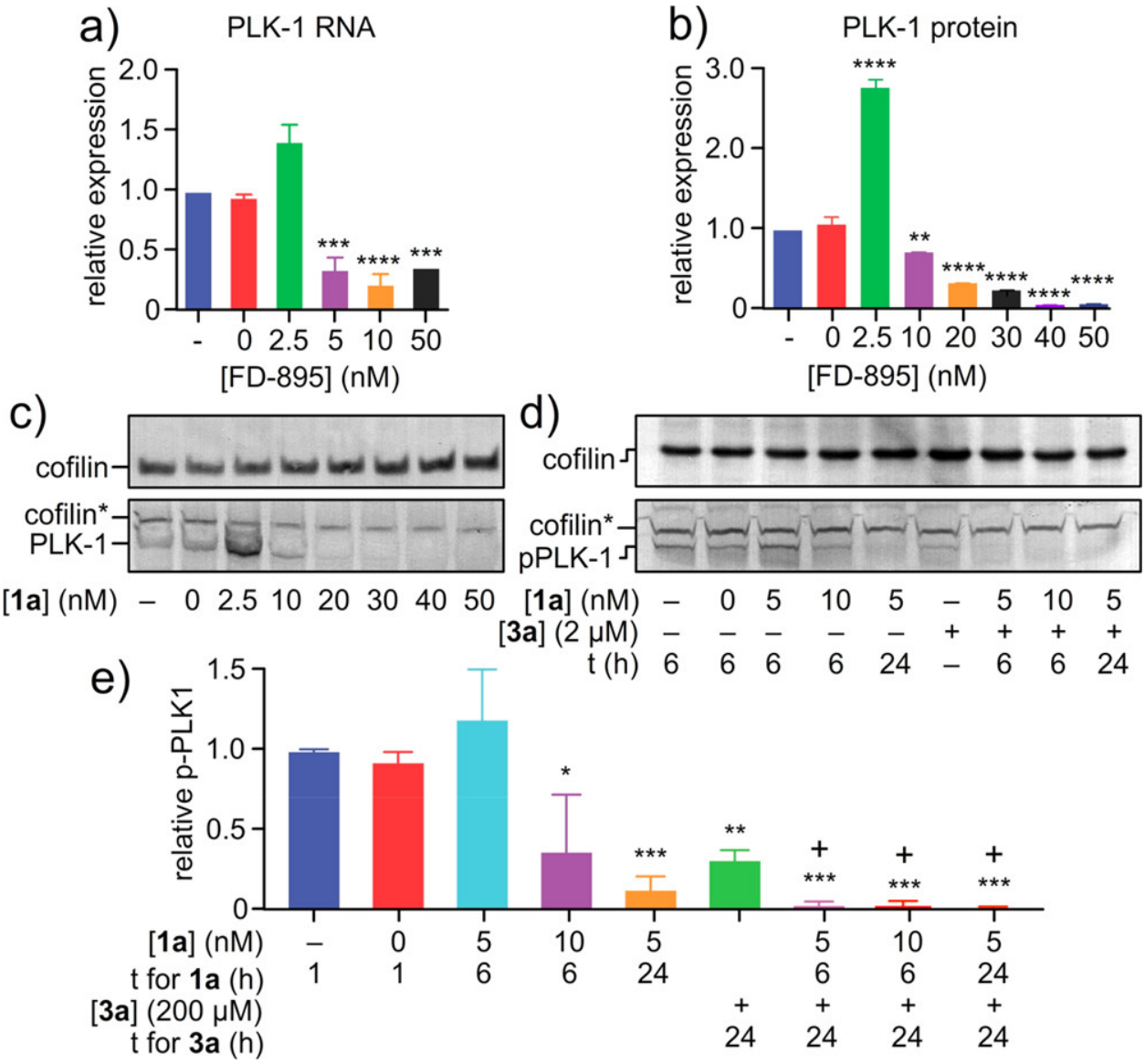

Figure 2.4 Demonstration of synergistic splice modulation of PLK-1. HCT-116 cells were treated with SPLM **1a** for 24 h and then expression of (a) *PLK-1* RNA or (b, c) PLK-1 protein was analyzed. (d, e) For combination studies, synchronized HCT-116 cells were treated with 5 nM or 10 nM **1a** for 6 or 24 h, 2 μM **3a** for 24 h, or a combination of **1a** and **3a**. Treatment efficacy was assessed by visualizing PLK-1 levels via Western blotting. The "+" sign above bars indicates synergy. Experiments were conducted in biological triplicate. Statistics were calculated using a standard one-way ANVOA; *p*-values were represented so that * signifies $p < 0.05$, ** signifies $p < 0.01$, *** signifies $p < 0.001$, and **** signifies $p < 0.0001$.

We also analyzed the effects of combination treatment on AURK protein expression. Because 2a inhibits AURK activation by blocking the kinase's ATP binding site, AURK phosphorylation levels were used to assess the efficacy of this cell cycle inhibitor. Synchronized

HCT-116 cells were treated with 1a, 2a, or a combination of 1a and 2a, and then phosphorylated AURKA (pAURKA) and phosphorylated AURKB (pAURKB) levels were examined by western blotting (Figure 2.3e-g). Although all treatments were found to reduce expression of pAURK to some extent, combination treatment most successfully decreased pAURK levels. In fact, in some treatment conditions, 1a and 2a were found to act synergistically to reduce pAURKA and pAURKB protein levels (Figure 2.3).

The effects of combination treatment were also evaluated for PLK-1 protein. Because 3a inhibits PLK-1 activation by targeting its ATP binding site, phosphorylated PLK-1 (pPLK-1) protein levels were used to measure efficacy of this inhibitor. Synchronized HCT-116 cells were treated with 1a, 3a, or a combination of 1a and 3a, followed by evaluating pPLK-1 levels by western blotting (Figure 2.3e). All treatments successfully reduced pPLK-1 expression, but combination treatment was found to be particularly effective in reducing pPLK-1. Synergy between 1a and 3a was observed for all conditions tested (Figure 2.4).

Interestingly, our studies suggest that SPLM response can be attenuated by exploring the structure activity relationships (SARs) within the SPLM. As shown in Figure S2.4, different SPLMs target AURK and PLK-1 to a different extent. These studies suggest the need to tailor the gene selectivity of splice modulation. While early evidence (Figure S2.4) suggest the potential to use medicinal chemical methods to encourage the mis-splicing of genes of therapeutic interest, the scope and potential of this interplay will require significant systems and gene-specific studies before the global regulatory network is revealed. While it is clear that SPLMs can play a role as tools to reduce the levels of a given target within a cell, and hence increase therapeutic potency, the development of methods that selectively engage splice modulation within a tumor cell would

have profound implications, suggesting a means to specifically activate and target cells with a high-degree of cell specificity.

Section 2.3 Conclusion

Nearly a decade ago, the concept of modulating the RNA levels of proteins associated with cell cycle regulatory proteins was suggested as a therapeutic option to treat diverse cancers. 31 Studies such as that led by Ashihara32 demonstrate the potential for RNA interference of PLK-1 as a therapeutic approach for non-small cell lung cancers. Here, we show how the small molecule 1a can be used in a complementary approach to modulate the levels of properly spliced cell cycle regulators AURKA, AURKB and PLK-1 across a series of cell lines. This splice-induced loss resulted in a reduction in AURKA, AURKB and PLK-1 protein, attributing to a net improvement in efficacy of AURK inhibitors 2a-2b or PLK-1 inhibitor 3a, with marked enhancements up to 90000-fold (Figure 2.2).

Overall, this study suggests the potential to engage small molecule SPLM pre-treatment as a therapeutic tool to edit the levels of therapeutically targeted proteins by mis-splicing their RNAs. Here, one can envision the use of cell-specific SPLMs such as 1a for therapeutic intervention that begins with application of a SPLM to down-regulate the expression of a chemotherapeutic target (i.e., AURKA, AURKB or PLK-1) at the RNA level, resulting in a net loss of a targeted protein, followed by treatment with a target-selective inhibitor. Comparable to RNAi and RNAsi approaches, synergistic applications of SPLMs suggests an expanded potential for the use of splice modulation as a strategy for drug enhancement. SPLM combination therapy may be particularly useful for enhancing clinical agents that suffer from off-target effects or dose-limiting toxicity and could therefore allow for previously abandoned lead molecules (therapeutics) to re-enter the clinic.

This suggestion was recently supported by studies in which FR901462, the natural product precursor to spliceostatin A (1d, Figure S2.1), synergistically-improved efficacy of the PARP1 inhibitor olaparib.20 Ongoing studies are now focused on exploring specificity of this SPLM combination therapy at a systems-wide level, with the overall goal of validating this strategy as mechanism-based approach to synergize chemotherapeutic treatment.

Section 2.4 Methods

Compounds

FD-895 (1a) and 17S-FD-895 (1g) were prepared by total synthesis.28 PF-03814735 (2a), danusertib (2b) and BI 2536 (3a) were purchased from Millipore-Sigma, Adipogen Corporation, and Selleck Chemical, respectively. All oligonucleotides were purchased by custom synthesis (Integrated DNA Technologies). Unless stated otherwise, all reagents and media were purchased from VWR or Fisher Scientific.

Cell culture

The HCT-116 cell line was cultured in McCoy's 5a (Life Technologies) supplemented with 10% fetal bovine serum (FBS), 2 mM L-glutamine, and 100 U mL−1 of penicillin and 100 μg mL−1 of streptomycin at 37 °C in an atmosphere of 5% CO2. Both the HeLa and Caov3 cell lines were maintained in DMEM (Life Technologies) supplemented with 10% FBS, 2 mM L-glutamine, and 100 U mL−1 of penicillin and 100 μg mL−1 of streptomycin at 37 °C in an atmosphere of 5% CO2.

Cellular drug treatments

Compounds were dissolved in DMSO (MilliporeSigma). Cells were treated with 1a, 2a, 2b, or 3a in media with ≥0.5% DMSO for 24–72 h.

Cell viability assays

HCT-116 cells were plated at 5 × 103 cells/well in McCoy's 5a containing 10% FBS. Cell were cultured for 24 h and then pre-treated with 1a for 24 h, then washed twice with 100 µL PBS. Next, cells were treated with cell cycle inhibitors ranging from 0–10 µM of 2a, 2b, or 3a for 72 h. Then, the cells were washed twice with 100 µL PBS, and 100 µL of media was added to each well, followed by 20 µL of CellTiter Aqueous One Solution (Promega). After 2 h at 37 °C, absorbance readings were taken at 490 nm (test wavelength) and 690 nm (reference wavelength). GI50 values were calculated in Prism (GraphPad) using ≥ 3 biological replicates.

Analysis of drug effects

CompuSyn (ComboSyn) was used to analyze cytotoxic effects of the combination of 1a with 2a, 2b, or 3a. The following equation was fitted to experimental data using nonlinear regression:

$$1 = \frac{D_a}{GI_{50a}\left(\frac{E}{100-E}\right)^{\frac{1}{ma}}} + \frac{D_b}{GI_{50b}\left(\frac{E}{100-E}\right)^{\frac{1}{mb}}} + \frac{CI \cdot D_a \cdot D_b}{GI_{50a} \cdot GI_{50b} \cdot \left(\frac{E}{100-E}\right)^{\frac{1}{2ma}} \cdot GI_{50b}\left(\frac{E}{100-E}\right)^{\frac{1}{2mb}}}$$

where D_a is the concentration of drug A, D_b in the concentration of drug B, GI_{50a} is the median effective drug concentration, E is the fraction of cells surviving, and m is the slope parameter of the individual drug's concentration-effect curve. When the combination index (CI) value > 1, antagonism is indicated, meaning that the observed efficacy is less than the expected additive effect. CI = 1 reflects additive effects, meaning the observed efficacy is within the range of expected additive effects. CI < 1 indicates synergy, meaning the observed efficacy is greater than the expected additive effects.33

Quantitative real time PCR (qPCR)

Cells were treated with 1a, 2a, 2b, or 3a in 0.5% DMSO for 24 h. Untreated cells were considered as a control. Total RNA was isolated using mirVana miRNA isolation kit (Life

Technologies). A 1 μg sample of RNA was subjected to DNAseI from a TURBO DNA free kit (Life Technologies). The cDNA was prepared by using SuperScript III reverse transcriptase kit (Life Technologies). The amount of unspliced RNA for different genes was determined using Power SYBR Green PCR master mix (Applied Biosystems) by qPCR using specific primers for each gene (Supplementary Table 1). qPCR using 2.5 μM of each primer was performed on 5 ng of the obtained cDNA. qPCR conditions were as follows: 95 °C for 10 min for one cycle, then 95 °C for 30 s, 55 °C for 60 s, 72 °C for 60 s, for 40 cycles using the MXPro. Quantification cycle (Cq) values were identified for each sample, and then RNA levels were calculated using $2^{-\Delta\Delta CT}$ method.34 GAPDH was used as a control for normalization.21 At least three biological replicates were conducted. Statistics were calculated using a standard one-way ANVOA; p-values were represented so that * signifies $p<0.0001$.

Western blot analyses

Cells were synchronized using a double thymidine block followed by treatment with 100 ng/mL nocodazole. Then cells were treated with 1a, 2a, 2b, or 3a in 0.5% DMSO for 6–24h. Untreated cells were considered as a control. Cells were washed twice with PBS, and lysed with modified RIPA buffer (Cell Signaling Technology) containing 1% of a human protease and phosphatase inhibitor cocktail (Cell Signaling Technology) at 4 °C. The protein content of the whole cell lysates was quantified using the Pierce BCA Assay (Thermo Fisher). Lysates in sample buffer comprised of 720 mM 2-mercaptoethanol, 0.001% bromophenol blue, 2% SDS, 10% glycerol, 80 mM Tris • HCl pH 6.8 were denatured at 95 °C for 5 min. Total cellular proteins (20–50 μg) were subjected to SDS PAGE using a 4–20% Criterion precast gel (Bio-Rad) followed by transfer to a 0.45 μm polyvinylidene difluoride (PVDF) membrane (Millipore). After blocking with 5% BSA for 1 h in 25 mL Tris-buffered saline with Tween 20 (TBST) comprised of 20 mM

Tris • HCl, 137 mM NaCl, 0.1% Tween-20 pH 7.6, the membrane was incubated with a primary antibody overnight at 4 °C. The primary antibodies included a rabbit anti-PLK-1 (4513, Cell Signaling Technology), rabbit antiphospho-PLK-1 (5472, Cell Signaling Technology), mouse anti-AURKA (610938, BD), rabbit anti-phospho-AURK (2914, Cell Signaling Technology), and mouse anti-cofilin (54532, Abcam). All primary antibodies were used at a 1:1000 dilution in TBST containing 5% BSA. After washing three times with 25 mL of TBST, the membranes were incubated with AP-labeled anti-rabbit (7054, Cell Signaling Technology) or AP-labeled anti-mouse (S372B, Promega) secondary antibodies with a dilution of 1:1000–7500 TBST containing 5% BSA for 60 min at rt. The membranes were washed three times with 25 mL TBST and protein-antibody complexes signals were detected using a BCIP/NBT (S3771, Promega) then stained blots were imaged on a conventional flatbed scanner (1260, Epson). Band signal was quantified using ImageStudio (LI-COR). At least three biological replicates were conducted. Statistics were calculated using a standard one-way ANVOA; p-values were represented so that * signifies $p<0.0001$.

Chapter 2, in full, is a reprint of the material as it appears: Trieger, K.A., La Clair, J.J., Burkart, M.D. "Splice Modulation Synergizes Cell Cycle Inhibition" *ACS Chem. Biol.* **2020** 15 (3), 669-674. The dissertation author is the primary co-author of this manuscript.

Section 2.5 Supplementary Information

Supplementary Information

Splice Modulation Synergizes Cell Cycle Inhibition

Kelsey A. Trieger,[†] James J. La Clair,[†] and Michael D. Burkart[†,*]

[†] Department of Chemistry and Biochemistry, University of California, San Diego, La Jolla, CA 92093-0358, United States

*Correspondence: Michael D. Burkart, Phone: 858-534-5673, e-mail: mburkart@ucsd.edu

Table of Contents

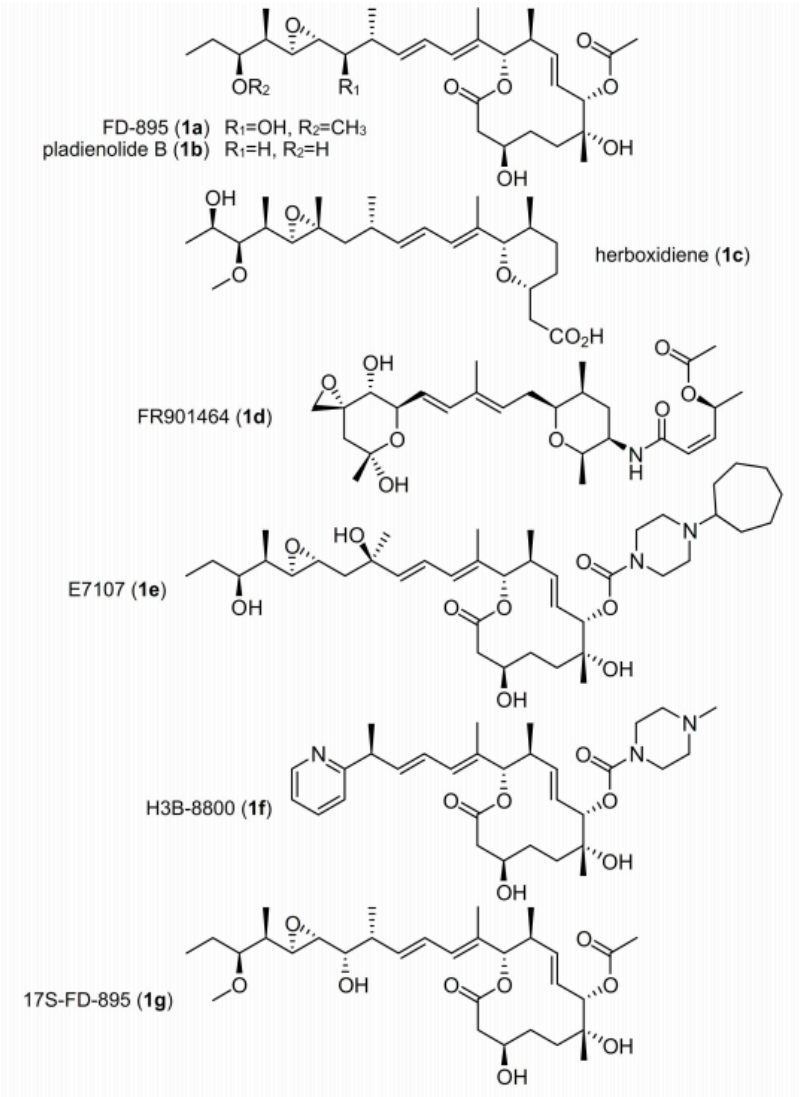

Supplementary Figure S1. Expanded set of splicing modulators including natural products FD-895 (**1a**), pladienolide B (**1b**), herboxidiene (**1c**), and FR901464 (**1d**). Structures of clinically-evaluated analogs E7107 (**1e**) and H3B-8800 (**1f**) along with clinical-candidate 17S-FD-895 (**1g**).

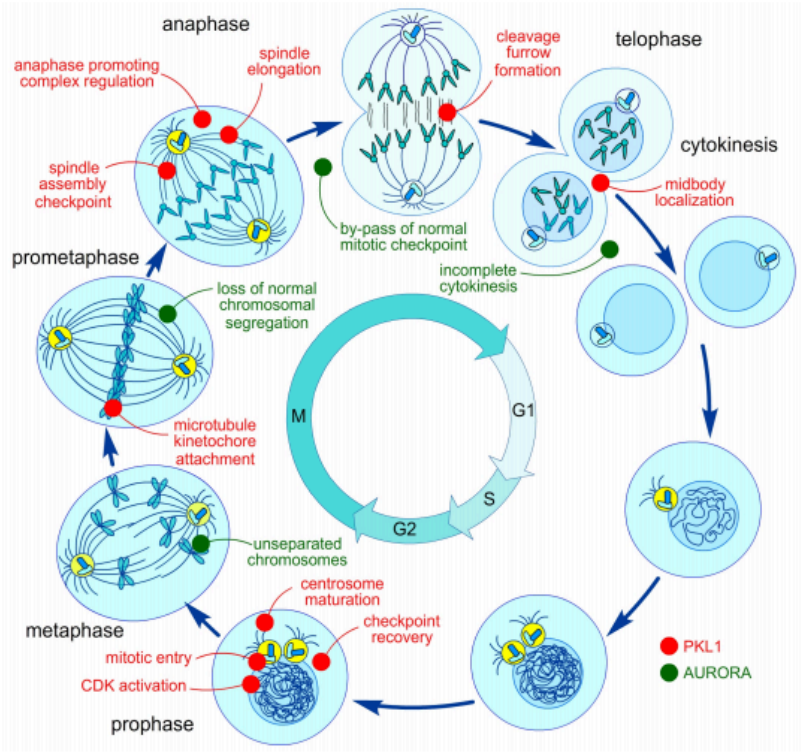

Supplementary Figure S2. Roles of polo-like kinase 1 (PLK-1) and aurora kinases (AURK) in the mitotic cycle. Both kinases play an interactive role in regulating each stage of passage through mitosis with effects arising from inhibition or reduced expression of PLK-1 (in red) and aurora kinases (in green).

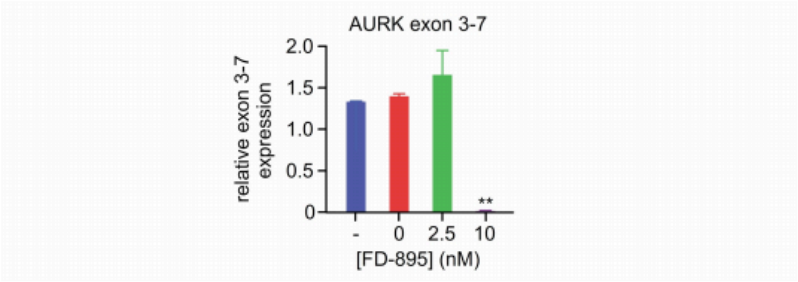

Supplementary Figure S3. AURKA gene regulation by FD-895. Increasing concentrations of FD-895 led to a decrease in the inclusion of exons 3-7 in AURKA RNA.

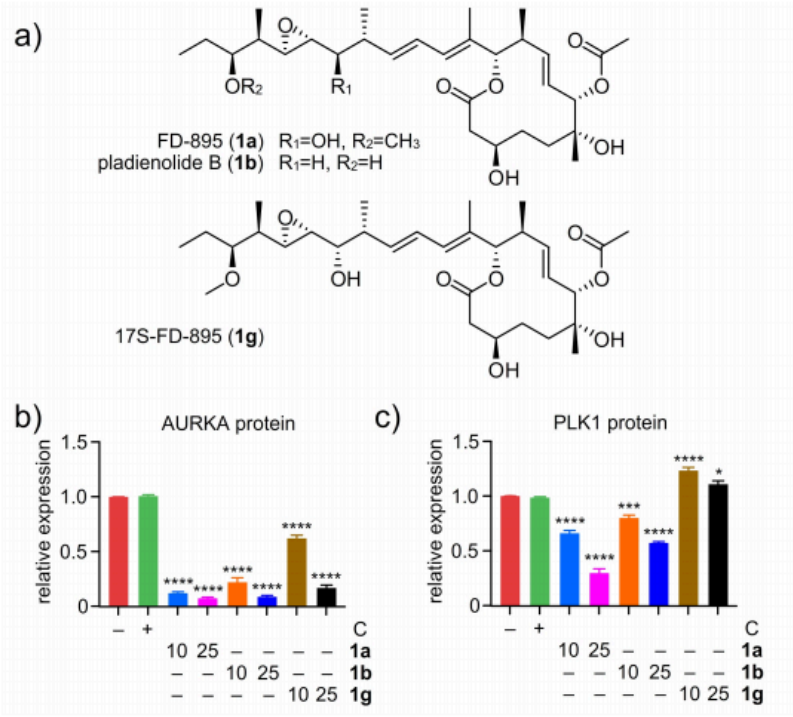

Supplementary Figure S4. Splice modulator selectivity. FD-895 (**1a**) and pladienolide B (**1b**) reduced AURKA and PLK-1 protein expression in a concentration-dependent manner. 17S-FD-895 (**1g**) reduced AURKA expression and modestly increased PLK-1 expression. Experiments were conducted in biological triplicate. Statistics were calculated using a standard one-way ANVOA; p-values were represented so that * signifies $p<0.05$, ** signifies $p<0.01$, *** signifies $p<0.001$, and **** signifies $p<0.0001$.

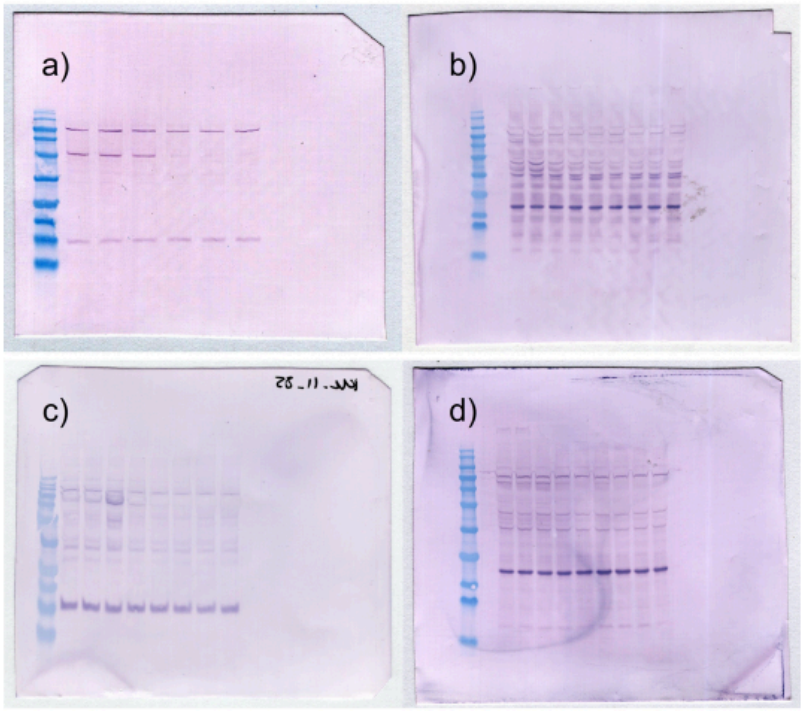

Supplementary Figure S5. Full scale scans of representative western blots used in this manuscript. **a)** Representative western blot used in Figure 3d. **b)** Representative western blot used in Figure 3e. **c)** Representative western blot used in Figure 4c. **d)** Representative western blot used in Figure 4d.

Supplementary Table 1. Sequences of the qPCR primers used in this study.

qPCR primers		
Primer	**Location**	**5' Sequence 3'**
GAPDH-FP	Exon 3	TGGTCACCAGGGCTGCTT
GAPDH-RP	Exon 4	AGCTTCCCGTTCTCAGCCTT
AURKA-FP	Intron 2	CCACCTTCGGCATCCTAAT
AURKA-RP	Intron 2	TCCAAGTGGTGCATATTCC
AURKB-FP	Intron 2	GGAGAGCTTAAAATTGCAG
AURKB-RP	Intron 2	TGCAGCTCTTCTGCAGCTC
PLK1-FP		CTCAACACGCCTCATCCTC
PLK1-RP		GTGCTCGCTCATGTAATTG
FP: forward primer; RP reverse primer		

Supplementary Table 2. Confidence intervals of GI_{50} values for cytotoxicity studies.*

Compounds	Cell Line	GI_{50} value (nM)	Standard error (nM)	Confidence interval
1a	HCT116	0.5-1.7	0.1-0.4	0.4-2.6
1a	Caov3	1.6-2.0	0.46-0.59	0.94-3.46
1a	HeLa	3.7-4.5	0.92-1.26	2.16–8.24
2a	HCT116	430.0	440.7	3453.0 - 5231.0
2a + 1 nM **1a**	HCT116	517.0	281.0	136.9 - 1886.0
2a + 5 nM **1a**	HCT116	0.05	0.05	0.01 - 0.18
2a	Caov3	5500	621	4303 - 6938
2a + 1 nM **1a**	Caov3	2800	450	1906 - 3979
2a + 5 nM **1a**	Caov3	0.08	0.06	0.01 - 0.22
2a	HeLa	10100	3371	5527 - 20150
2a + 1 nM **1a**	HeLa	4000	1084	2368 - 6667
2a + 5 nM **1a**	HeLa	0.20	0.10	0.01 - 0.42
2b	HCT116	2100	186	1737 - 2492
2b + 1 nM **1a**	HCT116	250.0	35.7	180.3 - 351.6
2b + 5 nM **1a**	HCT116	0.05	0.04	0.01 - 0.13
2b	Caov3	6000	402	5233 - 6942
2b + 1 nM **1a**	Caov3	900	230	468 - 1765
2b + 5 nM **1a**	Caov3	0.07	0.06	0.01 - 0.19
2b	HeLa	19500	4112	13180 - 31166
2b + 1 nM **1a**	HeLa	16300	4178	10281 - 28836
2b + 5 nM **1a**	HeLa	0.30	0.16	0.01 - 0.74
3a	HCT116	160.0	52.9	67. 0 - 444.6
3a + 1 nM **1a**	HCT116	0.90	0.33	0.33 - 2.28
3a + 5 nM **1a**	HCT116	0.004	0.002	0.001 - 0.008
3a	Caov3	25.9	9.6	6.2 - 79.8
3a + 1 nM **1a**	Caov3	12.8	5.4	1.7 - 48.8
3a + 5 nM **1a**	Caov3	0.20	0.05	0.07 - 0.30
3a	HeLa	13200	2662	8927 - 20456
3a + 1 nM **1a**	HeLa	10700	2369	7036 - 17217

* Data from these studies was obtained from and reported in Figure 2

Supplementary Table 3. Combination Index values for cytotoxicity studies.*

Figure	[**1a**] (nM)	[**2a**] (nM)	[**2b**] (nM)	[**2b**] (nM)	CI value
2a	1.0	1.0			2.35
	1.0	10.0			12.4
	1.0	50.0			28.4
	1.0	100.0			24.5
	1.0	500.0			12.2
	1.0	1,000.0			4.34
	1.0	5,000.0			0.190
	1.0	10,000.0			0.166
2a	5.0	1.0			0.0605
	5.0	10.0			0.0741
	5.0	50.0			0.0525
	5.0	100.0			0.0403
	5.0	500.0			0.0530
	5.0	1,000.0			0.0681
	5.0	5,000.0			0.627
	5.0	10,000.0			0.833
2b	1.0	1.0			12,700,000
	1.0	10.0			76,600,000
	1.0	50.0			404,000
	1.0	100.0			1,600
	1.0	500.0			1,790,000
	1.0	1,000.0			3,300
	1.0	5,000.0			10.7
	1.0	10,000.0			0.0962
2b	5.0	1.0			0.000218
	5.0	10.0			0.000329
	5.0	50.0			0.000348
	5.0	100.0			0.000372
	5.0	500.0			0.000567
	5.0	1,000.0			0.000810
	5.0	5,000.0			0.00275
	5.0	10,000.0			0.00519
2c	1.0	1.0			498,000,000
	1.0	10.0			30,400
	1.0	50.0			1,790,000
	1.0	100.0			1,790,000
	1.0	500.0			1,790,000
	1.0	1,000.0			76,600,000
	1.0	5,000.0			78.6
	1.0	10,000.0			0.0000407
2c	5.0	1.0			0.00811
	5.0	10.0			0.00642
	5.0	50.0			0.00642
	5.0	100.0			0.0156

	5.0	500.0			0.0157
	5.0	1,000.0			0.00234
	5.0	5,000.0			0.0000237
	5.0	10,000.0			0.0000108
2d	1.0		1.0		4,580
	1.0		10.0		6.75
	1.0		50.0		2.56
	1.0		100.0		2.30
	1.0		500.0		0.519
	1.0		1,000.0		0.268
	1.0		5,000.0		0.260
	1.0		10,000.0		0.0409
2d	5.0		1.0		0.0761
	5.0		10.0		0.0823
	5.0		50.0		0.0686
	5.0		100.0		0.0787
	5.0		500.0		0.0769
	5.0		1,000.0		0.0890
	5.0		5,000.0		0.181
	5.0		10,000.0		0.450
2e	1.0		1.0		587,000
	1.0		10.0		426,000
	1.0		50.0		154,000
	1.0		100.0		54,800
	1.0		500.0		2,090
	1.0		1,000.0		223
	1.0		5,000.0		8.74
	1.0		10,000.0		4.04
2e	5.0		1.0		0.00242
	5.0		10.0		0.01263
	5.0		50.0		0.00593
	5.0		100.0		0.00882
	5.0		500.0		0.0251
	5.0		1,000.0		0.0187
	5.0		5,000.0		0.0123
	5.0		10,000.0		0.0120
2f	1.0		1.0		307,000,000,000.
	1.0		10.0		307,000,000,000.
	1.0		50.0		307,000,000,000.
	1.0		100.0		307,000,000,000.
	1.0		500.0		1,108,000,000.
	1.0		1,000.0		307,000,000,000.
	1.0		5,000.0		1,108,000,000.
	1.0		10,000.0		8.53
2f	5.0		1.0		0.0591
	5.0		10.0		0.0344
	5.0		50.0		0.437

	5.0		100.0		0.135
	5.0		500.0		0.0156
	5.0		1,000.0		0.0156
	5.0		5,000.0		0.000324
	5.0		10,000.0		0.0000536
2g	1.0			1.0	4.03
	1.0			10.0	1.57
	1.0			50.0	1.49
	1.0			100.0	1.66
	1.0			500.0	0.807
	1.0			1,000.0	0.501
	1.0			5,000.0	0.00378
	1.0			10,000.0	0.000414
2g	5.0			1.0	0.0254
	5.0			10.0	0.00704
	5.0			50.0	0.00415
	5.0			100.0	0.00712
	5.0			500.0	0.0185
	5.0			1,000.0	0.00472
	5.0			5,000.0	0.0170
	5.0			10,000.0	0.0000336
2h	1.0			1.0	35,700,000
	1.0			10.0	240,000,000
	1.0			50.0	922,000
	1.0			100.0	4,470,000
	1.0			500.0	2,610
	1.0			1,000.0	4,330
	1.0			5,000.0	10.4
	1.0			10,000.0	0.0938
2h	5.0			1.0	0.000188
	5.0			10.0	0.000412
	5.0			50.0	0.000309
	5.0			100.0	0.000295
	5.0			500.0	0.000447
	5.0			1,000.0	0.000879
	5.0			5,000.0	0.00385
	5.0			10,000.0	0.00455
2i	1.0			1.0	307,000,000,000
	1.0			10.0	6,140,000
	1.0			50.0	76,600,000
	1.0			100.0	76,600,000
	1.0			500.0	1,790,000
	1.0			1,000.0	307,000,000,000
	1.0			5,000.0	144,000
	1.0			10,000.0	1.59
2i	5.0			1.0	0.0156
	5.0			10.0	0.0234

	5.0			50.0	0.135
	5.0			100.0	0.0496
	5.0			500.0	0.00811
	5.0			1,000.0	0.00811
	5.0			5,000.0	0.000142
	5.0			10,000.0	0.0000167

*Data from these studies was obtained from and reported in Figure 2

Section 2.6 References

(1) Sveen, A., Kilpinen, S., Ruusulehto, A., Lothe, R. A., and Skotheim, R. I. (2016) Aberrant RNA splicing in cancerexpression changes and driver mutations of splicing factor genes. Oncogene 35, 2413−2427.

(2) Seki-Asano, M., Okazaki, T., Yamagishi, M., Sakai, N., Takayama, Y., Hanada, K., Morimoro, S., Takatsuki, A., and Mizoue, K. (1994) Isolation and characterization of a new 12-membered macrolide FD895. J. Antibiot. 47, 1395−1401.

(3) Sakai, T., Sameshima, T., Matsufuji, M., Kawamura, N., Dobashi, K., and Mizui, Y. (2004) Pladienolides, new substances from culture of Streptomyces platensis Mer-11107. I. Taxonomy, fermentation, isolation and screening. J. Antibiot. 57, 173.

(4) Miller-Wideman, M., Makkar, N., Tran, M., Isaac, B., Biest, N., and Stonard, R. (1992) Herboxidiene, a new herbicidal substance from StreptomycesChromofuscus A7847. Taxonomy, fermentation isolation, physico-chemical and biological properties. J. Antibiot. 45, 914−921.

(5) Nakajima, H., Hori, Y., Terano, H., Okuhara, M., Manda, T., Matsumoto, S., and Shimomura, K. (1996) New antitumor substances, FR901463, FR901464 and FR901465. II. Activities against experimental tumors in mice and mechanism of action. J. Antibiot. 49, 1204−1211.

(6) Leon, B., Kashyap, M. K., Chan, W. C., Krug, K. A., Castro, J. E., La Clair, J. J., and Burkart, M. D. (2017) A challenging pie to splice: Drugging the spliceosome. Angew. Chem., Int. Ed. 56, 12052−12063.

(7) Pham, D., and Koide, K. (2016) Discoveries, target identifications, and biological applications of natural products that inhibit Splicing Factor 3B subunit 1. Nat. Prod. Rep. 33, 637−647.

(8) Kaida, D., Motoyoshi, H., Tashiro, E., Nojima, T., Hagiwara, M., Ishigami, K., Watanabe, H., Kitahara, T., Yoshida, T., Nakajima, H., Tani, T., Horinouchi, S., and Yoshida, M. (2007) Spliceostatin A targets SF3b and inhibits both splicing and nuclear retention of preMRNA. Nat. Chem. Biol. 3, 576−583.

(9) Kotake, Y., Sagane, K., Owa, T., Mimori-Kiyosue, Y., Shimizu, H., Uesugi, M., Ishihama, Y., Iwata, M., and Mizui, Y. (2007) Splicing factor SF3b as a target of the antitumor natural product pladienolide. Nat. Chem. Biol. 3, 570−575.

(10) Hasegawa, M., Miura, T., Kuzuya, K., Inoue, A., Won Ki, S., Horinouchi, S., Yoshida, T., Kunoh, T., Koseki, K., Mino, K., Sasaki, R., Yoshida, M., and Mizukami, T. (2011) Identification of SAP155 as the target of GEX1A (Herboxidiene), an antitumor natural product. ACS Chem. Biol. 6, 229−233.

(11) Martínez-Montiel, N., Rosas-Murrieta, N. H., MartínezMontiel, M., Gaspariano-Cholula, M. P., and Martínez-Contreras, R. D. (2016) Microbial and natural metabolites that inhibit splicing: A powerful alternative for cancer treatment. BioMed Res. Int. 2016, 3681094.

(12) Gao, Y., Vogt, A., Forsyth, C. J., and Koide, K. (2013) Comparison of splicing factor 3b inhibitors in human cells. ChemBioChem 14, 49−52.

(13) Lee, S. C., and Abdel-Wahab, O. (2016) Therapeutic targeting of splicing incancer. Nat. Med. 22, 976−986.

(14) Salton, M., and Misteli, T. (2016) Small molecule modulators of pre-mRNA splicing in cancer therapy. Trends Mol. Med. 22, 28−37.

(15) Seiler, M., Yoshimi, A., Darman, R., Chan, B., Keaney, G., Thomas, M., Agrawal, A. A., Caleb, B., Csibi, A., Sean, E., Fekkes, P., Karr, C., Klimek, V., Lai, G., Lee, L., Kumar, P., Lee, S. C., Liu, X., Mackenzie, C., Meeske, C., Mizui, Y., Padron, E., Park, E., Pazolli, E., Peng, S., Prajapati, S., Taylor, J., Teng, T., Wang, J., Warmuth, M., Yao, H., Yu, L., Zhu, P., Abdel-Wahab, O., Smith, P. G., and Buonamici, S. (2018) H3B-8800, an orally available small-molecule splicing modulator, induces lethality in spliceosome-mutant cancers. Nat. Med. 24, 497−504.

(16) Hong, D. S., Kurzrock, R., Naing, A., Wheler, J. J., Falchook, G. S., Schiffman, J. S., Faulkner, N., Pilat, M. J., O'Brien, J., and LoRusso, P. (2014) A phase I, open-label, single-arm, dose-escalation study of E7107, a precursor messenger ribonucleic Acid (pre-MRNA) splicesomeinhibitor administered intravenously on days 1 and 8 every 21 days to patients with solid tumors. Invest. New Drugs 32, 436−444.

(17) Cretu, C., Agrawal, A. A., Cook, A., Will, C. L., Fekkes, P., Smith, P. G., Lührmann, R., Larsen, N., Buonamici, S., and Pena, V. (2018) Structural basis of splicing modulation by antitumor macrolide compounds. Mol. Cell 70, 265−273.

(18) Finci, L. I., Zhang, X., Huang, X., Zhou, Q., Tsai, J., Teng, T., Agrawal, A., Chan, B., Irwin, S., Karr, C., Cook, A., Zhu, P., Reynolds, D., Smith, P. G., Fekkes, P., Buonamici, S., and Larsen, N. A. (2018) The cryo-EM structure of the SF3b spliceosome complex bound to a splicing modulator reveals a pre-mRNA substrate competitive mechanism of action. Genes Dev. 32, 309−320.

(19) Salton, M., Kasprzak, W. K., Voss, T., Shapiro, B. A., Poulikakos, P. I., and Misteli, T. (2015) Inhibition of vemurafenibresistant melanoma by interference with pre-mRNA splicing. Nat. Commun. 6, 7103.

(20) Yamano, T., Kubo, S., Yano, A., Kominato, T., Tanaka, S., Ikeda, M., and Tomita, N. (2019) Splicing modulator FR901464 is a potential agent for colorectal cancer in combination therapy. Oncotarget. 10, 352−367.

(21) Teng, T., Tsai, J. H., Puyang, X., Seiler, M., Peng, S., Prajapati, S., Aird, D., Buonamici, S., Caleb, B., Chan, B., Corson, L., Feala, J., Fekkes, P., Gerard, B., Karr, C., Korpal, M., Liu, X., T. Lowe, J., Mizui, Y., Palacino, J., Park, E., Smith, P. G., Subramanian, V., Wu, Z. J., Zou, J., Yu, L., Chicas, A., Warmuth, M., Larsen, N., and Zhu, P. (2017) Splicing modulators act at the branch point adenosine binding pocket defined by the PHF5A-SF3b complex. Nat. Commun. 8, 1552.

(22) Kumar, D., Kashyap, M. K., La Clair, J. J., Villa, R., Spaanderman, I., Chien, S., Rassenti, L. Z., Kipps, T. J., Burkart, M. D., and Castro, J. E. (2016) Selectivity in small molecule splicing modulation. ACS Chem. Biol. 11, 2716−2723.

(23) Vanzyl, E. J., Rick, K. R. C., Blackmore, A. B., MacFarlane, E. M., and McKay, B. C. (2018) Flow cytometric analysis identifies changes in S and M phases as novel cell cycle alterations induced by the splicing inhibitor isoginkgetin. PLoS One 13, No. e0191178.

(24) Kashyap, M. K., Kumar, D., Villa, R., La Clair, J. J., Benner, C., Sasik, R., Jones, H., Ghia, E. M., Rassenti, L. Z., Kipps, T. J., Burkart, M. D., and Castro, J. E. (2015) Targeting the spliceosome in Chronic Lymphocytic Leukemia with the macrolides FD-895 and pladienolideB. Haematologica 100, 945−954.

(25) Salaun, P., Rannou, Y., and Claude, P. (2008) Cdk1, Plks, Auroras, and Neks: The mitotic bodyguards. Adv. Exp. Med. Biol. 617, 41−56.

(26) Carnero, A. (2002) Targeting the cell cycle for cancer therapy. Br. J. Cancer 87, 129.

(27) Meulenbeld, H. J., Mathijssen, R. H., Verweij, J., de Wit, R., and de Jonge, M. J. (2012) Danusertib, an aurora kinase inhibitor. Expert Opin. Invest. Drugs 21, 383−393.

(28) Schöffski, P., Jones, S. F., Dumez, H., Infante, J. R., Van Mieghem, E., Fowst, C., Gerletti, P., Xu, H., Jakubczak, J. L., English, P. A., Pierce, K. J., and Burris, H. A. (2011) Phase I, open-label, multicentre, dose-escalation, pharmacokinetic and pharmacodynamic trial of the oral aurora kinase inhibitor PF-03814735 in advanced solid tumours. Eur. J. Cancer 47, 2256−2264.

(29) Villa, R., Mandel, A. L., Jones, B. D., La Clair, J. J. La, and Burkart, M. D. (2012) Structure of FD-895 revealed through total synthesis. Org. Lett. 14, 5396−5399.

(30) Hofheinz, R.-D., Al-Batran, S.-E., Hochhaus, A., Jager, E.,¨ Reichardt, V. L., Fritsch, H., Trommeshauser, D., and Munzert, G. (2010) An open-label, phase I study of the Polo-like Kinase-1 inhibitor, BI 2536, in patients with advanced solid tumors. Clin. Cancer Res. 16, 4666−4674.

(31) Ashihara, E., Kawata, E., and Maekawa, T. (2010) Future prospect of RNA interference for cancer therapies. Curr. Drug Targets 11, 345−360.

(32) Kawata, E., Ashihara, E., and Maekawa, T. (2011) RNA interference against polo-like kinase-1 in advanced non-small cell lung cancers. J. Clin. Bioinf. 1, 6.

(33) Foucquier, J., and Guedj, M. (2015) Analysis of drug combinations: current methodological landscape. Pharmacol. Res. Perspect. 3, No. e00149.

(34) Arocho, A., Chen, B., Ladanyi, M., and Pan, Q. (2006) Validation of the 2-DeltaDeltaCt calculation as an alternate method of data analysis for quantitative PCR of BCR-ABL P210 transcripts. Diagn. Mol. Pathol. 15, 56−61.

Chapter 3. Stereochemical Attenuation of Splice Modulation

Section 3.1 Introduction

RNA splicing plays a central role in cell regulation, development, and disease progression, but the complexity of this macromolecular assembly process has left RNA splicing underexplored in cancer. In recent years, it has become clear that alternative RNA splicing becomes mis-regulated in and plays a role in the progression of a wide range of cancers [1,2]. However, this therapeutic vulnerability has not been well explored due to a lack of RNA-targeting methods and little information on the splicing changes that take place during cancer progression. Understanding the relationship between splicing and cancer progression will allow for expansion of our therapeutic arsenal in tackling cancer.

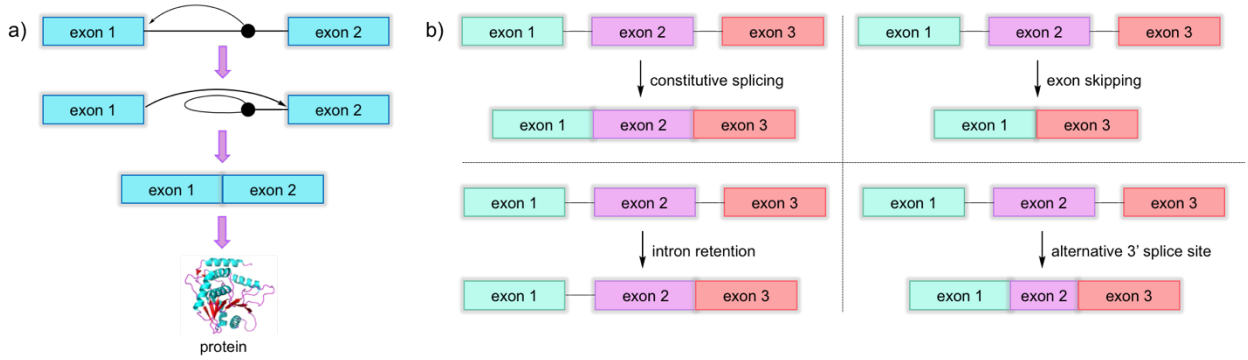

Figure 3.1 *RNA splicing.* **(A)** The splicing reaction begins when the branch point adenine (black circle) reacts with the 5' splice site (ss). The 5' ss then reacts with the 3' ss, ligating the exon ends together. **(B)** Exons can be constitutively spliced, where all exons are present in every mRNA product, or alternatively spliced, where exon and intron inclusion in the mRNA product can vary based on the directives of various splicing factors.

Splicing serves to remove noncoding sequences (introns) from precursor messenger RNA (pre-mRNA), and ligate coding sequences (exons), forming mRNA that can then be translated into protein (Figure 3.1) [3]. This reaction is carried out by a macromolecular machine called the spliceosome, a ribonucleoprotein (RNP) complex containing five small nuclear RNAs (snRNA) and over 200 associated proteins. The splicing reaction begins when the branch point adenine

(BPA) within an intron attacks the 5' splice site, forming the intron lariat. This process is highly regulated; the spliceosome prevents premature reaction of the BPA by shielding it until ready for catalysis, at which point the spliceosome arranges the secondary structure of the pre-mRNA intron in such a way that the BPA is positioned near the 5' splice site. Specifically, two spliceosomal proteins, splicing factor 3b 1 (SF3B1) and PHD finger protein 5a (PHF5A), are responsible for binding and positioning the BPA for the start of the splicing reaction. After the pre-mRNA is successfully spliced, the resulting intron lariat is discarded, and the spliceosome disassembles.

Because aberrant splicing has been identified as a major contributor to cancer progression and metastasis, drugs that regulate RNA splicing could serve as powerful therapeutics for cancer. Splice modulators (SPLMs) are a class of chemotherapeutics that regulate aberrant splicing profiles in tumors, thereby inducing tumor cell apoptosis [4]. These drugs affect splicing by binding to the spliceosomal pocket formed by proteins SF3B1 and PHF5A in the same spot that typically binds the BPA of the pre-mRNA (Figure 3.2). SPLM occupation of this binding pocket interrupts normal interactions between the pre-mRNA and the spliceosome, thereby preventing initiation of splicing, or inducing usage of an alternative BPA within the intron [5]. In this way, SPLM treatment alters splicing of thousands of different genes involved in splicing, metabolism, the cell cycle, and more. Overall, SPLMs interfere with the overused splicing machinery that cancer cells become dependent upon for expansion, thereby limiting the tumor's ability to produce proteins necessary for growth and survival.

Though splice modulators share some unifying structural features, such as a long side chain and 6- or 12-membered ring, this class of compounds is quite structurally diverse. Structural

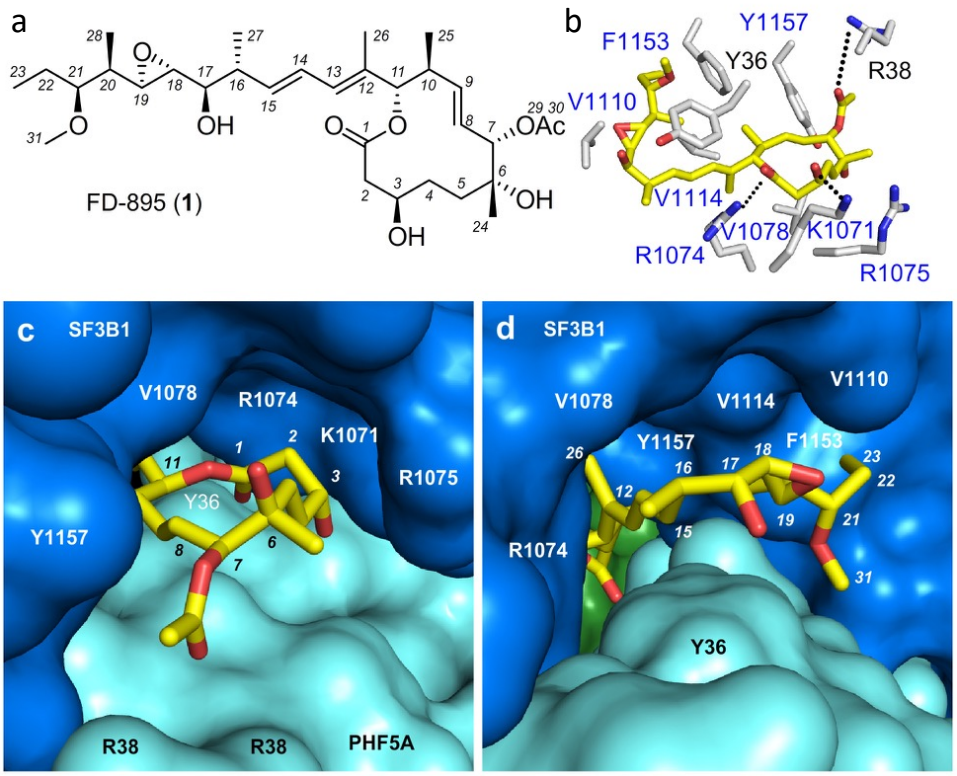

Figure 3.2 Binding of FD-895 to the SF3B1•PHF5A pocket. a) Structure of FD-895 (**1**) bound to the human core SF3B complex including: b) a depiction of the key amino acid residues within the binding pocket and surface rendering of the pocket illustrating the regions occupied by the c) core and d) side chain. Protein components are given by SF3B1 (dark blue) and PHF5A (light blue).

differences from one SPLM to another lead to significant changes in splicing activity based on SPLM orientation within the spliceosome binding pocket (Figure 3.2). Therefore, although most SPLMs affect the splicing of the same category of genes, each SPLM affects the splicing of individual genes to a different extent. In 2004, the Burkart laboratory began synthesizing splice modulators and structural analogs in order to investigate the structure-activity relationship of these compounds [6,7]. Through these efforts, we have been able to obtain splice modulators with optimized features. For example, the synthetic splice modulator 17S-FD-895 shows enhanced stability compared to its parent natural products [8]. Having found that changing the structural features of splice modulators could favorably alter drug properties, we became interested in further exploring the structure-activity relationships (SARs) of FD-895.

In this series of studies, we explored the relationship between structural features of the splice modulator FD-895 and RNA splicing selectivity. To this end, we synthesized a panel of splice-modulating analogs of the natural product FD-895. We then used these analogs to explore the role of drug structure in potency, gene selectivity, and splicing activity.

Section 3.2 Results and Discussion

Using synthetic methods recently developed at gram scales,12 we began by adapting routes to prepare analogs of FD-895 (**1**) with inversion of the stereochemistry at 10 of the 11 stereocenters (C3, C7, C10, C11, C16, C17, C18, C19, C20 and C21). Our approach developed through the Stille coupling of macrolide core (C1-C11) and side chain (from C12-C28) components. Isomers with inversion at C3, C7, C10 or C11 were prepared by synthesis of the corresponding isomeric macrolide core and coupling it to a desired side chain in a final step. Side chain analogs at C16, C17, C18, C19, C20, and C21 were prepared in an analogous manner. Further information on synthetic routes, procedures, and compound validation are provided in the supplementary information.

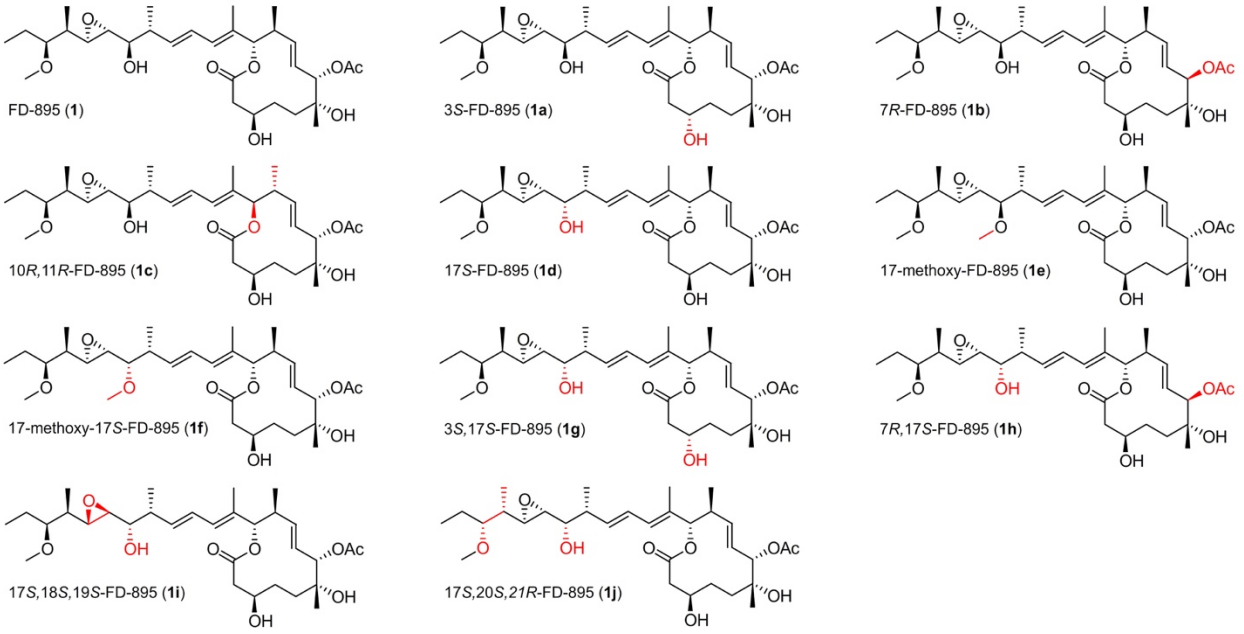

Figure 3.3 Structures of SPLM analogs. A panel of FD-895 analogs including stereochemical and functional modifications within the core at C3, C7, C10 and C11 and side chain at C17, C18, C19, C20, C21. Red indicates the position of modification.

In order to evaluate the impact of the FD-895 analogs on inhibiting tumor cell growth, we treated HCT116 colorectal carcinoma cells with analogs **1a-1j** for 72 hours and then measured tumor cell viability using the MTS assay (Table 1). The natural product FD-895 **1** was found to have GI_{50} value = 1.7 nM. Comparatively, the analogs were equally or less active than **1**, but all were found to retain some tumor-inhibiting activity (GI_{50} value $\leq$ 1 μM) except for analog **1c**.

The range in potencies of the analogs allowed us to classify the importance of structural and stereochemical features in FD-895. Modifications to the macrolide core decreased tumor-inhibiting activity. Epimerization of the C3 or C7 centers (analogs **1a,b**) led to near hundredfold reductions in activity, and epimerization of the C10,11 center (**1c**) led to a complete loss in activity, indicating that the spatial arrangement of the macrolide core in the spliceosomal binding pocket affects drug activity. The one exception to this rule was analog **1a**, representing epimerization of the C3 center for the 17S-FD-895 analog, which showed no reduction in activity. Modifications along the side chain had more variable effects on activity. For instance, epimerization of C17 (**1d**)

or the installment of a methoxy group at C17 (**1e**) did not change drug activity. However, epimerization of the epoxide at C18,19 (**1i**) or co-epimerization of the C20,21 centers (**1j**) led to decreases in activity by 260- and 150- fold, respectively. Overall, this data implies that spatial arrangement of SPLMs in the spliceosomal binding pocket directs drug activity.

Table 3.1 GI_{50} values for analogs **1-1j**. HCT116 were treated with analogs **1-1j** ranging from 0.1-5000 nM for 72 hours, then cell viability was measured using the MTS assay. Full cell viability graph included in Figure S3.1, and confidence intervals provided in Table S3.1.

Analog	**GI_{50} value (nM)**
FD-895 (**1**)	1.72
C3 FD-895 (**1a**)	2.21
C7 FD-895 (**1b**)	431.8
C10,11 FD-895 (**1c**)	36553
17S-FD-895 (**1d**)	2.06
17-methoxy FD-895 (**1e**)	2.21
17-methoxy 17S-FD-895 (**1f**)	37.65
C3 17S-FD-895 (**1g**)	131.2
C7 17S-FD-895 (**1h**)	806.2
C18,19 17S-FD-895 (**1i**)	445.5
C20,21 17S-FD-895 (**1j**)	262.2

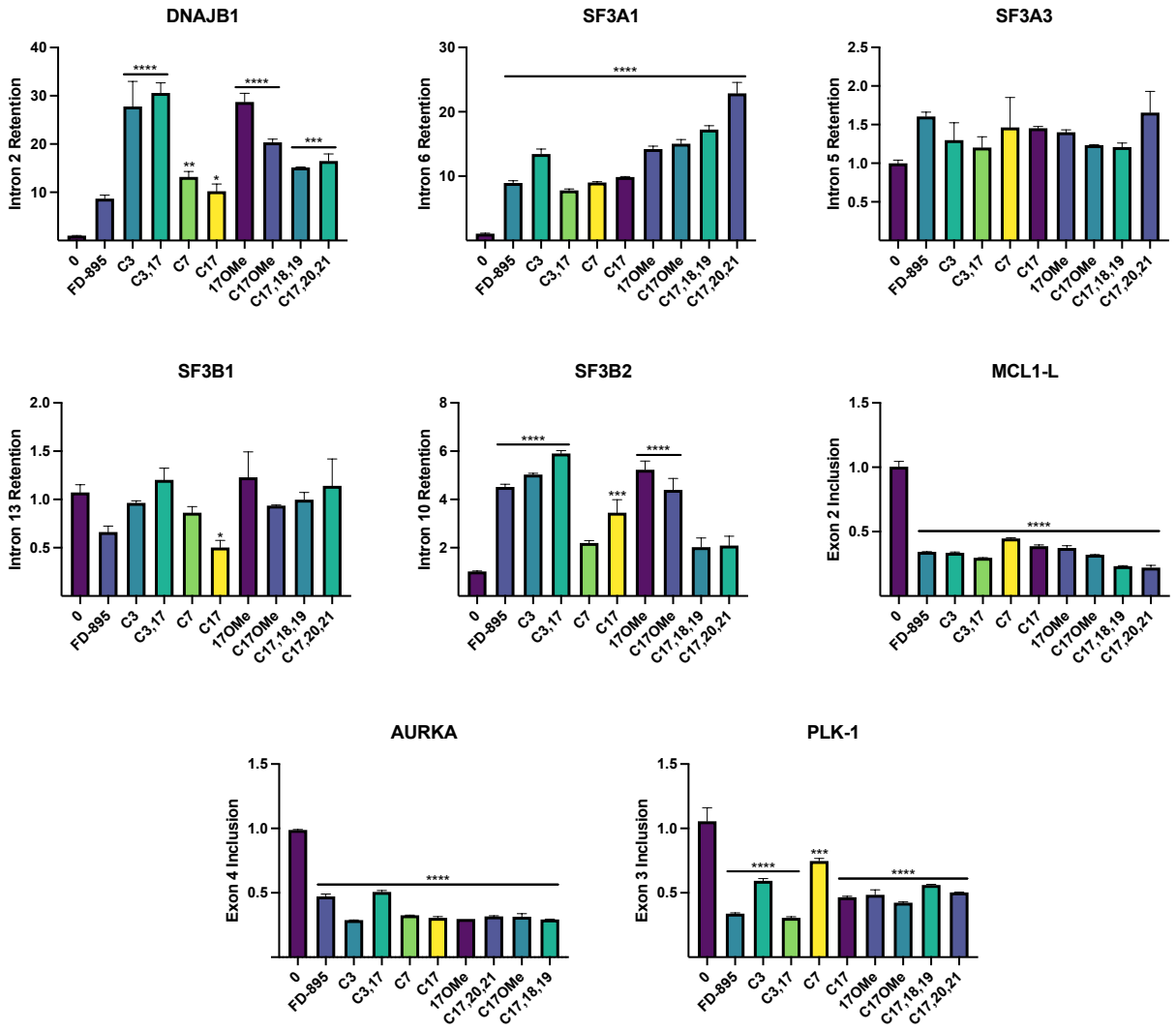

Figure 3.4 Structure-splicing profiles for RNA splice modulators after four-hour treatment. HCT116 tumor cells were treated with analogs **1, 1, 1a, 1b, 1d-g, 1i, and 1j** at 20 times the GI_{50} value for each analog (listed in table 1) for four hours and then cellular RNA was isolated and purified for qPCR. Primers were designed to evaluate intron retention or exon skipping, direct responses to splice modulator treatment. Genes evaluated included those involved in splicing regulation (SF3A1, SF3A3, SF3B1, SF3B2), apoptosis (MCL-1L), protein folding (DNAJB1), and cell cycle regulation (AURKA, PLK-1) relative to the unspliced control GAPDH.

To probe the structure-splicing relationship of the FD-895 analogs, we next evaluated the impact of treatment on tumor splicing *in situ.* For these studies, we used only the analogs that were considered active (GI_{50} value ≤ 500 nM). Here, we treated HCT116 tumor cells with analogs **1, 1a, 1b, 1d-g, 1i, and 1j** at 20 times the GI_{50} value for each analog, allowing us to normalize each analog relative to each other and thereby evaluate changes in gene response due to splicing

selectivity rather than compounding effects due to differences in potency. We treated cells for four hours so that we could evaluate early changes in splicing activity, and then cellular RNA was isolated and purified for qPCR (Figures 3.4 and 3.5). None of the concentrations tested led to significant changes in cell viability over the four-hour time window, ensuring that changes in gene expression were not due to cell death (Figure S3.7). For these studies, we evaluated the expression of genes involved in splicing regulation (SF3A1, SF3A3, SF3B1, SF3B2), apoptosis (MCL-1_L), protein folding (DNAJB1), and cell cycle regulation (AURKA, PLK-1) relative to the unspliced control GAPDH. Primers were designed to evaluate intron retention or exon skipping, direct responses to splice modulator treatment. The master splicing regulator alternative splicing factor (SF2) was also evaluated, with the primers for this gene designed to evaluate overall gene expression, which changes in response to splice modulator treatment.

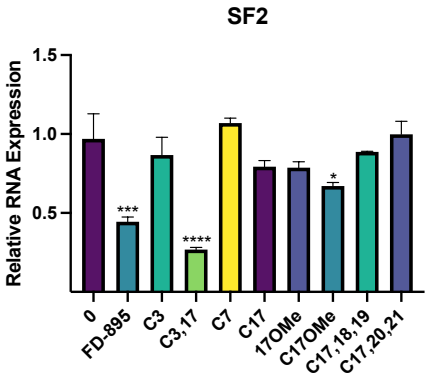

Figure 3.5 Structure-activity profiles for RNA splice modulators after four-hour treatments. HCT116 tumor cells were treated with analogs **1, 1, 1a, 1b, 1d-g, 1i, and 1j** at 20 times the GI_{50} value for each analog (listed in table 1) for four hours and then cellular RNA was isolated and purified for qPCR. Primers were designed to evaluate gene expression, which changes in response splice modulator treatment for the alternative splicing regulator (SF2) relative to the unspliced control GAPDH.

We found that splicing activity typically corresponded to drug activity for the analogs; however, each analog also displayed a unique splicing signature. For instance, in looking at the gene DNAJB1, we found that the natural product FD-895 (**1**) was not able to significantly induce intron 2 retention for this gene, but all other analogs tested were able to induce intron 2 retention

in DNAJB1. Interestingly, both C3 analogs **1a** and **1g** induced intron 2 retention to similar extent, despite analog **1g** being over 50 times less potent than analog **1a**. It was also notable that relatively inactive analogs like **1b** and **1i**, with GI_{50} values of 431.8 and 445.5 nM respectively, were able to induce intron 2 retention to a greater extent than **1** in DNAJB1.

Another unique finding from these studies was that all analogs tested were able to alter the expression of splicing factor expression, as seen with the intron 6 retention in SF3A1 induced by SPLM treatment. This indicates that these analogs affect splicing *in situ* by two different mechanisms: directly, by interfering with spliceosomal interactions with pre-mRNA, and indirectly, by altering the ratio of proteins involved in spliceosome formation. It was also found that all analogs tested were able to reduce the expression of oncogenes MCL-1_L, AURKA, and PLK-1 by inducing exon skipping for these genes.

A handful of analogs were also selected to evaluate the late-phase effects of splice modulator treatment on tumor splicing *in situ*. For these studies, HCT116 tumor cells were treated with analogs **1-1j** at 500 nM for 24 hours and then cellular RNA was isolated and purified for qPCR (Figures 3.6 and 3.7). Additional studies were conducted with HCT116 tumor cells treated with analogs **1-1j** at 100 or 250 nM for 24 hours to evaluate splicing effects at a range of drug concentrations (Figures S3.2, S3.3, S3.4, and S3.5). None of the concentrations tested led to significant changes in cell viability over the 24-hour time window, ensuring that changes in gene expression were not due to cell death (Figure S3.6). The majority of primers were designed to evaluate intron retention or exon skipping, direct responses to splice modulator treatment. Genes evaluated included those involved in splicing regulation (SF3A1, SF3A3, SF3B1, SF3B2), apoptosis (MCL-1_L), and protein folding (DNAJB1), relative to the unspliced control GAPDH. A handful of primers were also designed to evaluate overall gene expression, which changes in

response to splice modulator treatment, for genes involved in the cell cycle (AURKA, PLK-1) as well as splicing regulation (SF2).

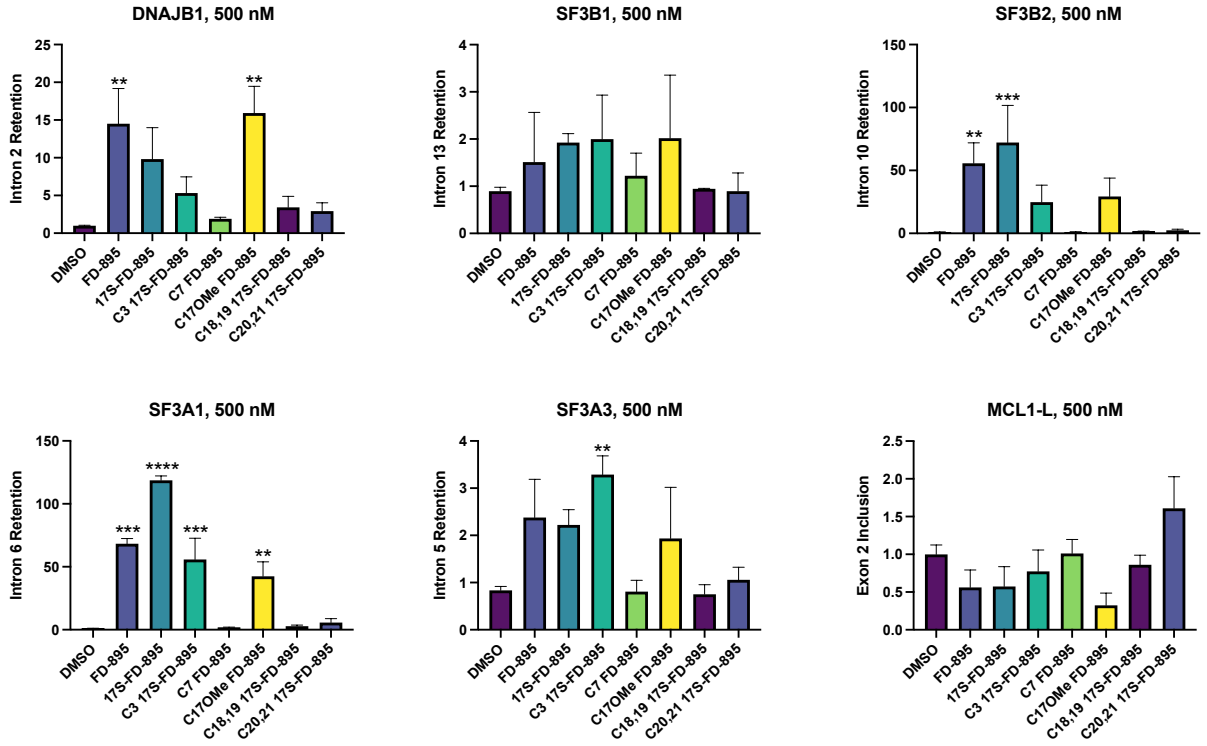

Figure 3.6 Structure-splicing profiles for RNA splice modulators after 24-hour treatment. HCT116 tumor cells were treated with analogs **1, 1b, 1d, 1e, 1g, 1h,** and **1j** at 500 nM for 24 hours and then cellular RNA was isolated and purified for qPCR. Primers were designed to evaluate intron retention or exon skipping, direct responses to splice modulator treatment. Genes evaluated included those involved in splicing regulation (SF3A1, SF3A3, SF3B1, SF3B2), apoptosis (MCL-1L), and protein folding (DNAJB1), relative to the unspliced control GAPDH.

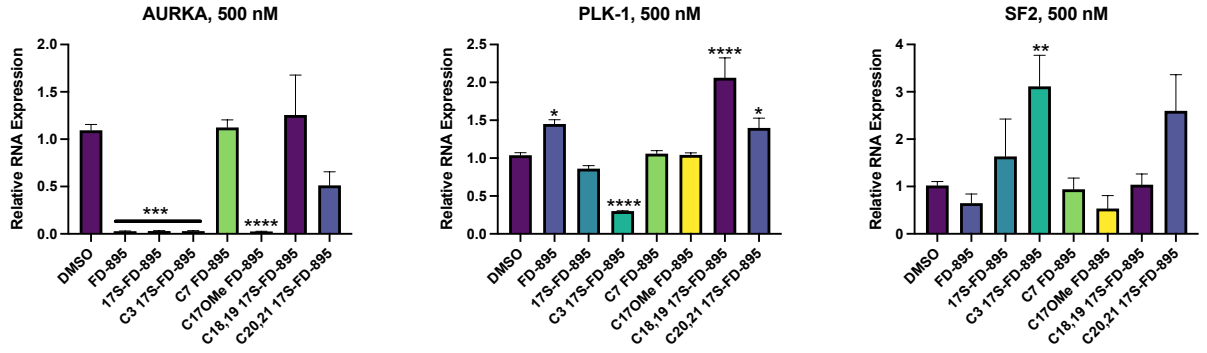

Figure 3.7 Structure-activity profiles for RNA splice modulators. HCT116 tumor cells were treated with analogs **1, 1b, 1d, 1e, 1g, 1h,** and **1j** at 500 nM for 24 hours and then cellular RNA was isolated and purified for qPCR. Primers were designed to evaluate gene expression, which changes in response splice modulator treatment. Genes evaluated included those involved in splicing regulation (SF2) as well as the cell cycle (AURKA, PLK-1), relative to the unspliced control GAPDH.

We found that splicing activity typically corresponded to drug activity for the analogs; however, each analog also displayed a unique splicing signature. The natural product FD-895 (**1**), a strong splicing modulator, altered the splicing of many of the genes tested, including DNAJB1, SF3A1, SF3B2, PLK-1, and AURKA. Epimerization of the C17 center (analog **1d**) led to a modest switch in splicing activity; **1d** reduced AURKA to a similar extent as **1**, but increased intron retention of SF3A1 and SF3B2 to a greater extent than **1**. Epimerization of C3 (analog **1g**), which displayed weaker drug activity, was found to be a surprisingly potent splicing modulator; **1g** was the only analog that increased intron retention of SF3A3 or altered the expression of SF2, and most potently reduced PLK-1 RNA expression. In addition, **1g** induced intron retention of SF3A1 and altered the expression of AURKA. **1g** was one of the few analogs that showed greater splicing activity for particular genes despite its reduction in drug activity, indicating that the C3 position is important for splicing selectivity not necessarily drug overall drug activity. Analog **1b** displayed a complete loss of splicing activity, indicating that proper arrangement of the C7 substituent in the SF3B1•PHF5A pocket is crucial for splicing activity. Methylated analog **1e**, which had comparable potency to FD-895, was found to be a slightly weaker splice modulator; **1e** altered gene expression to an equal or lesser extent for DNAJB1, AURKA, and SF3A1. Analog **1i** showed a drastic reduction in splicing activity, correlating with its decrease in drug activity, for all genes tested except for PLK-1, for which **1i** increased the RNA expression. Analog **1j** showed a similar splicing profile to **1i**, and was only found to affect the RNA expression of PLK-1 and AURKA. The reductions in both drug and splicing activity for analogs with epimerized centers along the side chain point to the importance of the side chain in guiding overall splicing effects.

Section 3.3 Conclusions

These studies have provided new information on the role of splice modulator structure in drug activity and spliceosome interactions. From the nine SPLM analogs of FD-895 generated for this work, we were able to identify trends in how small stereochemical or structural modifications in the side chain or macrolide core regions attenuated drug activity. Epimerization of stereocenters in either region typically led to a loss in activity, consistent with structural data indicating higher-energy conformations and differential 3D intramolecular interactions for these analogs. Epimerization of the C3 (**1a**) and C17 (**1d**) centers proved an exception to this rule, showing activity levels similar to the parent natural product FD-895 (**1**). Interestingly, these analogs also displayed unique splicing-selectivity profiles, particularly the C3 (**1g**) analog, which shows enhanced selectivity for the genes SF2 and SF3A3 after 24-hour treatment (Figures 3.4 and 3.5). X-ray crystallography studies [5] show the C3 center positioned near regions of the SF3B1•PHF5A pocket that interact with incipient pre-mRNA; this structural information combined with our structure-splicing relationship studies indicate that the C3 region is crucial for determining gene-specific splicing activity and modifying this region can lead to preferential targeting of some genes.

We also found that some analogs had unique splicing selectivity profiles independent of their cytotoxic potential. For instance, epimerization (**1d**) or methylation of the C17 (**1e**) center did not significantly alter GI_{50} value compared to FD-895 (**1**), but after 24 hours (Figure 3.4) **1d** was found to induce higher levels of intron 6 retention in SF3A1 and intron 10 retention in SF3B2, and **1e** was found to have reduced splicing selectivity overall compared to **1** or **1d**. Overall, this information implies that cytotoxic potency does not necessarily correlate with splicing selectivity. Instead, a more complex relationship exists, accounting for SPLM fit in the SF3B1•PHF5A pocket and SPLM interactions with pre-mRNA.

Section 3.4 Methods

Compounds

Splice modulator **1-1j** were prepared by total synthesis as described in the supplementary information section. All oligonucleotides were purchased by custom synthesis (Integrated DNA Technologies). Unless stated otherwise, all reagents and media were purchased from VWR or Fisher Scientific.

Cell culture

The HCT-116 cell line was cultured in McCoy's 5a (Life Technologies) supplemented with 10% fetal bovine serum (FBS), 2 mM L-glutamine, and 100 U mL−1 of penicillin and 100 μg mL−1 of streptomycin at 37 °C in an atmosphere of 5% CO2.

Cellular drug treatments

Compounds were dissolved in DMSO (MilliporeSigma). Cells were treated with **1-1j** in media with ≥0.5% DMSO for 4–72 h.

Cell viability assays

HCT-116 cells were plated at 5×10^3 cells/well in McCoy's 5a containing 10% FBS. Cells were cultured for 24 h and then treated with analogs **1-1j** for 4-72 h, then washed twice with 100 μL PBS. 100 μL of media was added to each well, followed by 20 μL of CellTiter Aqueous One Solution (Promega). After 2 h at 37 °C, absorbance readings were taken at 490 nm (test wavelength) and 690 nm (reference wavelength). GI_{50} values were calculated in Prism (GraphPad) using ≥ 3 biological replicates.

Quantitative real time PCR (qPCR)

Cells were treated with **1-1j** in 0.5% DMSO for 4 or 24 h. Untreated cells were considered as a control. Total RNA was isolated using mirVana miRNA isolation kit (Life Technologies). A

1 μg sample of RNA was subjected to DNAseI from a TURBO DNA free kit (Life Technologies). The cDNA was prepared by using SuperScript III reverse transcriptase kit (Life Technologies). The amount of unspliced RNA for different genes was determined using Power SYBR Green PCR master mix (Applied Biosystems) by qPCR using specific primers for each gene (Supplementary Table 1). qPCR using 2.5 μM of each primer was performed on 5 ng of the obtained cDNA. qPCR conditions were as follows: 95 °C for 10 min for one cycle, then 95 °C for 30 s, 55 °C for 60 s, 72 °C for 60 s, for 40 cycles using the MXPro. Quantification cycle (Cq) values were identified for each sample, and then RNA levels were calculated using $2^{-\Delta\Delta CT}$ method.34 GAPDH was used as a control for normalization.21 At least three biological replicates were conducted. Statistics were calculated using a standard one-way ANVOA; p-values were represented so that * signifies $p<0.0001$.

Chapter 3, in part, is material being prepared for submission under the title "Stereochemical Attenuation of Splice Modulation" Chan, W. C.*; **Trieger, K. A.***; Patel, A.; La Clair, J. J.; Burkart, M. D. *authors contributed equally. The dissertation author is the primary co-author of this manuscript.

Section 3.5 Supplementary Information

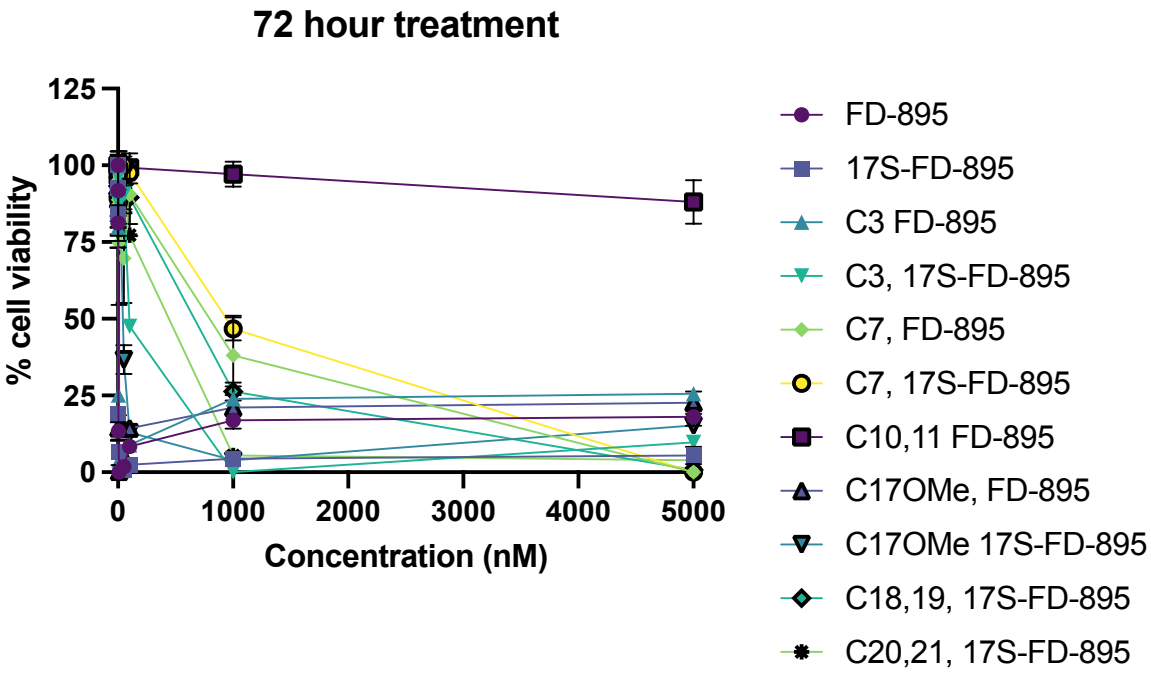

Figure S3.1 Cell viability studies for 72-hour treatments. HCT116 cells were treated with analogs **1-1j** with concentrations ranging from 0.1-5000 nM for 72 hours and then cell viability was measured using the MTS assay. GI_{50} values were calculated using GraphPad.

Table S3.1 GI_{50} values for analogs **1-1j**. HCT116 were treated with analogs **1-1j** ranging from 0.1-5000 nM for 72 hours, then cell viability was measured using the MTS assay. GI_{50} values and confidence intervals were calculated using GraphPad. Full cell viability graph included in Figure S3.1.

Analog	**GI_{50} value (nM)**	**95% confidence interval**
FD-895 (**1**)	1.72	1.004 to 2.828
C3 FD-895 (**1a**)	2.21	1.148 to 4.044
C7 FD-895 (**1b**)	431.8	176.9 to 999.4
C10,11 FD-895 (**1c**)	36553	26507 to 56115
17S-FD-895 (**1d**)	2.06	1.466 to 2.858
17-methoxy FD-895 (**1e**)	2.21	1.110 to 4.175
17-methoxy 17S-FD-895 (**1f**)	37.65	25.77 to 55.17
C3 17S-FD-895 (**1g**)	131.2	88.69 to 199.0
C7 17S-FD-895 (**1h**)	806.2	553.9 to 1163
C18,19 17S-FD-895 (**1i**)	445.5	319.8 to 620.6
C20,21 17S-FD-895 (**1j**)	262.2	178.6 to 391.8

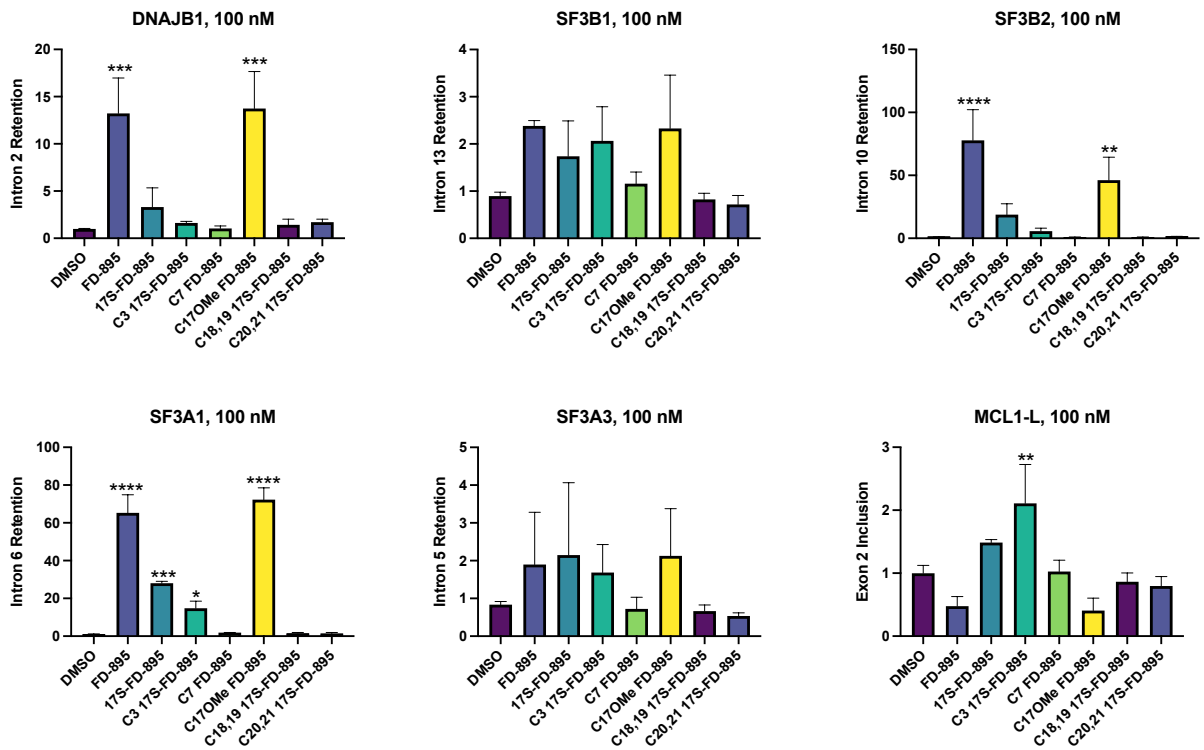

Figure S3.2 Structure-splicing profiles for RNA splice modulators at 100 nM. HCT116 tumor cells were treated with analogs **1, 1b, 1d, 1e, 1g, 1h,** and **1j** at 100 nM for 24 hours and then cellular RNA was isolated and purified for qPCR. Primers were designed to evaluate intron retention or exon skipping, direct responses to splice modulator treatment. Genes evaluated included those involved in splicing regulation (SF3A1, SF3A3, SF3B1, SF3B2), apoptosis (MCL-1L), and protein folding (DNAJB1), relative to the unspliced control GAPDH.

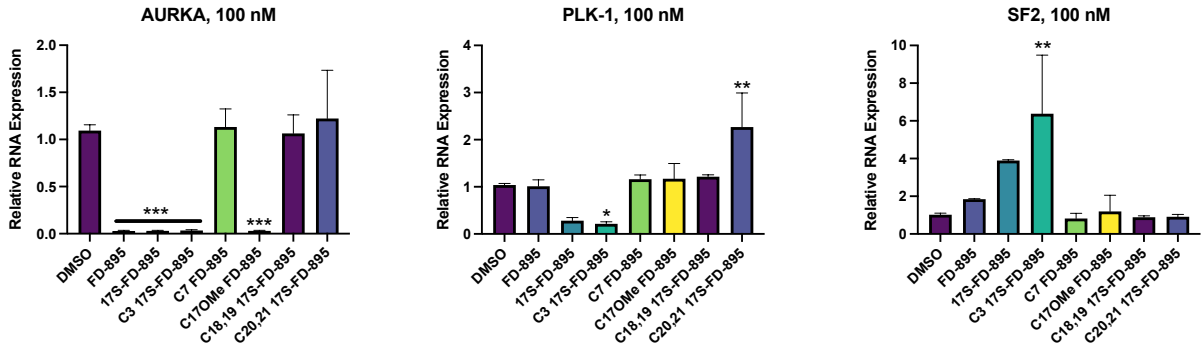

Figure S3.3 Structure-activity profiles for RNA splice modulators at 100 nM. HCT116 tumor cells were treated with analogs **1, 1b, 1d, 1e, 1g, 1h,** and **1j** at 100 nM for 24 hours and then cellular RNA was isolated and purified for qPCR. Primers were designed to evaluate gene expression, which changes in response splice modulator treatment. Genes evaluated included those involved in splicing regulation (SF2) as well as the cell cycle (AURKA, PLK-1), relative to the unspliced control GAPDH.

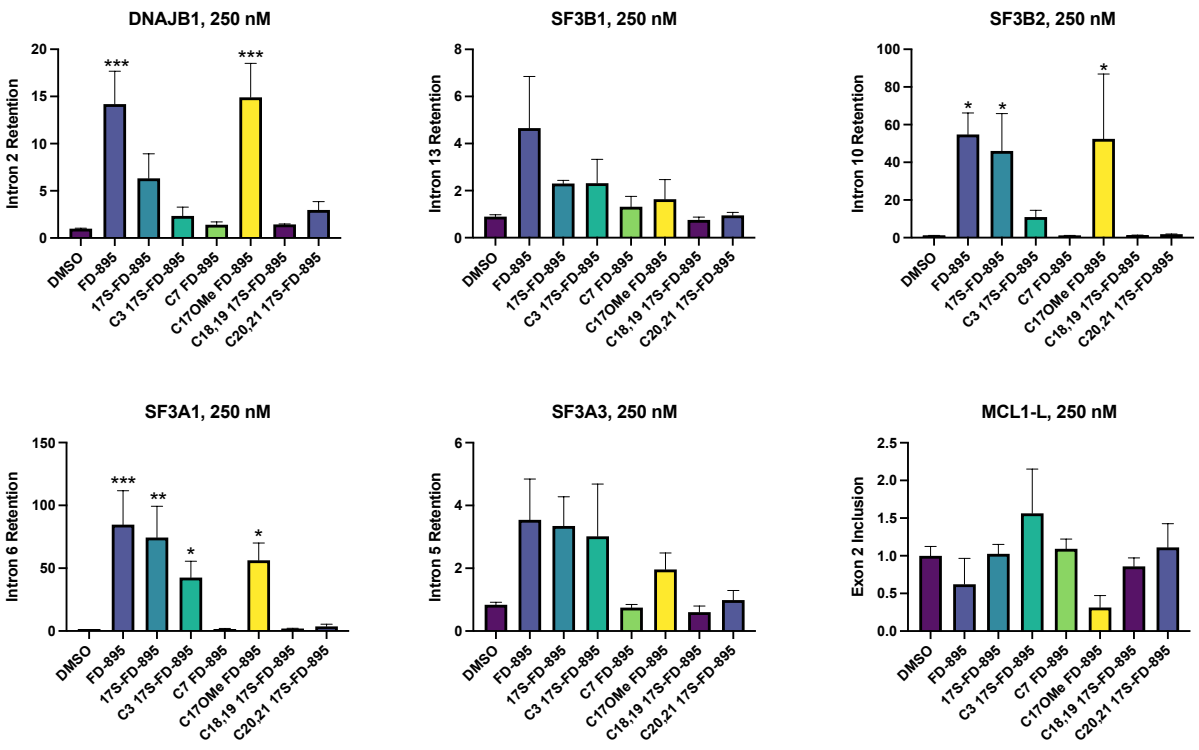

Figure S3.4 Structure-splicing profiles for RNA splice modulators at 250 nM. HCT116 tumor cells were treated with analogs **1, 1b, 1d, 1e, 1g, 1h,** and **1j** at 250 nM for 24 hours and then cellular RNA was isolated and purified for qPCR. Primers were designed to evaluate intron retention or exon skipping, direct responses to splice modulator treatment. Genes evaluated included those involved in splicing regulation (SF3A1, SF3A3, SF3B1, SF3B2), apoptosis (MCL-1L), and protein folding (DNAJB1), relative to the unspliced control GAPDH.

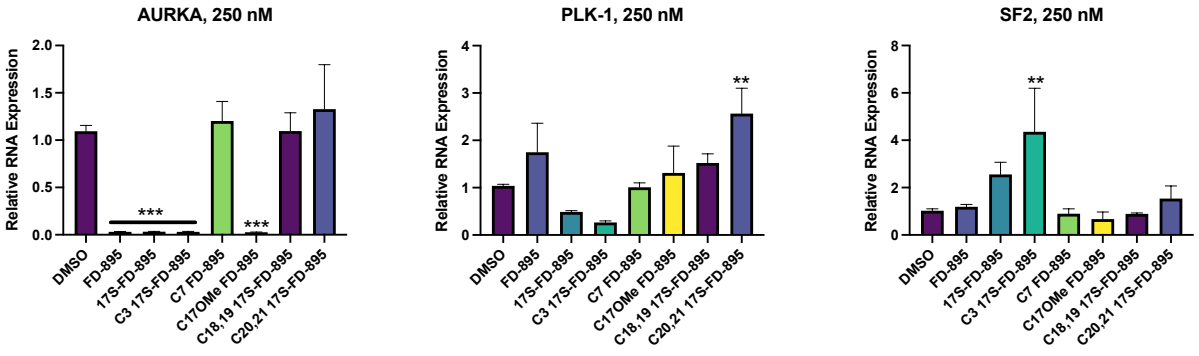

Figure S3.5 Structure-activity profiles for RNA splice modulators at 250 nM. HCT116 tumor cells were treated with analogs **1, 1b, 1d, 1e, 1g, 1h,** and **1j** at 250 nM for 24 hours and then cellular RNA was isolated and purified for qPCR. Primers were designed to evaluate gene expression, which changes in response splice modulator treatment. Genes evaluated included those involved in splicing regulation (SF2) as well as the cell cycle (AURKA, PLK-1), relative to the unspliced control GAPDH.

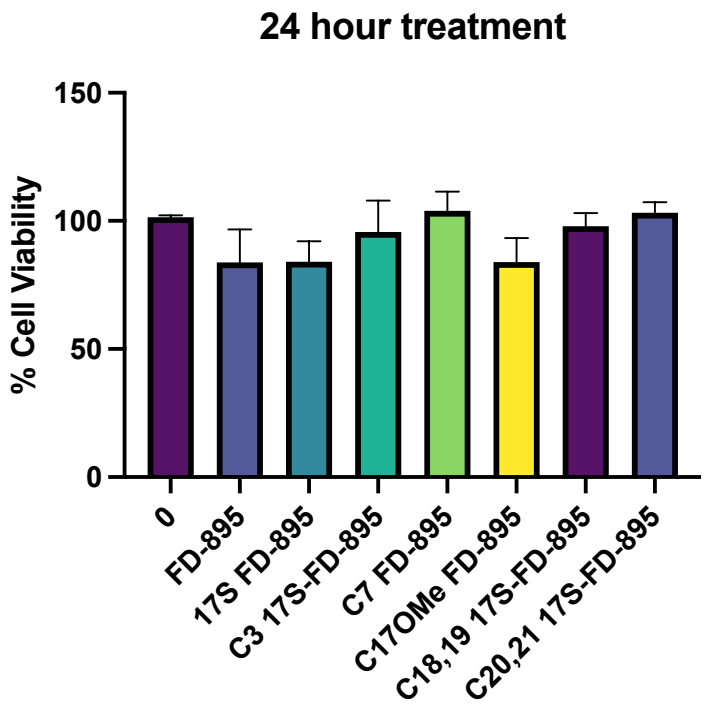

Figure S3.6 Cell viability studies for 24-hour treatments. HCT116 tumor cells were treated with analogs **1, 1b, 1d, 1e, 1g, 1h,** and **1j** at 500 nM for 24 h and then cell viability was measured using the MTS assay. No significant changes in cell viability were identified.

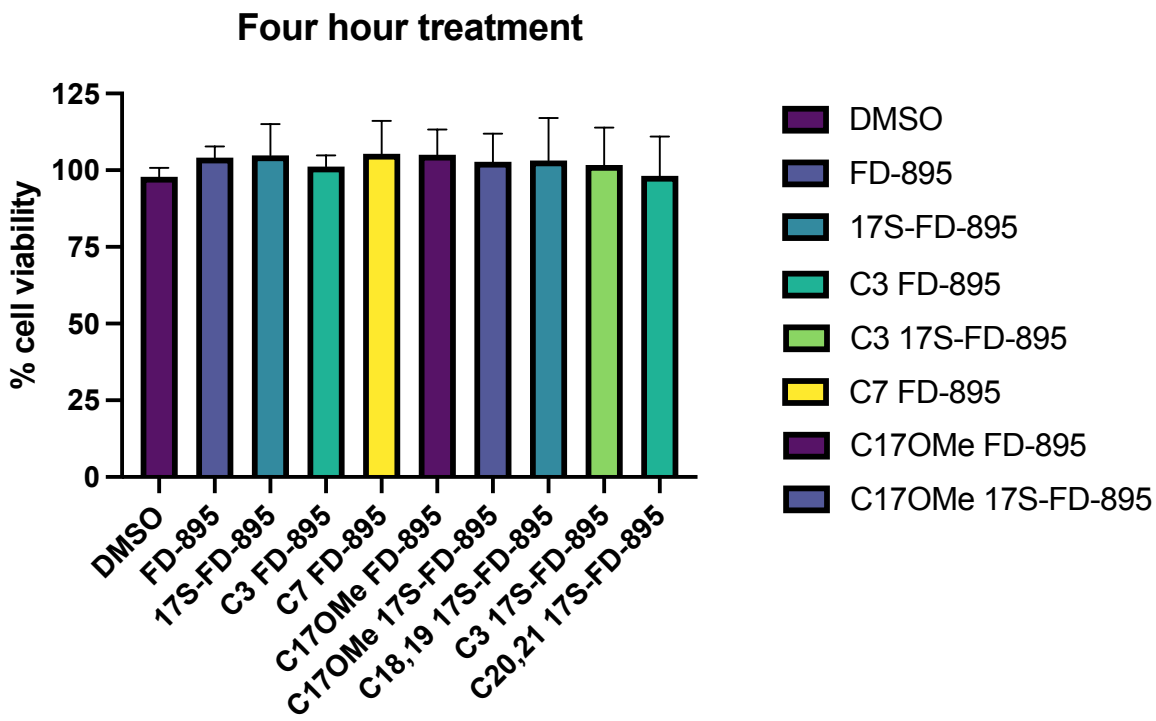

Figure S3.7 Cell viability studies for four-hour treatments. HCT116 tumor cells were treated with analogs **1a-1c, 1e-1g,** and **1j** at 20x the GI_{50} value for each analog (GI_{50} values listed in in table 1) for four hours and then cell viability was measured using the MTS assay. No significant changes in cell viability were identified.

A. General synthetic methods: Chemical reagents were obtained from Acros Organics, Alfa Aesar, Chem-Impex Int., CreoSalus, Fischer Scientific, Fluka, Oakwood Chemical, Sigma-Aldrich, Spectrum Chemical Mfg. Corp., or TCI Chemicals. Deuterated NMR solvents were obtained from Cambridge Isotope Laboratories. All reactions were conducted with rigorously dried anhydrous solvents that were obtained by passing through a column composed of activated A1 alumina or purchased as anhydrous. Anhydrous *N*,*N*-dimethylformamide was obtained by passage over activated 3Å molecular sieves and a subsequent NaOCN column to remove traces of dimethylamine. Triethylamine (Et_3N) was dried over Na and freshly distilled. Ethyl-*N,N*-diisopropylamine (Et*N-i*-Pr_2) was distilled from ninhydrin, then from KOH. Anhydrous CH_3CN was obtained by distillation from CaH_2. All reactions were performed under positive pressure of Ar in oven-dried glassware sealed with septa, with stirring from a Teflon coated stir bars using an IKAMAG RCT-basic stirrer (IKA GmbH). Solutions were heated on adapters for IKAMAG RCT-basic stirrers. Analytical Thin Layer Chromatography (TLC) was performed on Silica Gel 60 F254 precoated glass plates (EM Sciences). Preparative TLC (pTLC) was conducted on Silica Gel 60 plates (EM Sciences). Visualization was achieved with UV light and/or an appropriate stain (I_2 on SiO_2, $KMnO_4$, bromocresol green, dinitrophenylhydrazine, ninhydrin, and ceric ammonium molybdate). Flash chromatography was carried out on Fischer Scientific Silica Gel, 230-400 mesh, grade 60 or SiliaFlash Irregular Silica Gel P60, 40-63 μm mesh, grade 60. Yields correspond to isolated, chromatographically and spectroscopically homogeneous materials. ^1H NMR and ^{13}C NMR spectra were recorded on a Varian VX500 spectrometer equipped with an Xsens Cold probe. Chemical shift δ values for ^1H and ^{13}C spectra are reported in parts per million (ppm) and multiplicities are abbreviated as s = singlet, d = doublet, t = triplet, q = quartet, m = multiplet, br = broad. All ^{13}C NMR spectra were recorded with complete proton decoupling. FID files were

processed using MestraNova 12.0.3. (MestreLab Research). Electrospray (ESI) mass spectrometric analyses were performed using a ThermoFinnigan LCQ Deca spectrometer, and high-resolution analyses were conducted using a ThermoFinnigan MAT900XL mass spectrometer with electron impact (EI) ionization. A Thermo Scientific LTQ Orbitrap XL mass spectrometer was used for high-resolution electrospray ionization mass spectrometry analysis (HR-ESI-MS). FTIR spectra were obtained on a Nicolet magna 550 series II spectrometer as thin films on either KBr or NaCl discs, and peaks are reported in wavenumbers (cm^{-1}). Optical rotations $[\alpha]_D$ were measured using a Perkin-Elmer Model 241 polarimeter with the specified solvent and concentration and are quoted in units of deg cm^2 g^{-1}. Spectral data and procedures are provided for all new compounds and copies of select spectra have been provided.

Typical procedure for the Stille Coupling of 2-2j and 3-3 for the synthesis of 1-1j.

Reagents:

CuCl, anhydrous, beads, 99.99% (Sigma-Aldrich): beads were powdered prior to addition

KF, anhydrous, powder, 99.9% (Sigma-Aldrich): used without further purification

XPhos Pd G2 (Sigma-Aldrich): used without further purification

t-BuOH, anhydrous, 99.5% (Sigma-Aldrich): used without further purification

Vinylstannane **2-2j** (1.5 eq) and core **3-3f** (1 eq) were combined in a 50 mL flask and dried *via* rotary evaporation of benzene. To the mixture was then sequentially added CuCl (1.5 eq), KF (1.5 eq) and XPhos Pd G2 (0.05 eq) and anhydrous *t*-BuOH (10 mL). The reaction vessel was purged under Ar, heated to 50 °C and stirred overnight, at which point solution turns into a gray cloudy mixture. The mixture was then filtered through a plug of Celite and eluted with acetone (20 mL). The elutants were concentrated on a rotary evaporator to yield a crude brown semi-solid. Pure **1-1j** was obtained as a white semi-solid by flash chromatography over neutral silica gel, eluting with a gradient of hexanes to 1:3 acetone/hexanes.

Procedures for the synthesis of FD-895 (1).

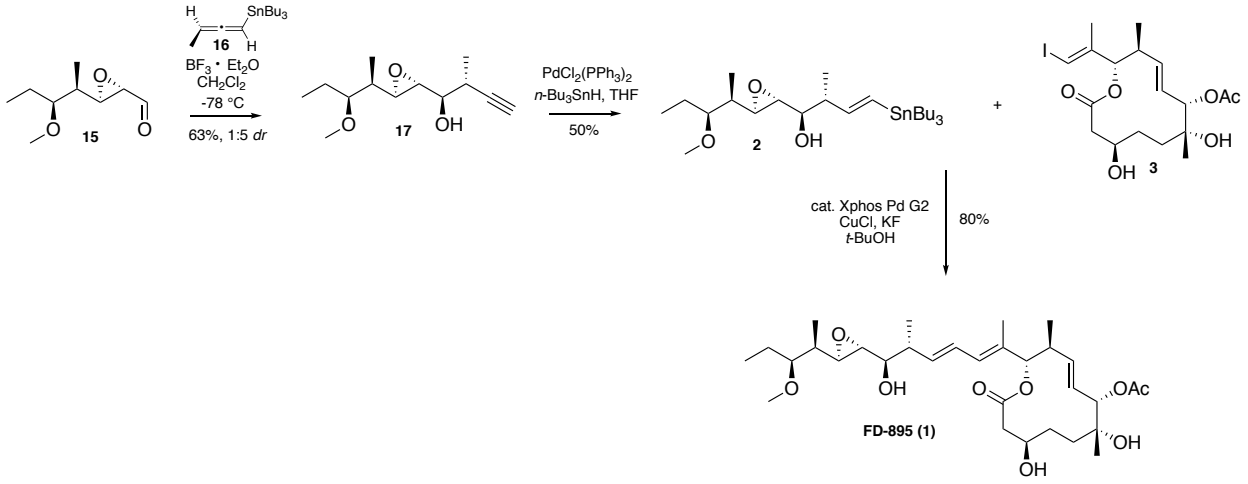

Marshall addition of allenylstannane 16 to aldehyde 15 to afford alkyne 17

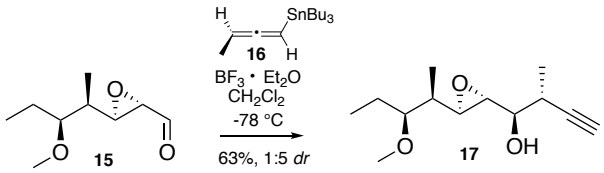

Reagents:

BF_3•Et_2O, 46.5% BF_3 (Alfa Aesar): used without further purification

(1*R*,2*R*)-1-((2*R*,3*R*)-3-((2*R*,3*S*)-3-Methoxypentan-2-yl)oxiran-2-yl)-2-methylbut-3-yn-1-ol (5). Aldehyde **15** (0.701 g, 4.08 mmol) and allenylstannane **16** (2.10 g, 6.10 mmol) in a 100 mL flask were dissolved in anhydrous CH_2Cl_2 (40.0 mL) and purged with an Ar atmosphere. The mixture was cooled to -78 °C and BF_3•Et_2O (0.753 mL, 6.10 mmol) was added dropwise over 5 min. The reaction was stirred for 1 h at -78 °C. A mixture of MeOH (5 mL) and satd. $NaHCO_3$ (1 mL) was added, and the solution was warmed to rt. The phases were separated, and the aqueous phases were extracted with Et_2O (3 × 100 mL). The organic phases were combined, dried with Na_2SO_4 and concentrated on a rotary evaporator. Alkyne **17** (0.692 g, 63%) was obtained in a 1:5 mixture of diastereomers (by NMR) as a colorless oil by flash chromatography, eluting with a gradient of hexanes to 1:3 Et_2O/hexanes.

Note 1: Desired diastereomer was isolated in the next step.

Note 2: The remaining C18-C19 epoxide diastereomer from the Sharpless epoxidation was resolved after purification of the next step.

Alkyne **17**: TLC (2:1 hexanes/EtOAc): R_f = 0.50; ^{1}H NMR ($CDCl_3$, 400 MHz) δ 3.55 (s, 3H), 3.41 (m, 1H), 3.21 (ddd, *J* = 10.4, 6.4, 3.9 Hz, 1H), 3.07 (dd, *J* = 4.6, 2.3 Hz, 1H), 3.0 (dd, *J* = 8.1, 2.2 Hz, 1H), 2.67 (m, 1H), 2.16 (d, *J* = 2.5 Hz, 1H), 2.07 (bs, 1H), 1.57 (m, 3H), 1.31 (d, *J* =

6.9 Hz, 3H), 0.97 (d, *J* = 7.0 Hz, 3H), 0.90 (t, *J* = 7.4 Hz, 3H); ^{13}C NMR ($CDCl_3$, 100 MHz) δ 83.8, 77.4, 73.7, 71.2, 59.5, 59.4, 58.3, 39.0, 31.1, 23.9, 17.2, 10.4, 10.2; ESI–MS m/z 249.14 $[M+Na]^+$; FTIR (film) νmax 3430, 3310, 2967, 2935, 2878, 1457, 1379, 1260, 1093 cm^{-1}; HR–ESI–MS m/z calcd. for $C_{13}H_{22}O_3Na$ $[M+Na]^+$: 249.1461, found 249.1462. $[\alpha]^{25}_D$ = +10.2 ° (c = 1.0, CH_2Cl_2).

Hydrostannylation of alkyne 17

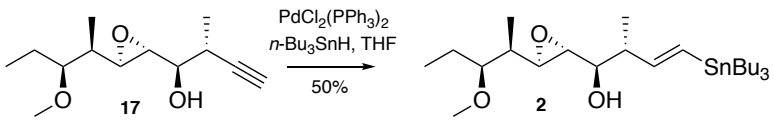

Reagents:

n-Bu_3SnH, 97% contains 0.05% BHT as stabilizer (Acros Organics): used without further purification

$PdCl_2(PPh_3)_2$ (Oakwood Chemical): dried *via* azeotropic distillation of benzene

(1*R*,2*R*,*E*)-1-((2*R*,3*R*)-3-((2*R*,3*S*)-3-Methoxypentan-2-yl)oxiran-2-yl)-2-methyl-4-(tributylstannyl)but-3-en-1-ol (2). $PdCl_2(PPh_3)_2$ (0.155 g, 0.221 mmol) was added to a solution of alkyne **17** (0.501 g, 2.21 mmol) in a 50 mL flask in anhydrous THF (20 mL). The mixture was cooled to 0 °C and *n*-Bu_3SnH (1.79 mL, 6.63 mmol) was added dropwise. The mixture was stirred for 45 min at 0 °C, at which point the resulting mixture was concentrated to yield a black crude oil. The material was extracted into hexanes, filtered through a pad of Celite and was eluted with hexanes. The elutant was concentrated on a rotary evaporator, and this process was repeated twice until a clear black solution was achieved. Pure vinylstannane **2** (0.110 g, 50%) was obtained as a mixture of 1:5 α:β regioisomers by flash chromatography, eluting with a gradient of hexanes to CH_2Cl_2 to 1:20 Et_2O/CH_2Cl_2. The desired regioisomer and diastereomer can be obtained in 95+% purity by additional flash chromatography, eluting with a gradient of hexanes to CH_2Cl_2 to 1:20 Et_2O/CH_2Cl_2.

Note 1: Unwanted diastereomer obtained from previous reaction was removed after flash chromatography

Vinylstannane **2**: TLC (10:1 hexanes/Et_2O): R_f = 0.28 (CAM stain); ^1H NMR (C_6D_6, 500 MHz) δ 6.20 (m, 2H), 6.19 (d, *J* = 6.8 Hz, 1H), 3.34 (td, *J* = 4.9, 1.8 Hz, 1H), 3.23 (s, 3H), 3.16 (td, *J* = 6.3, 4.2 Hz, 1H), 2.98 (dd, *J* = 8.0, 2.3 Hz, 1H), 2.84 (dd, *J* = 4.3, 2.3 Hz, 1H), 2.51 (td, *J* = 6.9, 5.2 Hz, 1H), 1.61 (m, 6H), 1.48 – 1.32 (m, 7H), 1.19 (d, *J* = 6.9 Hz, 3H), 1.02 – 0.92 (m, 19H), 0.86 (t, *J* = 7.4 Hz, 3H); ^{13}C NMR (C_6D_6, 500 MHz) δ 154.5, 150.5, 150.4, 150.4, 150.3, 83.8, 83.3, 72.8, 59.0, 57.5, 57.3, 57.2, 39.0, 39.0, 29.3, 27.4, 23.5, 15.9, 15.8, 13.4, 10.5, 9.6, 9.4; HR–ESI–MS m/z calcd. for $C_9H_{17}O_3$ $[M+H]^+$ 519.2843, found 519.2839; $[\alpha]^{25}_D$ = -2.3° (c = 1.0, CH_2Cl_2).

Stille coupling of stannane 2 and core 3

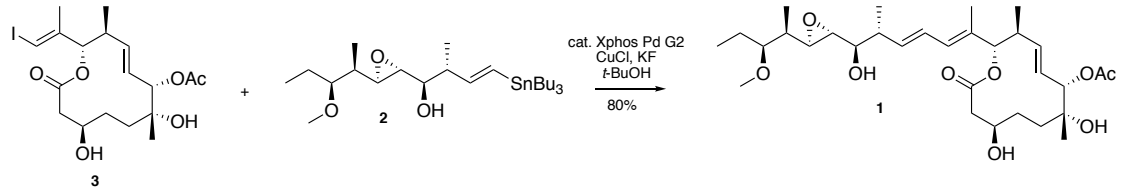

FD-895 (**1**): Yield: 80%, 121 mg; TLC (1:3 acetone/CH_2Cl_2): R_f = 0.28 (CAM stain); NMR data provided in Table S1; FTIR (film) ν_{max} 3447, 2963, 2930, 2875, 1739, 1457, 1374, 1239, 1176, 1089, 1021 cm^{-1}; HR-ESI-MS *m/z* calcd. for $C_{31}H_{50}IO_9Na$ $[M+Na]^+$: 589.3370, found 589.3376; $[\alpha]^{25}_D$ = +6.8 ° (c = 1.0, CH_2Cl_2).

Table S3.2. NMR data for FD-895 (**1**) in C_6D_6

Position	δ_H, mult (*J* in Hz)	δ_C	^{1}H, ^{1}H-COSY	^{1}H, ^{1}H-NOESY	^{1}H, ^{13}C-HMBC
1		172.1			
2’	2.30, dd (14.8,	38.6	2’’w, 3	2’’, 3	1, 3, 4
2’’	2.20, dd (14.8,		2’, 3	2’, 3, 4’, 5’	1, 3w
3	3.51, m	69.4	3OHw	2’, 2’’, 4’, 5’, 5’’,	
3-OH	3.66, d (11.0)		3	3, 6OH, 17OH	
4’	1.60, m	30.4	3w, 4’’, 5’	2’, 3, 8, 24	3, 5
4’’	1.25, m		3, 5’	3w, 5’, 7	3, 5
5’	1.54, m	35.9	5’’	2'', 3, 5’, 8	4, 6, 24w
5’’	1.23, m		4’	3, 4’, 7	4, 6, 7, 24w
6		73.3			
6-OH	1.85, s			3, 3OH, 17OH	
7	5.26, s	79.2	8	4’’, 5’’, 8, 24	8, 9, 24, 26, 29
8	5.83, dd (15.2,	126.5	7, 9	4’w, 5’, 7, 9, 10	6w, 9, 10
9	5.63, dd (15.2,	140.7	8, 10	4’’, 5’’, 7, 8, 10, 11,	7, 8, 10, 11w,
10	2.38, m	41.1	11, 25	7, 8, 9, 11w, 25, 26	8, 9, 11, 25
11	5.24, d (1.8)	82.6	10	9, 10w, 13, 25, 26w	1, 9, 10, 12, 14,
12		131.6			
13	6.10, dd (10.9,	131.7	14, 26	11, 14, 15, 25, 26w,	11, 14, 15, 26
14	6.23, dd (15.0,	126.2	13, 15	13, 15, 16, 26, 27	12, 13, 16
15	5.53, dd (15.0,	138.3	14, 16	13, 14, 16, 17, 18, 27	13, 14, 16, 17, 27
16	2.39, m	42.6	17, 27	14, 15, 17, 18, 27	13w, 14, 15, 17,
17	3.10, m	75.3	16, 18	15, 16, 18, 19, 27	16w, 27w
17-OH	2.14, bs		17	3w, 3OH, 6OH, 17w	
18	2.66, dd (5.8, 2.2)	60.6	17, 19	15w, 16, 17, 20, 27,	17, 20
19	2.87, dd (8.3, 2.3)	59.7	18w, 20	17, 20, 21, 28, 31	17, 20, 21, 28
20	1.26, m	39.4	19, 28	18, 19, 21, 23, 28	18, 19, 21, 23,
21	3.15, td (6.4, 4.1)	83.6	20, 22’,	19, 20, 22’, 22’’, 23,	19, 20, 22w, 23,
22’	1.63, m	23.9	22’’, 23	21, 22’’, 23	20, 21, 23
22’’	1.37, ddd (14.0,		22’, 23	21, 22’, 23	20, 21, 23
23	0.84, t (7.5)	10.0	22’, 22’’	21, 22’, 22’’	21, 22
24	1.02, s	24.8		4’, 5’, 6OH, 7	5, 6, 7
25	0.70, d (6.8)	16.4	10	9, 10, 11, 13w, 26	9, 10, 11
26	1.57, d (1.3)	11.9		10, 11, 14, 25	11, 12, 13, 14, 15
27	1.14, d (6.8)	17.0	16	14, 15, 16, 17, 18w	15, 16, 17
28	0.83, d (7.1)	10.6	20	17, 18, 19, 21, 31w	19, 20, 21
29		169.0			
30	1.62, s	20.7			29
31	3.25, s	57.8		19, 23	21

Stille coupling of stannane 2 and Core 3a to afford 3*S*-FD-895 (1a).

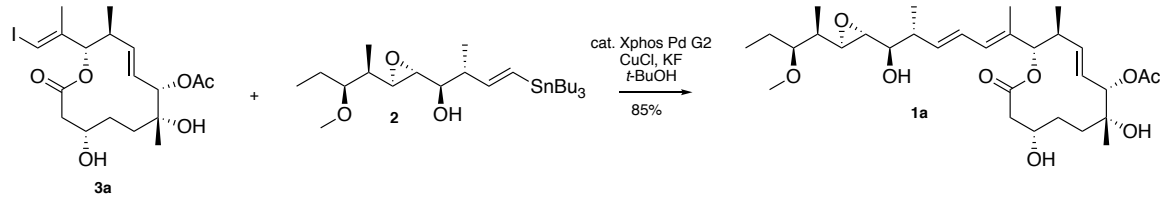

3*S*-FD-895 (**1a**): Yield: 85%, 65.1 mg; TLC (1:3 acetone/CH_2Cl_2): R_f = 0.18 (CAM stain); NMR data provided in Table S2; FTIR (film) ν_{max} 3447, 2963, 2930, 2875, 1739, 1457, 1374, 1239, 1176, 1089, 1021 cm^{-1}; HR-ESI-MS *m/z* calcd. for $C_{31}H_{50}IO_9Na$ $[M+Na]^+$: 589.3310, found 589.3311; $[\alpha]^{25}_D$ = +9.4 ° (c = 1.0, CH_2Cl_2).

Table S3.3 NMR data for 3*S*-FD-895 (1a) in C_6D_6

Position	δ_H, mult (*J* in	δ_C	^1H, ^1H-	^1H, ^1H-NOESY	^1H, ^{13}C-HMBC
1		169.6			
2’	2.47, m	40.0	2’’, 3	3, 5’	1, 3, 4w
2’’	2.38, m		2’, 3	3	1, 3, 4
3	4.25, bs	67.3	2’, 2’’w	2’w, 2’’, 4’, 4’’	
3-OH					
4’	1.35, m	27.5	3w, 4’’, 5’’	3, 5’, 5’’, 7	2w, 3w, 5w
4’’	1.33, m		3w, 4’, 5’	3, 5’, 5’’	3w, 5w
5’	1.88, dt (13.5,	30.7	4’’, 5’’	4’’	4, 6, 24
5’’	1.82, m		4’, 5’	4’, 24	4, 6, 7, 24
6		73.4			
6-OH					
7	5.26, d (9.8)	79.3	8	4’, 8, 9, 24	8, 9, 24w, 29
8	5.93, dd (15.2,	126.6	7, 9, 10w	5’w, 7, 9, 10	6w, 10
9	5.62, dd (15.3,	140.4	8, 10	7, 8, 10, 11, 25	7, 10, 11w, 25w
10	2.47, m	41.2	9w, 11, 25	8w, 25	8, 9, 11, 25w
11	5.20, d (10.7)	82.2	10	10w, 13, 25	1, 9, 10, 12, 13,
12		132.1			
13	6.17, d (11.0)	131.4	14, 26w	8, 15, 27w	11, 15, 26
14	6.26, dd (15.0,	126.3	13, 15	15, 27	12, 13, 16
15	5.54, dd (15.0,	137.9	14, 16	7, 13, 14, 16w, 27	12, 13, 16, 17, 27
16	2.38, m	42.6	15, 17w, 27	14,15, 27	14, 15, 17, 18, 27
17	3.10, t (6.6)	75.2	16, 18	16w, 18w 27	15, 16, 18, 27
17-OH					
18	2.68, dd (5.8,	60.6	17, 19w	17, 19, 20, 28	17, 19w, 20w
19	2.86, dd (8.2,	59.6	18w, 20	20w, 28	17w, 18w, 20,
20	1.27, ddd (8.2,	39.3	19, 28	18, 21, 22’, 22’’, 28	19, 28w
21	3.14, td (6.3, 4.1)	83.5	20, 22’,	20, 22’, 22’’, 23, 28	19, 20w, 22w,
22’	1.63, m	23.8	21, 22’’, 23	22’’, 23w	20, 21, 23
22’’	1.39, m		21, 22’, 23	22’, 23	20, 21, 23
23	0.84, t (7.5)	10.0	22’, 22’’	21, 22’, 22’’	21, 22
24	1.11, s	24.8		2’’	5, 6, 7
25	0.73, d (6.8)	16.5	10	10	9, 10, 11
26	1.60, s	11.9	13	10, 14	11, 12, 13
27	1.15, d (6.7)	17.1	16	15, 16, 17	15, 16, 17
28	0.85, d (7.8)	10.6	20	20, 21	19, 20
29		169.1			
30	1.66, s	20.8			29

31	3.25, s	57.7		21, 22', 23, 24	21

Stille coupling of stannane 2 and core 3b to afford 7*R*-FD-895 (1b).

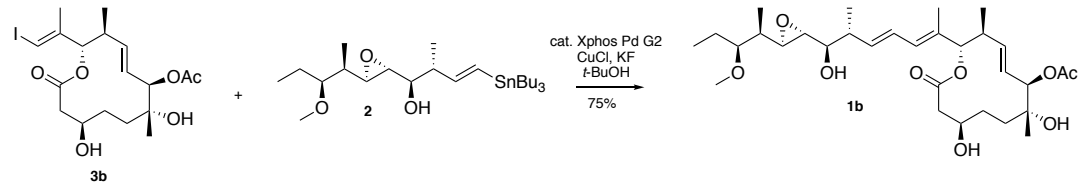

7*R*-FD-895 (1b): Yield: 75%, 99.1 mg; TLC (1:3 acetone/CH_2Cl_2): R_f = 0.28 (CAM stain); NMR data provided in Table S3; FTIR (film) ν_{max} 3447, 2963, 2930, 2875, 1739, 1457, 1374, 1239, 1176, 1089, 1021 cm^{-1}; HR-ESI-MS *m/z* calcd. for $C_{31}H_{50}IO_9Na$ $[M+Na]^+$: 589.3348 found 589.3351; $[\alpha]^{25}_D$ = +10.9 ° (c = 1.0, CH_2Cl_2).

Table S3.4 NMR data for 7*R*-FD-895 (1b) in C_6D_6

Position	δ_H, mult (*J* in	δ_C	^{1}H, ^{1}H-	^{1}H, ^{1}H-NOESY	^{1}H, ^{13}C-HMBC
1		172.3			
2’	2.35, m	39.0	2’, 3	3, 4’’w, 5’	1, 3, 4
2’’	2.29, dd (14.6,		2’’, 3	3, 4’’, 5’	1, 3, 4
3	3.57, bs	69.6	3OH, 4’	2’, 2’’, 4’, 4’’w, 5’w, 5’’,	N/A
3-OH	3.67, d (10.6)		3	4’, 5’’	conformers
4’	1.66, m	30.6	3, 4’’, 5’,	3, 3OH, 5’, 5’’, 7w	conformers
4’’	1.82, m		3, 4’, 5’,	3w, 5’, 5’’, 7w	2
5’	1.58, m	36.5	4’, 4’’,	4’	conformers
5’’	0.95, m		4’, 4’’, 5’	4’’	conformers
6		73.8			
6-OH					
7	5.40, m	77.9	8	4’, 8, 10, 15, 24, 27w	5, 6, 8, 9, 29
8	5.92, dd (15.4,	128.0	7, 9	7, 9, 10, 11, 13w, 14w,	7, 10
9	5.38, m	130.7	8, 10	4’, 8, 10, 11, 15, 18, 25	7, 10
10	2.47, tq (10.1,	41.0	11, 25	8, 9, 25, 26	8, 9, 11, 25
11	5.36, d (10.7)	82.9	10	4’, 8, 10, 13, 25	1, 9, 10, 12w, 13,
12		131.9			
13	6.15, d (10.9)	131.5	14, 26w	8, 9, 11, 15, 28	11, 15, 26
14	6.26, dd (15.0,	126.2	13, 15	15, 16, 22’, 26, 27	12, 13, 16
15	5.50, dd (15.0,	138.2	14, 16	8w, 13, 14, 16, 17, 18w, 27	13, 16, 17, 27
16	2.37, m	42.7	15, 17, 26	14, 15, 27	14, 15, 17, 18, 27
17	3.06, t (6.6)	75.3	16, 18	16w, 19, 27	15, 16, 18, 19, 27
17-OH					
18	2.65, dd (5.7,	60.7	17	10, 15, 16, 19, 20, 27w,	17, 19, 20w
19	2.85, dd (8.2,	59.7	20	10w, 16w, 17w, 18, 20w,	18, 20, 28
20	1.30, m	39.4	19, 28	18, 23, 28	18, 19, 27, 28
21	3.14, td (6.3,	83.6	20, 22’,	19, 20, 22’, 22’’w, 23, 28	19w, 20, 23, 28,
22’	1.57, m	23.8	23	21, 22β, 23	20, 21, 23
22’’	1.36, m		23	21, 22α, 23	20, 21, 23
23	0.84, t (7.5)	10.0	22’, 22’’	21, 22’, 22’’	21, 22
24	1.00, s	24.7		3OH, 5’, 5’’, 7	5, 6, 7
25	0.76, d (6.8)	17.1	10	9, 10, 11, 20, 26	9, 10, 11
26	1.62, bs	11.5		10, 11, 14	11, 12, 13, 14, 15
27	1.12, d (6.8)	16.9	16	14, 15, 16, 17w	15, 16, 17
28	0.84, d (7.0)	10.6	20	19, 21	19, 20, 21
29		169.2			
30	1.67, s	20.4			29

31	3.24, s	57.8		19, 21, 22', 23, 28	21

Procedures for the synthesis of 10*R*,11*R*-FD-895 (1c).

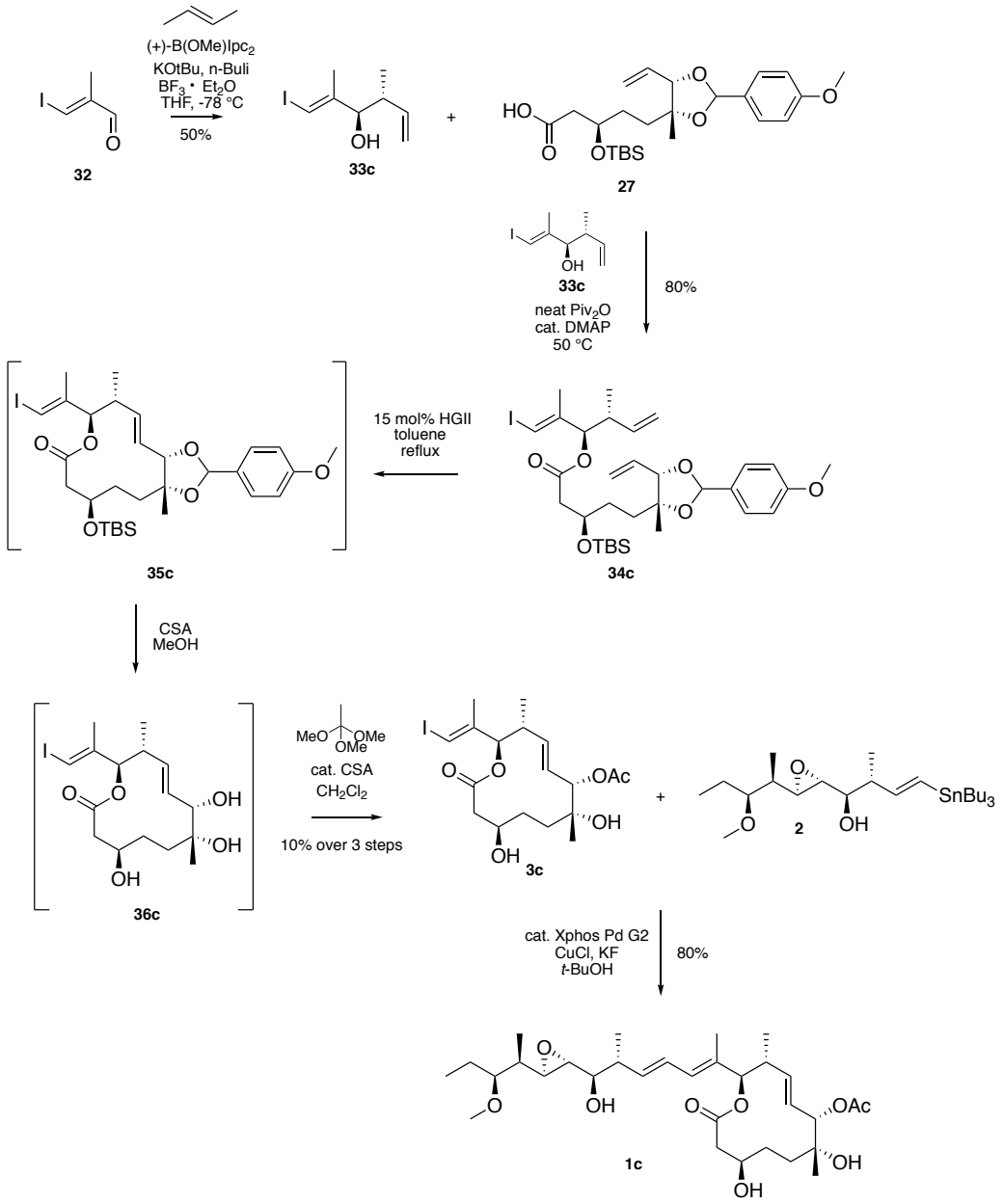

Crotylation of aldehyde 32 to vinyl iodide 33c

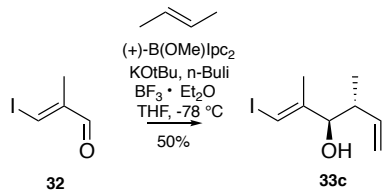

Reagents:

Trans-2-butene (Acros Organics): used without further purification

(+)-B-methoxydiisopinocampheylborane (Sigma): used without further purification

KO*t*-Bu (Chem-Impex): used without further purification

n-BuLi (2.5 M in hexane) (Acros Organics): used without further purification

BF_3•Et_2O (Alfa Aesar): used without further purification

(*E*)-But-2-ene (20.0 mL, 0.200 mol) was condensed and added to a 11 L reaction flask containing anhydrous THF (300 mL) at -78 °C. KO*t*-Bu (11.4 g, 0.101 mol) was added, and the mixture was stirred at -78 °C for 30 min. *n*-BuLi (2.5 M in hexane, 40.0 mL, 0.100 mol) was added dropwise over 15 min, and the resulting yellow mixture was stirred at -78 °C for an additional 30 min. A solution of (+)-B-methoxydiisopinocampheylborane (25.3 g, 0.800 mmol) in anhydrous THF (100 mL) was added dropwise over 15 min, and the mixture turned clear. After stirring the mixture for 30 min, BF_3•Et_2O (17.0 mL, 0.134 mol) was added dropwise over 10 min, and the mixture was stirred for an additional 10 min. After cooling the mixture to -94 °C, a solution of **32** (12.1 g, 61.7 mmol) in anhydrous THF (75 mL) was added dropwise over 45 min. The mixture was allowed to warm to rt and stirred for 16 h. H_2O (200 mL) was added, and the mixture was concentrated on a rotary evaporator. Vinyl iodide **33c** (7.80 g, 50%) was obtained at a 10:1 *dr* by flash chromatography, eluting with CH_2Cl_2.

Vinyl iodide **33:** TLC (CH_2Cl_2): R_f = 0.40 ($KMnO_4$); ^1H NMR (500 MHz, $CDCl_3$) δ 6.26 (s, 1H), 5.72 (m, 1H), 5.18 (d, *J* = 16.0 Hz, 1H), 5.18 (d, *J* = 11.3 Hz, 1H), 3.87 (dd, *J* = 8.1, 2.9 Hz, 1H), 2.36 (h, *J* = 7.4 Hz, 1H), 1.88 (d, *J* = 2.9 Hz, 1H), 1.82 (bs, 3H), 0.92 (d, *J* = 6.8 Hz, 3H); ^{13}C NMR (125 MHz, $CDCl_3$) δ 148.1, 140.0, 117.4, 80.2, 80.0, 42.4, 19.4, 16.6; HR-ES-MS *m/z* calcd. for $C_8H_{13}IONa$ $[M+Na]^+$: 274.9998, found 274.9997; $[\alpha]^{25}_D$ = +21.4 ° (c = 1.0, CH_2Cl_2).

Esterification of acids 27 with alcohol 33c to afford 34c

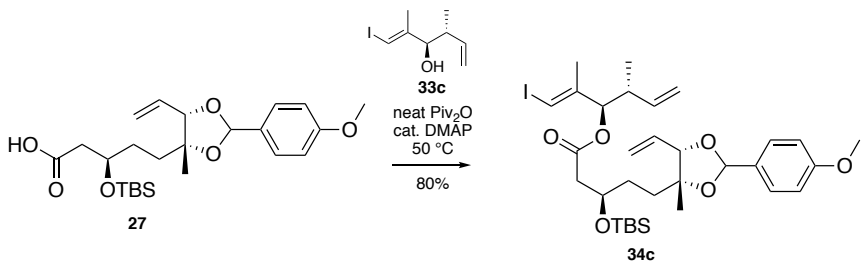

Reagents:

DMAP, 98% (Sigma-Aldrich): used without further purification

Pivalic anhydride, 99% (Alfa Aesar): used without further purification

3*S*,4*S*,*E*)-1-Iodo-2,4-dimethylhexa-1,5-dien-3-yl-(3*R*)-3-((*tert*-butyldimethylsilyl)oxy)-5-((4*R*,5*S*)-2-(4-methoxyphenyl)-4-methyl-5-vinyl-1,3-dioxolan-4-yl)pentanoate (34). DMAP (150 mg, 1.22 mmol) and pivalic anhydride (3.71 mL, 18.3 mmol) were added sequentially to a 250 mL flask containing **27** (5.51 g, 12.2 mmol) and alcohol **33** (3.23 g, 12.8 mmol). The mixture was purged with Ar and stirred neat at 50 °C for 8 h. Pivalic anhydride was removed from the mixture under airflow. Crude material was then loaded directly onto silica gel in hexanes and eluted with a gradient of hexanes to 1:10 Et_2O/hexanes. Pure esters **34** (6.72 g, 80%) were obtained as a clear oil.

Esters **34**: TLC (1:4 Et_2O/hexanes): R_f = 0.40 and 0.38 (CAM stain); ^1H NMR (500 MHz, C_6D_6) δ 7.57 (d, *J* = 8.7 Hz, 2H), 7.55 (d, *J* = 8.7 Hz, 2H), 6.86 (d, *J* = 8.6 Hz, 2H), 6.82 (d, *J* = 8.6 Hz, 2H), 6.22 (s, 1H), 6.20 (s, 1H), 5.93 (s, 1H), 5.83 (m, 1H), 5.79 (m, 2H), 5.63 (m, 1H), 5.60 (m, 1H), 5.33 (dt, *J* = 17.2, 1.6 Hz, 1H), 5.22 (d, *J* = 8.1 Hz, 1H), 5.19 (d, *J* = 8.1 Hz, 1H), 5.09 (dq, *J* = 10.4, 1.4 Hz, 1H), 4.96 (m, 2H), 4.27 (m, 1H), 4.22 (m, 1H), 4.12 (dt, *J* = 6.6, 1.3 Hz, 1H), 3.29 (s, 3H), 3.26 (s, 3H), 2.46 (dd, *J* = 15.0, 6.3 Hz, 1H), 2.42 (dd, *J* = 15.0, 6.6 Hz, 1H), 2.30 (dd, *J* = 15.0, 5.6 Hz, 1H), 2.25 (m, 1H), 2.22 (dd, *J* = 15.0, 5.7 Hz, 1H), 1.98 (dt, *J* = 13.0, 4.0 Hz, 1H), 1.87 (m, 1H), 1.79 (m, 1H), 1.71 (d, *J* = 1.1 Hz, 3H), 1.69 (d, *J* = 1.1 Hz, 3H), 1.67 (m, 1H), 1.25 (s, 3H), 1.24 (m, 2H), 1.21 (s, 3H), 1.01 (s, 9H), 0.98 (s, 9H), 0.67 (d, *J* = 5.3 Hz, 3H), 0.65 (d, *J* = 5.3 Hz, 3H), 0.14 (s, 3H), 0.14 (s, 3H), 0.12 (s, 3H), 0.09 (s, 3H); ^{13}C NMR (125 MHz, C_6D_6) δ 170.3, 170.3, 160.8, 160.6, 144.8, 144.7, 139.8, 133.6, 132.9, 131.2, 128.6, 128.4, 128.2, 128.1, 127.6, 118.0, 117.9, 115.8, 115.8, 114.0, 113.9, 102.7, 102.3, 87.9, 86.0, 83.3, 82.4, 82.1, 80.4, 80.3, 69.9, 69.8, 54.8, 42.9, 42.6, 40.5, 40.5, 32.9, 31.9, 31.4, 28.9, 26.2, 26.2, 22.7, 22.1, 20.0, 18.3, 18.3, 16.5, 16.4, -4.4, -4.4, -4.5; FTIR (film) ν_{max} 2956, 2929, 2856, 1739, 1616, 1517, 1378, 1249, 1170, 1070 cm^{-1}; HR-ES-MS *m/z* calcd. for $C_{32}H_{49}NO_5S_2SiNa$ $[M+Na]^+$: 707.2203, found 707.2199; $[\alpha]^{25}_D$ = -13.1 ° (c = 1.0, CH_2Cl_2).

Ring-closing metathesis of ester 34c

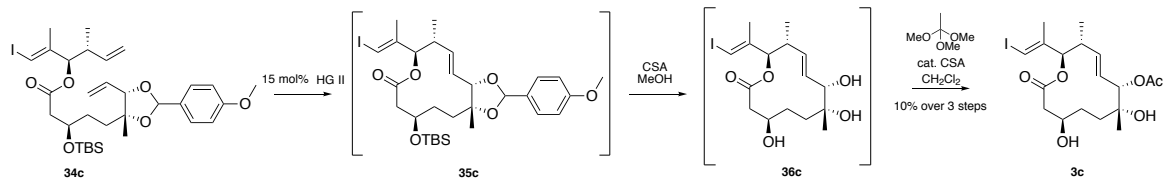

Reagents:

2nd Generation Hoyveda Grubbs catalyst, 97% (Sigma-Aldrich): used without further purification

(1*S*)-(+)-10-Camphorsulfonic acid, 98% (TCI Chemicals): used without further purification

Trimethyl orthoformate, 99% (Sigma-Aldrich): used without further purification

(2*R*,3*R*,6*S*,7*R*,10*R*,*E*)-7,10-dihydroxy-2-((*E*)-1-iodoprop-1-en-2-yl)-3,7-dimethyl-12-oxooxacyclododec-4-en-6-yl acetate (3c) Esters **34c** (5.15 g, 7.52 mmol) in a two-necked 3 L flask equipped with a 1 L addition funnel were dissolved into anhydrous, degassed toluene (700 mL). The mixture was purged with Ar and heated to reflux. 2nd Generation Hoyveda-Grubbs catalyst (706 mg, 1.13 mmol) in anhydrous, degassed toluene (700 mL) purged under Ar was dropwise added to the solution of 34 in boiling toluene. After stirring for 20 min the mixture turned from a clear green color into a black solution and was further stirred at reflux for 5 h. The mixture was then cooled to rt and concentrated by a rotary evaporator. The crude black semi-solid was then suspended in hexanes and filtered through a pad of Celite and eluted with hexanes. The elutants were concentrated on a rotary evaporator to yield a crude green oil. Crude

lactones **35c** were then dissolved in 1:3 MeOH/CH_2Cl_2 (300 mL) in a 1 L flask. (1*S*)-(+)-10-Camphorsulfonic acid (3.45 g, 14.9 mmol) was added as a solid in one portion. The mixture was stirred for 5 h, at which point TLC analyses indicated complete conversion of starting material. Satd. $NaHCO_3$ (50 mL) was added, and the mixture was extracted into CH_2Cl_2 (3 × 200 mL). The organics were collected and concentrated on a rotary evaporator to a crude oil. Crude triol **36c** was subjected to dry column vacuum chromatography over silica and the column was washed with CH_2Cl_2 (500 mL). Crude triol **36c** was eluted with acetone, concentrated, and carried forward without further purification. Trimethyl orthoformate (400 μL, 3.13 mmol) was added dropwise as a solution of CH_2Cl_2 (20 mL) to a mixture of crude triol **36c** and (1*S*)-(+)-10-camphorsulfonic acid (120 mg, 0.259 mmol). The mixture was stirred at 0 °C for 1 h, at which point satd. NH_4Cl (5 mL) was added. The mixture was stirred for 20 min and extracted into CH_2Cl_2 (150 mL). The organics were concentrated on a rotary evaporator. Pure core **3c** (25.1 mg, 10% over three steps) was obtained as a mixture of two isomers by flash chromatography, eluting with a gradient of CH_2Cl_2 to 1:3 acetone/CH_2Cl_2.

Core **3**: TLC (1:8 acetone/CH_2Cl_2): R_f = 0.328 (CAM stain); ^{1}H NMR (500 MHz, C_6D_6) δ 6.19 (s, 1H), 5.82 (dd, *J* = 15.3, 9.8 Hz, 1H), 5.45 (dd, *J* = 15.3, 10.1 Hz, 1H), 5.18 (d, *J* = 9.8 Hz, 1H), 5.09 (d, *J* = 10.6 Hz, 1H), 4.11 (bs, 1H), 2.30 (m, 2H), 2.21 (m, 1H), 2.08 (d, *J* = 14.9 Hz, 1H), 1.76 (bs, 1H), 1.64 (m, 1H), 1.62 (s, 3H), 1.61 (d, *J* = 1.1 Hz, 3H), 1.55 (m, 1H), 1.44 (m, 1H), 1.22 (m, 2H), 1.04 (s, 3H), 0.51 (d, *J* = 6.7 Hz, 3H); ^{13}C NMR (125 MHz, C_6D_6) δ 171.7, 169.0, 143.8, 139.8, 126.9, 84.4, 80.0, 79.0, 73.2, 69.3, 41.1, 38.4, 35.8, 30.2, 24.7, 20.8, 19.1, 16.1; FTIR (film) ν_{max} 3502, 3058, 2959, 2873, 1733, 1616, 1368, 1243, 1168, 1021 cm^{-1}; HR-

ESI-MS *m/z* calcd. for $C_{18}H_{27}IO_6Na$ $[M+Na]^+$: 489.0745, found 489.0742; $[\alpha]^{25}_D$ = -38.5 ° (c = 1.0, CH_2Cl_2).

Stille coupling of stannane 2 and core 3c to afford 10*R*,11*R*-FD-895 (1c).

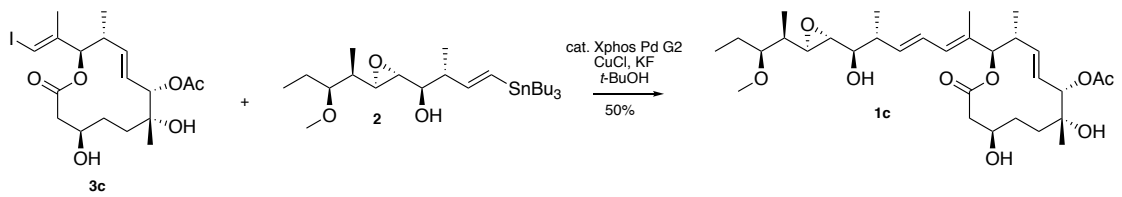

10*R*,11*R*-FD-895 (1c): Yield: 50%, 6.60 mg; TLC (1:3 acetone/CH_2Cl_2): R_f = 0.28 (CAM stain); NMR data provided in Table S4; FTIR (film) ν_{max} 3447, 2963, 2930, 2875, 1739, 1457, 1374, 1239, 1176, 1089, 1021 cm^{-1}; HR-ESI-MS *m/z* calcd. for $C_{31}H_{50}IO_9Na$ $[M+Na]^+$: 589.3348 found 589.3351; $[\alpha]^{25}_D$ = +10.9 ° (c = 1.0, CH_2Cl_2).

Table S3.5 NMR data for 10*R*,11*R* -FD-895 (1c) in C_6D_6

Position	δ_H, mult (*J* in	δ_C	^{1}H, ^{1}H-	^{1}H, ^{1}H-NOESY	^{1}H, ^{13}C-HMBC
1		169.6			
2’	2.38, m	40.1	2’, 3	3w, 5’	1, 3, 4
2’’	2.25, dd (13.3,		2’, 3	3	1, 3, 4
3	4.14, m	67.8	2’, 2’’w	2’w, 2’’, 4’, 4’’,	
3-OH					
4’	1.29, m	27.5	3, 4’’, 5’,	3, 4’’, 5’, 5’’	5, 3
4’’	1.20, m		3w, 4’, 5’,	3, 4’, 5’, 5’’, 24	5
5’	1.83, m	30.7	4’, 4’’, 5’’	2’, 4’, 4’’, 8, 25	3w, 4, 6, 7w, 24
5’’	1.75, dt (13.4,		4’, 4’’, 5’	4’, 4’’, 24	3w, 4, 6, 7, 24, 30
6		73.5			
6-OH	1.75, s				
7	5.23, d (9.8)	79.3	8	4’, 8w, 9, 24	8, 9, 24w, 29
8	5.90, dd (15.2,	126.6	7, 9, 10w	5’, 7, 9, 10	6, 10
9	5.58, dd (15.3,	140.3	8, 10	4’, 7, 8, 10, 11, 25	7, 10
10	2.43, m	41.2	11, 25	8, 9, 11, 25, 26	8, 9, 11, 25
11	5.18, d (10.8)	82.1	10	9, 10w, 13, 25, 26w	1, 9, 10, 12, 13,
12		132.2			
13	6.17, d (10.8)	131.3	14, 26w	9, 11, 15, 25, 26	11, 15, 26
14	6.27, dd (15.1,	126.5	13, 15	15, 16, 26, 27	12, 13, 16
15	5.53, dd (15.1,	137.8	14, 16	13, 14, 16, 17, 18w,	13, 16, 17
16	2.36, m	42.8	15, 17, 27	14, 15, 17, 18, 27	14, 15, 17, 18, 27
17	3.12, m	74.8	16, 18	15, 16, 18, 19, 27	15w, 16, 19, 25
17-OH	1.55, bs				
18	2.69, dd (5.1,	60.3	17, 19w	14w, 15, 16, 17, 19,	17, 19, 20
19	2.90, dd (8.1,	59.4	18w, 20	17, 18w, 20, 22’w,	17w, 18, 20, 21w
20	1.31, m	39.2	19, 28	19, 21, 28	19, 23
21	3.14, m	83.6	20, 22’,	20, 22’, 22’’, 23	19, 20, 22w, 23,
22’	1.60, m	23.9	21, 22’’,	21, 22’’, 23	20, 21, 23
22’’	1.39, m		21, 22’, 23	19w, 21, 22’, 23, 31	20, 21, 23
23	0.84, t (7.5)	10.1	22’, 22’’	20, 21, 22’, 22’’,	21, 22
24	1.06, s	24.8		4’w, 4’’, 5’w, 5’’, 7	5, 6, 7
25	0.72, d (6.7)	16.5	10	5’, 9, 10, 11,13, 26	9, 10, 11
26	1.58, s	12.0	13	10, 14, 25w	11, 12, 13, 14
27	1.11, d (6.8)	16.9	16	14, 15, 16, 17, 18w	15, 16, 17
28	0.87, d (7.0)	10.5	20	18, 19, 20, 21, 22’	19, 20, 21
29		169.2			
30	1.63, s	20.8			29

31	3.24, s	57.7		19w, 21, 22’’, 23	21

Stille coupling of stannane 2d and core 3 to afford 17*S*-FD-895 (1d).

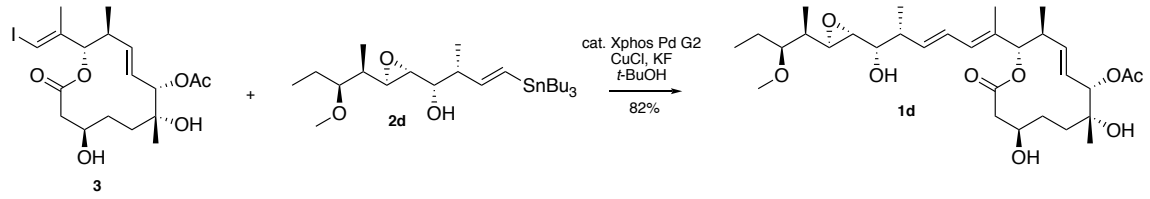

17S-FD-895 (**1d**): Yield: 80%, 66.4 mg; TLC (1:3 acetone/CH_2Cl_2): R_f = 0.28 (CAM stain); NMR data provided in Table S5; FTIR (film) ν_{max} 3447, 2963, 2930, 2875, 1739, 1457, 1374, 1239, 1176, 1089, 1021 cm^{-1}; HR-ESI-MS *m/z* calcd. for $C_{31}H_{50}IO_9Na$ $[M+Na]^+$: 589.3345, found 589.3347; $[\alpha]^{25}_D$ = +8.8 ° (c = 1.0, CH_2Cl_2).

Table S3.6 NMR data for 17*S*-FD-895 (1d) in C_6D_6

Position	δ_H, mult (*J* in	δ_C	^{1}H, ^{1}H-	^{1}H, ^{1}H-NOESY	^{1}H, ^{13}C-HMBC
1		171.8			
2’	2.29, dd (14.8,	38.2	2’, 3	3, 3OHw, 4’/5’w	3
2’’	2.19, dd (14.8,		2’’, 3	3, 4’/5’	1
3	3.49, td (11.1,	69.0	3OH,	2’, 2'', 3OH, 4’/5’,	
3-OH	3.63, d (11.2)		3	2’, 3, 4’’, 6OH	3
4’	1.57, m	30.0	3w, 4’’,	2’’, 3, 5’’, 24	
4’’	1.25, m		3, 4’, 5’,	3OHw, 5’, 7, 9, 24w	3w
5’	1.55, m	35.5	3, 4’’	2’’, 3OH, 4’’, 6OH,	
5’’	1.20, m		5’	3, 4’, 7w, 24	4w, 6w, 7w
6		72.5			
6-OH	1.75, s			3OH, 5’’w, 7w, 8,	5, 6, 17
7	5.26, d (1.5)	78.8	8	4’’, 8, 9w, 24	8, 29
8	5.83, dd (15.2,	140.3	7, 9	4’/5’, 7, 9, 10w, 25	7, 10w
9	5.62, dd (15.2,	126.0	8, 10	4’/5’, 7, 8, 10, 25	10, 25w
10	2.39, m	40.8	9, 11, 25	7w, 8, 9w, 11w, 25,	11
11	5.24, d (2.4)	82.2	10	9, 10, 13, 25, 26	1, 12, 13, 26
12		131.0			
13	6.11, d (10.7)	131.4	14, 26w	11, 14, 15, 25, 26w	11, 14w, 15, 26
14	6.26, dd (15.2,	126.1	13, 15	13, 15, 16, 26, 27w	12w, 13w
15	5.80, dd (15.2,	137.6	14, 16	13, 14, 27	12, 13, 14, 16,
16	2.36, m	41.2	15, 17, 27	14, 17, 27	15
17	3.42, q (3.7)	73.0	16,	15, 16, 17OH, 18,	
17-OH	1.55, bs			17, 19	16, 17
18	2.56, dd (3.8,	57.3	17, 19w	15w, 16, 17, 19w,	
19	3.01, dd (8.3,	59.3	18, 20	15w, 17, 17OH,	20
20	1.33, m	38.9	19, 21, 28	18, 19w, 21, 23, 28	
21	3.15, m	83.4	22’, 22’’	19, 20, 22’, 22’’, 23	19, 28
22’	1.63, m	23.5	21, 23	21w, 22’’, 23	20w, 21, 23
22’’	1.40, dt (14.0,		21, 23	21w, 22’, 23	20w, 21, 23
23	0.85, t (7.5)	9.7	22’, 22’’	20, 21, 22’, 22’’	21, 22
24	1.00, s	24.4		4’/5’, 4’’w, 5’’,	5, 6 ,7
25	0.70, d (6.7)	16.1	10	7, 9, 10, 13, 26	8, 10, 11
26	1.59, d (1.3)	11.5	13	10, 11w, 14, 25	11, 12, 13, 14w,
27	1.12, d (7.0)	16.9	16	9, 14, 15, 16, 17, 18	15, 16, 17
28	0.88, d (6.9)	10.5	20	18, 19, 20, 21	19, 20, 21
29		168.7			
30	1.61, s	20.4			29
31	3.23, s	57.4		21, 22’, 22’’, 23	21

Procedures for the synthesis of 17-O-Me-FD-895 and 17*S*-O-Me-FD-895

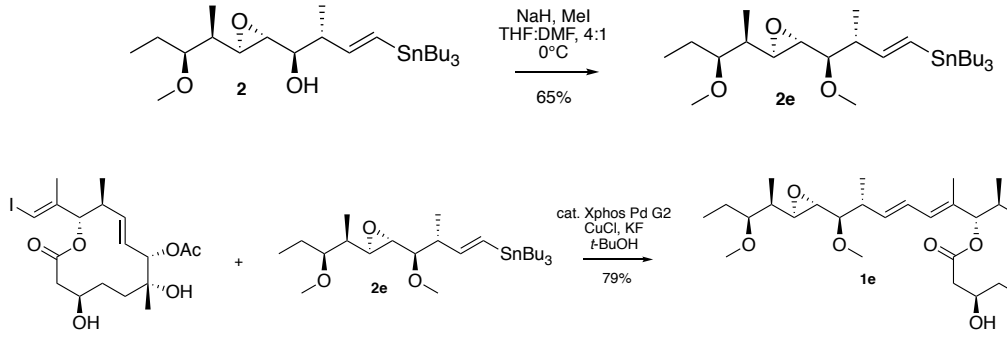

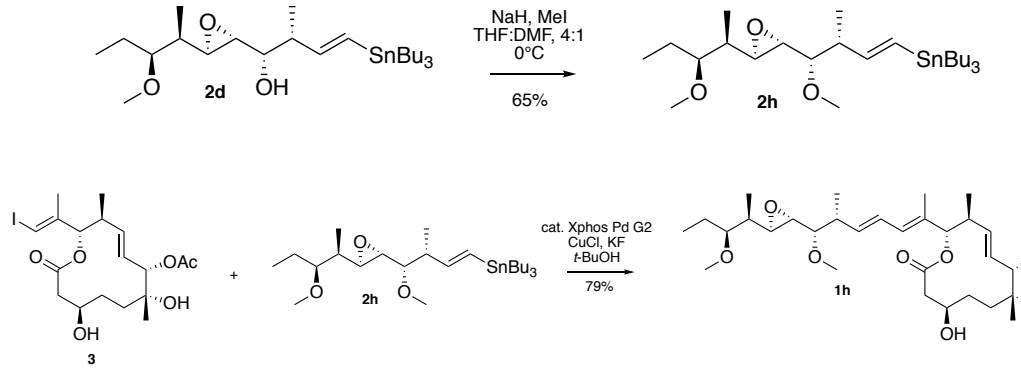

Methylation of stannane 2 to afford stannane 2e

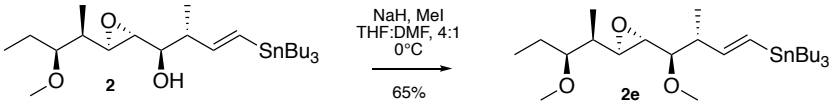

Reagents:

NaH, 60% in mineral oil (Alfa Aesar): used without further purification

MeI, 98% (Sigma-Aldrich): used without further purification

Tributyl((3*R*,4*R*,*E*)-4-methoxy-4-((2*S*,3*R*)-3-((2*R*,3*S*)-3-methoxypentan-2-yl)oxiran-2-yl)-3-methylbut-1-en-1-yl)stannane (2e). MeI (0.0586 mL, 0.941 mmol) was added at rt to a solution of stannane **2** (50.0 mg, 0.0941 mmol) in a mixture of anhydrous THF (10 mL) and anhydrous DMF (3 mL) in a 50 mL flask. The mixture was cooled to 0 °C and NaH (60% in mineral oil, 8.85 mg, 0.221 mmol) was added in portions ensuring the mixture remained at 0 °C. The mixture was slowly warmed to rt and stirred for 16 h. After cooling the mixture to 0 °C, a solution of phosphate buffered saline pH 7 (5 mL) was added dropwise. The volatiles were concentrated on a rotary evaporator. The mixture was extracted with hexane (3 × 50 mL). The combined organic phases were washed with brine, dried over Na_2SO_4, filtered and concentrated on a rotary evaporator. Pure stannane **2e** (34.9 mg, 70%) was obtained as a colorless oil by flash chromatography, eluting with a gradient of hexanes to 10% Et_2O/hexanes.

Vinylstannane **2e**: TLC (1:10 Et_2O/hexanes): R_f = 0.50 (CAM stain); ^1H NMR (500 MHz, C_6D_6) δ 6.35 (dd, *J* = 19.1, 6.8 Hz, 1H), 6.16 (d, *J* = 19.1 Hz, 1H), 3.50 (s, 3H), 3.45 (m, 1H), 3.23 (s, 3H), 3.19 (m, 1H), 2.83 (dd, *J* = 4.4, 2.3 Hz, 1H), 2.75 (dd, *J* = 4.4, 2.3 Hz, 1H), 2.60 (td, *J* = 6.9, 5.2 Hz, 1H), 1.61 (m, 8H), 1.39 (m, 8H), 1.19 (d, *J* = 6.9 Hz, 3H), 1.01 (d, *J* = 7.1 Hz, 3H), 1.00

(d, J = 8.1 Hz, 3H), 0.95 (t, J = 7.4 Hz, 12H), 0.84 (t, J = 7.4 Hz, 3H); ^{13}C NMR (125 MHz, C_6D_6) δ 151.7, 127.3, 86.2, 83.5, 60.2, 58.4, 58.4, 57.6, 56.9, 44.9, 39.7, 32.0, 29.6, 27.8, 23.1, 23.1, 15.6, 14.4, 14.0, 10.9, 10.0, 9.8; FTIR (film) ν_{max} 3454, 3310, 2973, 2937, 2890, 1459, 1101, 840 cm^{-1}; HR-ESI-MS *m/z* calcd. for $C_{25}H_{50}O_3Sn$ $[M+H]^+$ 533.2998, found 533.2994; $[\alpha]^{25}_D$ = +10.4 ° (c = 1.0, CH_2Cl_2).

Stille Coupling of stannane 2e and core 3 to afford 17-O-Methyl-FD-895 (1e)

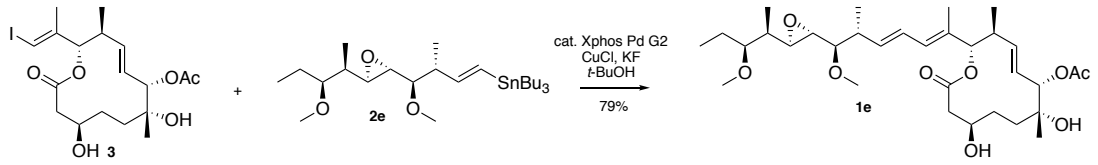

17-O-Methyl-FD-895 (**1e**): Yield: 79%, 8.81 mg; TLC (1:3 acetone/hexanes): R_f = 0.40 (CAM stain); NMR data provided in Table S6; FTIR (film) ν_{max} 3447, 2963, 2930, 2875, 1739, 1457, 1374, 1239, 1176, 1089, 1021 cm^{-1}; HR-ESI-MS *m/z* calcd. for $C_{31}H_{50}IO_9Na$ $[M+Na]^+$: 603.7642, found 603.7641; $[\alpha]^{25}_D$ = +36.9 ° (c = 1.0, CH_2Cl_2).

Table S3.7 NMR data for 17-O-Me-FD-895 (1e) in C_6D_6

Position	δ_H, mult (*J* in	δ_C	^1H, ^1H-	^1H, ^1H-NOESY	^1H, ^{13}C-
1		172.1			
2’	2.29, dd (14.8,	38.6	2’’, 3	3, 4’w	1, 3, 4w
2’’	2.20, dd (14.8,		2’, 3	3, 5’	1
3	3.48, m	69.3	2’w, 2’’w,	2’, 2’’, 4’, 5’’	
3-OH	3.62, d (11.1)		3	3, 6OH	
4’	1.57, m	30.4	3, 4’’, 5’,	3, 5’’, 7, 8	5, 6, 3, 24
4’’	1.26, m		4’, 5’, 5’’	2’’, 3, 5’’, 9	3
5’	1.54, m	35.9	4’, 4’’, 5’’	2’’, 4’’, 8	4, 6, 24
5’’	1.18, m		4’, 4’’, 5’	4’	6, 7
6		73.6			
6-OH	1.77, s				
7	5.24, d (5.5)	79.2	8	4’’/5’’, 8, 9, 24w,	8w, 9, 24w, 29
8	5.82, dd (15.2,	126.4	7, 9	4’/5’, 7w, 9, 10,	6w, 9w, 10
9	5.62, dd (15.1,	140.7	8, 10	4’’/5’’, 7, 8, 10,	7, 8w, 10, 25
10	2.39, tq (10.4,	41.1	9, 11, 25	8, 9w, 25, 26	8, 9w, 11, 12,
11	5.26, d (6.3)	82.6	10	10, 13, 25, 26	1, 9, 10, 13,
12		131.7			
13	6.12, dd (10.9,	131.4	14, 26	8w, 11, 14, 15,	11, 15, 26
14	6.23, ddd	125.7	13, 15	8w, 13, 15, 16, 26	13w, 16
15	5.64, dd (15.2,	138.7	14, 16	13, 14, 16, 17	12, 13, 14w,
16	2.48, dq (14.4,	42.6	15, 17, 27	14, 15, 17w, 27w,	14, 15, 17, 18,
17	2.62, t (7.1)	86.2	16, 18	15w, 16, 20, 32	15, 16, 18, 27,
17-OH					
18	2.68, m	60.6	17	15, 16, 20, 32	17, 19w, 20
19	2.68, m	59.1	20	17, 20, 28w,	20, 21w
20	1.22, m	39.6	19, 28	17w, 21w, 22’,	19
21	3.20, m	83.5	20, 22’,	20, 22’, 22’’, 23	19w, 20w,
22’	1.64, m	23.7	21w, 22’’,	21, 22’’	20, 21, 23
22’’	1.37, dp (17.0,		22’, 23	21, 22’	20, 21, 23
23	0.82, t (7.4)	10.0	22’, 22’’	20, 21, 22’w,	21, 22
24	1.01, s	24.8		4’/5’, 7	5, 6, 7
25	0.71, d (6.8)	16.4	10	9w, 10, 11w, 13,	9, 10, 11
26	1.59, d (1.3)	11.8	13	8, 10, 11, 14, 25	11, 12, 13,
27	1.14, d (6.8)	17.0	16	14, 15, 16, 17	15, 16, 17
28	0.87, d (7.1)	10.8	20	22’, 22’’	19, 20, 21
29		169.0			
30	1.61, s	20.7			29
31	3.25, s	57.7		20w, 22’, 22’’w,	21

32	3.50, s	58.5		6OH, 17, 31w	17

Methylation of stannane 2d to afford stannane 2f

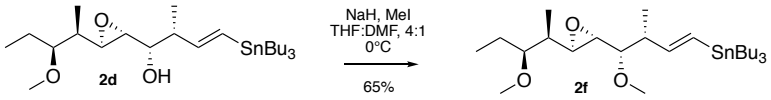

Reagents:

NaH, 60% in mineral oil (Alfa Aesar): used without further purification

MeI, 98% (Sigma-Aldrich): used without further purification

Tributyl((3*R*,4*R*,*E*)-4-methoxy-4-((2*S*,3*R*)-3-((2*R*,3*S*)-3-methoxypentan-2-yl)oxiran-2-yl)-3-methylbut-1-en-1-yl)stannane (2f). MeI (0.0586 mL, 0.941 mmol) was added at rt to a solution of stannane **2d** (50.0 mg, 0.0941 mmol) in a mixture of anhydrous THF (10 mL) and anhydrous DMF (3 mL) in a 50 mL flask. The mixture was cooled to 0 °C and NaH (60% in mineral oil, 8.85 mg, 0.221 mmol) was added in portions ensuring the mixture remained at 0 °C. The mixture was slowly warmed to rt and stirred for 16 h. After cooling the mixture to 0 °C, a solution of phosphate buffered saline pH 7 (5 mL) was added dropwise. The volatiles were concentrated on a rotary evaporator. The mixture was extracted with hexane (3 × 50 mL). The combined organic phases were washed with brine, dried over Na_2SO_4, filtered and concentrated on a rotary evaporator. Pure stannane **2f** (31.5 mg, 65%) was obtained as a colorless oil by flash chromatography, eluting with a gradient of hexanes to 10% Et_2O/hexanes.

Vinylstannane **2f**: TLC (1:10 Et_2O/hexanes): R_f = 0.50 (CAM stain); ^1H NMR (500 MHz, C_6D_6) δ 6.39 (dd, *J* = 19.1, 6.8 Hz, 1H), 6.26 (d, *J* = 19.1 Hz, 1H), 3.25 (s, 3H), 3.23 (s, 3H), 3.21 (m, 1H), 3.04 (dd, *J* = 4.4, 2.3 Hz, 1H), 2.83 (m, 2H), 2.75 (dd, *J* = 4.4, 2.3 Hz, 1H), 1.61 (m, 8H), 1.39 (m, 8H), 1.19 (d, *J* = 6.9 Hz, 3H), 1.01 (d, *J* = 7.1 Hz, 3H), 1.00 (d, *J* = 8.1 Hz, 3H), 0.95 (t,

J = 7.4 Hz, 12H), 0.84 (t, *J* = 7.4 Hz, 3H); ^{13}C NMR (125 MHz, C_6D_6) δ 150.7, 127.5, 84.7, 83.3, 59.7, 58.3, 57.6, 57.4, 45.3, 39.4, 29.4, 27.5, 23.5, 16.7, 13.8, 10.3, 9.8, 9.5; FTIR (film) ν_{max} 3454, 3310, 2973, 2937, 2890, 1459, 1101, 840 cm^{-1}; HR-ESI-MS *m/z* calcd. for $C_{25}H_{50}O_3Sn$ $[M+H]^+$ 533.2998, found 533.2994; $[\alpha]^{25}_D$ = -8.6° (c = 1.0, CH_2Cl_2).

Stille coupling of stannane 2f and core 3 to afford 17*S*-O-Methyl-FD-895 (1f).

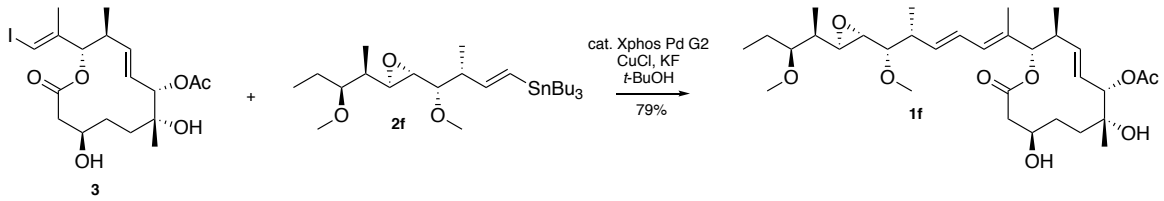

17-O-Methyl-FD-895 (**1f**): Yield: 81%, 4.21 mg; TLC (1:3 acetone/hexanes): R_f = 0.40 (CAM stain); NMR data provided in Table S9; FTIR (film) ν_{max} 3447, 2963, 2930, 2875, 1739, 1457, 1374, 1239, 1176, 1089, 1021 cm^{-1}; HR-ESI-MS *m/z* calcd. for $C_{31}H_{50}IO_9Na$ $[M+Na]^+$: 603.7642, found 603.7643; $[\alpha]^{25}_D$ = +36.9 ° (c = 1.0, CH_2Cl_2).

Table S3.8 NMR data for 17*S*-O-Me-FD-895 (1f) in C_6D_6

Position	δ_H, mult (*J* in	δ_C	^{1}H, ^{1}H-COSY	^{1}H, ^{1}H-NOESY	^{1}H, ^{13}C-HMBC
1		172.1			
2’	2.29, dd (14.8,	38.6	2’’, 3	3, 4’w	1, 3, 4w
2’’	2.20, dd (14.8,		2’, 3	3, 5’	1
3	3.48, m	69.3	2’w, 2’’w,	2’, 2’’, 4’, 5’’	
3-OH	3.62, d (11.1)		3	3, 6OH	
4’	1.57, m	30.4	3, 4’’, 5’,	3, 5’’, 7, 8	5, 6, 3, 24
4’’	1.26, m		4’, 5’, 5’’	2’’, 3, 5’’, 9	3
5’	1.54, m	35.9	4’, 4’’, 5’’	2’’, 4’’, 8	4, 6, 24
5’’	1.18, m		4’, 4’’, 5’	4’	6, 7
6		73.6			
6-OH	1.77, s				
7	5.24, d (5.5)	79.2	8	4’’/5’’, 8, 9, 24w,	8w, 9, 24w, 29
8	5.82, dd (15.2,	126.4	7, 9	4’/5’, 7w, 9, 10,	6w, 9w, 10
9	5.62, dd (15.1,	140.7	8, 10	4’’/5’’, 7, 8, 10,	7, 8w, 10, 25
10	2.39, tq (10.4,	41.1	9, 11, 25	8, 9w, 25, 26	8, 9w, 11, 12,
11	5.26, d (6.3)	82.6	10	10, 13, 25, 26	1, 9, 10, 13,
12		131.7			
13	6.12, dd (10.9,	131.4	14, 26	8w, 11, 14, 15, 25,	11, 15, 26
14	6.23, ddd (15.1,	125.7	13, 15	8w, 13, 15, 16, 26	13w, 16
15	5.64, dd (15.2,	138.7	14, 16	13, 14, 16, 17	12, 13, 14w,
16	2.48, dq (14.4,	42.6	15, 17, 27	14, 15, 17w, 27w,	14, 15, 17, 18,
17	2.62, t (7.1)	86.2	16, 18	15w, 16, 20, 32	15, 16, 18, 27,
17-OH					
18	2.68, m	60.6	17	15, 16, 20, 32	17, 19w, 20
19	2.68, m	59.1	20	17, 20, 28w,	20, 21w
20	1.22, m	39.6	19, 28	17w, 21w, 22’,	19
21	3.20, m	83.5	20, 22’,	20, 22’, 22’’, 23	19w, 20w, 23w
22’	1.64, m	23.7	21w, 22’’,	21, 22’’	20, 21, 23
22’’	1.37, dp (17.0,		22’, 23	21, 22’	20, 21, 23
23	0.82, t (7.4)	10.0	22’, 22’’	20, 21, 22’w,	21, 22
24	1.01, s	24.8		4’/5’, 7	5, 6, 7
25	0.71, d (6.8)	16.4	10	9w, 10, 11w, 13,	9, 10, 11
26	1.59, d (1.3)	11.8	13	8, 10, 11, 14, 25	11, 12, 13,
27	1.14, d (6.8)	17.0	16	14, 15, 16, 17	15, 16, 17
28	0.87, d (7.1)	10.8	20	22’, 22’’	19, 20, 21
29		169.0			
30	1.61, s	20.7			29
31	3.25, s	57.7		20w, 22’, 22’’w,	21

32	3.50, s	58.5		6OH, 17, 31w	17

Stille coupling of stannane 2d and core 3a to afford 3*S*,17*S*-FD-895 (1g).

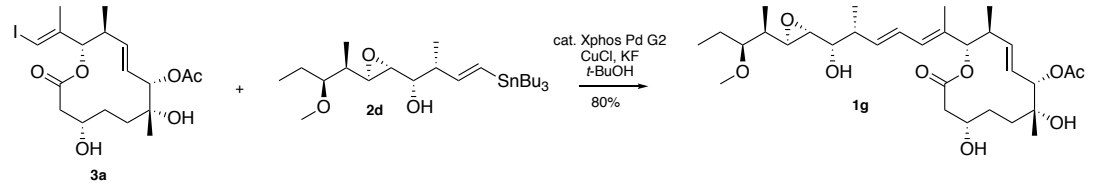

3*S*,17*S*-FD-895 (1g): Yield: 80%, 14.2 mg; TLC (1:3 acetone/CH_2Cl_2): R_f = 0.17 (CAM stain); NMR data provided in Table S7; FTIR (film) ν_{max} 3447, 2963, 2930, 2875, 1739, 1457, 1374, 1239, 1176, 1089, 1021 cm^{-1}; HR-ESI-MS *m/z* calcd. for $C_{30}H_{50}O_9Na$ $[M+Na]^+$: 589.3341, found 589.3342; $[\alpha]^{25}_D$= +12.4° (c = 1.0, CH_2Cl_2).

Table S3.9 NMR data for 3*S*,17*S*-FD-895 (**1g**) in C_6D_6

Position	δ_H, mult (*J* in	δ_C,	^{1}H, ^{1}H-	^{1}H, ^{1}H-NOESY	^{1}H, ^{13}C-
1		169.9			
2’	2.43, dd (13.3,	40.2	2’’, 3	3w, 5’	1, 3, 4w
2’’	2.30, dd (13.1,		2’, 3	3	1, 3, 4
3	4.20, m	67.8	2’, 2’’w	2’w, 2’’, 4’, 4’’	
3OH					
4’	1.34, m	27.6	4’’, 5’, 5’’	3, 5’’, 7	
4’’	1.29, m		3w, 4’, 5’w,	3, 24	2, 3w, 5w
5’	1.85, td (13.4,	30.9	4’, 4’’, 5’’	2’, 4’’, 8	4w, 6, 24w
5’’	1.78, td (13.6,		4’, 4’’, 5’	4’, 4’’, 24	4, 6, 7, 24w
6		73.6			
6OH	1.92, bs			5’’, 24	
7	5.25, d (9.8)	79.3	8	4’, 8, 9, 24	8, 9, 29
8	5.91, dd (15.2,	126.5	7, 9, 10w	5’, 7, 9, 10	6w, 10
9	5.61, dd (15.2,	140.5	8, 10	4’, 7, 8, 10w, 25	7, 10, 25w
10	2.47, m	41.3	9, 11, 25	8w, 25, 26	8, 9, 11, 25w
11	5.20, d (10.6)	82.3	10	9, 10w, 13, 25, 26w	1, 9w, 10, 12,
12		131.6			
13	6.19, d (10.9,	131.8	14, 26w	11, 15, 25w	11, 15, 26
14	6.27, ddd (15.1,	126.6	13, 15	15, 16, 26, 27	12, 13, 16
15	5.81, dd (15.0,	137.6	14, 16	14, 16, 27	12, 13, 16,
16	2.36, m	41.5	15, 17w, 27	14, 15, 17, 27	14, 15, 17w,
17	3.44, t (3.4)	73.0	16, 18	15, 16, 18, 19, 27	15, 16w, 18,
17OH					
18	2.57, dd (3.8,	59.7	17, 19	17, 20, 27, 28	17w
19	3.02, dd (8.2,	57.7	18, 20	17, 20w, 28	20
20	1.33, m	39.2	19, 21, 28	18, 21, 28	18w, 19,
21	3.14, td (6.2, 4.4)	83.8	20, 22’, 22’’	20, 22’w, 22’’, 23	19, 20w, 23
22’	1.63, m	23.9	21, 22’’, 23	21w, 22’’, 23	20, 21
22’’	1.41, m		21, 22’, 23	22’, 23	20, 21, 23
23	0.86, t (7.4)	10.2	22’, 22’’	20, 21, 22’, 22’’	21, 22
24	1.08, s	24.8		5’’, 7	5, 6, 7
25	0.73, d (6.8)	16.5	10	9, 10, 11	9, 10, 11
26	1.61, d (1.3)	12.0	13	10, 14	11, 12, 13
27	1.12, d (7.0)	17.3	16	14, 15, 16, 17, 18w	15, 16, 17
28	0.89, d (7.0)	10.9	20	18w, 19w, 20, 22’	19, 20, 21
29		169.4			
30	1.64, s	20.9			29
31	3.23, s	57.7		19w, 21, 22’’, 23	21

Stille coupling of stannane 2d and 3b to afford 7*R*,17*S*-FD-895 (1h).

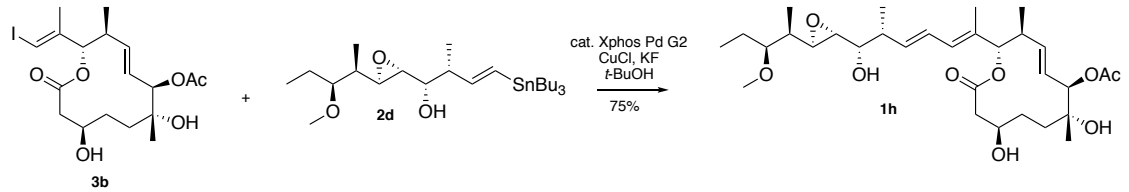

7*R*,17*S*-FD-895 (1h): Yield: 75%, 5.01 mg; TLC (1:3 acetone/CH_2Cl_2): R_f = 0.28 (CAM stain); NMR data provided in Table S8; FTIR (film) ν_{max} 3447, 2963, 2930, 2875, 1739, 1457, 1374, 1239, 1176, 1089, 1021 cm^{-1}; HR-ESI-MS *m/z* calcd. for $C_{30}H_{50}O_9Na$ $[M+Na]^+$: 589.3341, found 589.3345; $[\alpha]^{25}_D$= +20.1° (c = 1.0, CH_2Cl_2).

Table S3.10 NMR data for 7*R*,17*S* -FD-895 (**1h**) in C_6D_6

Position	δ_H, mult (*J* in Hz)	δ_C	^{1}H, ^{1}H-COSY	^{1}H, ^{1}H-NOESY	^{1}H, ^{13}C-HMBC
1	4.65, d (9.3)	172.3			
2’	2.35, m	39.3	2’, 3	3, 4’’w	1, 3, 4
2’’	2.30, dd (14.6,		2’’, 3	3, 4’’	1, 3, 4w
3	3.58, ddt (10.8,	69.6	2’’, w3OH,	3OH, 4’’,	
3-OH	3.70, d (10.7)		3	2’., 2’’, 3,	2w, 3
4’	1.80, m	30.6	3, 4’’, 5’, 5’’	3OHw, 5’, 7w,	conformers
4’’	1.62, m		3w, 4’, 5’,	2’w, 5’’	conformers
5’	1.58, m	36.5	4’w , 4’’, 5’’	4’, 5’’	conformers
5’’	0.97, m		4’, 4’’, 5’	3w, 4’’	conformers
6		73.8			
6-OH	1.68, bs			3OH, 24	
7	5.41, m	82.9	8	8, 10w, 24, 26	5, 6, 8, 9, 14, 29
8	5.93, dd (15.3,	127.9	7, 9	4’’/ 5’, 7, 9, 10	7, 10
9	5.39, m	130.7	8, 10	4’, 8, 10, 25	7, 8, 10
10	2.48, tq (10.3,	41.1	11, 25	8, 9w, 25, 26	8, 9, 11, 25w
11	5.36, d (10.6)	78.0	10	10w, 13, 25,	1, 10, 12, 13, 26
12		131.6			
13	6.17, d (10.7)	131.6	14, 26w	11, 14, 15, 16,	11, 15, 26
14	6.29, dd (15.1,	126.4	13, 15	15, 16, 26, 27	12, 13, 16
15	5.80, dd (15.1,	137.8	14, 16	13, 14, 16, 17w,	12, 13,14, 10w,
16	2.38, m	41.5	15, 17, 27	14, 15w, 17, 18,	14, 15, 17, 18
17	3.43, m	72.8	16, 17OH,	15, 16, 17OH,	15, 18, 19
17-OH	1.67, m		17	3, 3OH, 24	
18	2.57, dd (3.8,	59.6	17	15, 17, 20, 27,	17
19	3.02, dd (8.2,	57.6	20	17, 17OH, 20,	17w, 18w, 20,
20	1.33, m	39.0	19, 28	18, 21, 23	19, 28
21	3.15, m	83.7	20, 22’, 22’’	22’, 22’’, 23	19, 20, 22w, 23
22’	1.63, m	23.8	21, 22’’, 23	20w, 22’’	20, 21, 23
22’’	1.40, dp (14.2,		21, 22’, 23	22’, 23	20, 21, 23
23	0.85, t (7.4)	10.0	22’, 22’’	20, 21, 22’w,	21, 22
24	1.02, s	24.7		3, 3OH, 6OH, 7,	5, 6, 7
25	0.77, d (6.8)	16.9	10	9, 10, 11, 26w	9, 10, 11
26	1.64, d (1.2)	11.9		10, 14	11, 12, 13
27	1.12, d (7.0)	17.3	16	14w, 15w, 16,	15, 16, 17
28	0.89, d (7.0)	10.8	20	18, 19, 20, 21	19, 20, 21
29		169.3			
30	1.68, s	20.4			29

31	3.24, s	57.7		22’, 22’’, 23	21

Procedures for the Synthesis of Stannane 2i (17*S*,18*S*,19*S*-FD-895)

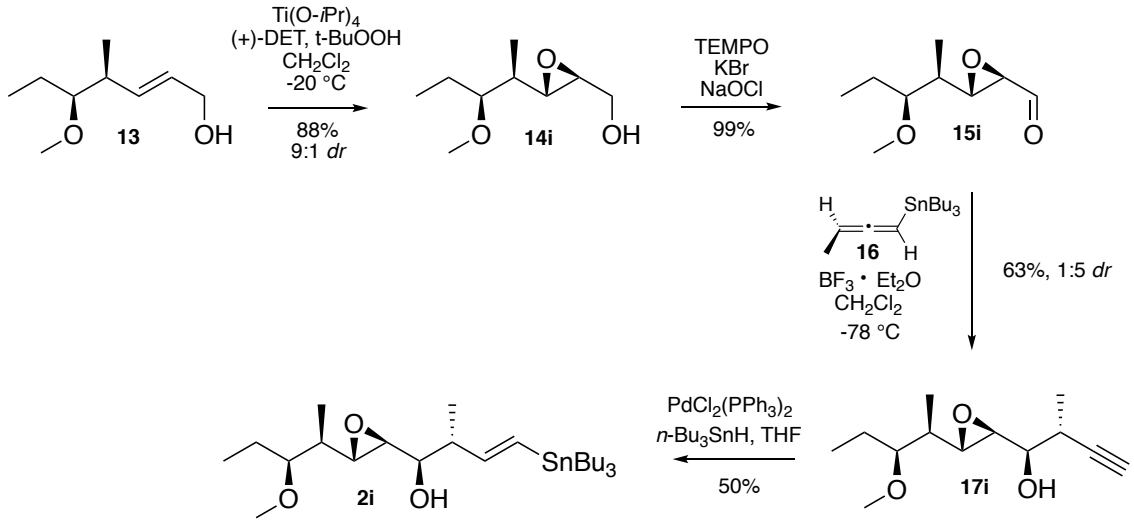

Epoxidation of Alcohol 13

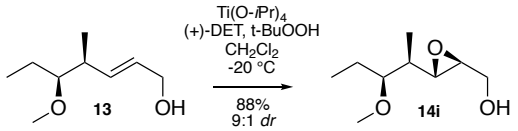

Reagents:

Ti(O*i*-Pr)$_4$, 97% (Sigma-Aldrich): vacuum distilled at 90 °C, 5 mbar

(-)-Diethyltartrate, 99% (Alfa Aesar): used without further purification

t-Butylhydroperoxide, 3.3 M in toluene: dried from a 70% solution in water according to methods developed by the Sharpless laboratory

((2S,3S)-3-((2R,3S)-3-Methoxypentan-2-yl)oxiran-2-yl)methanol (14i). *t*-Butylhydroperoxide (3.3 M, 19.2 mL, 65.1 mmol) was added to a 500 mL flask containing a stirring solution of Ti(O*i*-Pr)$_4$ (0.650 mL, 3.15 mmol), (-)-diethyl tartrate (0.550 mL, 3.15 mmol) and powdered 4Å molecular sieves (1 g) in anhydrous CH_2Cl_2 (100 mL). The mixture was cooled to -20 °C and stirred for 30 min. A solution of alcohol **13** (5.0 g, 31.9 mmol) in CH_2Cl_2 (25 mL) was added dropwise. The reaction was stirred at -20 °C for 4 h. The reaction was quenched *via* addition of 10% NaOH (10 mL). The mixture was then extracted into CH_2Cl_2 and concentrated on a rotary evaporator. Pure epoxyalcohol **14i** (5.50 g, 88%) was obtained as a 6:1 mixture of diastereomers by flash chromatography, eluting with a gradient of hexanes to 1:1 EtOAc/hexanes.

Note 1: Diastereomers were not separable and carried on directly to the next step.

Epoxyalcohol **14i**: TLC (1:2 EtOAc/hexanes): R_f = 0.10 (CAM stain); ^{1}H NMR (500 MHz, C_6D_6) δ 3.59 (tq, *J* = 15.9, 12.6, 2.7 Hz, 1H), 3.37 (m, 12.0, 7.1, 4.4 Hz), 3.02 (s, 3H), 2.77 (dd, *J*

= 7.1, 2.3 Hz, 1H), 2.74 (dd, *J* = 4.7, 2.5 Hz, 1H), 2.70 (dt, *J* = 7.3, 4.8 Hz, 1H), 2.36 (t, *J* = 6.1Hz, 1H), 1.44 (m, 1H), 1.37 (m, 1H), 1.30 (dtd, *J* = 14.0, 7.5, 5.2 Hz, 1H), 0.96 (d, *J* = 7.0 Hz, 3H) 0.77 (t, *J* = 7.4 Hz, 3H); ^{13}C NMR (125 MHz, C_6D_6) δ 83.8, 62.2, 58.0, 57.9, 57.7, 38.8, 24.0, 10.4, 10.1; FTIR (film) ν_{max} 3422, 2972, 2930, 2879, 1468, 1103 cm^{-1}; HR-ESI-MS *m/z* calcd. for $C_9H_{18}O_3$ $[M]^+$: 174.1250, found 174.1249; $[\alpha]^{25}_D$ = +182.4 ° (c = 1.0, $CHCl_3$).

Oxidation of Epoxyalcohol 14i

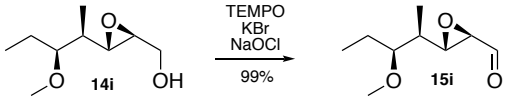

Reagents:

TEMPO, 99% (Oakwood Chemical): used without further purification

KBr, (Spectrum Chemical Mfg. Corp.): used without further purification

NaOCl, 2 M, 10-15% active chlorine (Spectrum Chemical Mfg. Corp.): used without further purification

(2*R*,3*S*)-3-((2*R*,3*S*)-3-Methoxypentan-2-yl)oxirane-2-carbaldehyde (15i). A solution of KBr (0.242 g, 2.04 mmol) in H_2O (10 mL), satd. $NaHCO_3$ (20 mL) and TEMPO (0.266 g, 1.70 mmol) were added sequentially to a 500 mL flask containing a solution of epoxyalcohol **14i** (4.42 g, 25.4 mmol) in CH_2Cl_2 (150 mL). The mixture was cooled to 0 °C and a solution of NaOCl (2 M, 17 mL, 34.0 mmol) and satd. $NaHCO_3$ (20 mL) were added dropwise *via* an addition funnel. The mixture was allowed to warm to rt and stirred for 2 h. The phases were separated, and the aqueous phase was extracted with CH_2Cl_2 (3 × 100 mL). The combined organic phases were washed with brine (100 mL), dried over Na_2SO_4, filtered and concentrated on a rotary evaporator. Aldehyde **15i** (4.41 g, 99%) was obtained without further purification and was carried on directly to the next step.

Note 1: Diastereomers obtained from epoxidation were not separable at this step and thus carried forward.

Aldehyde **15i**: TLC (1:2 EtOAc/hexanes): R_f = 0.55 (CAM stain); ^{1}H NMR (500 MHz, C_6D_6) δ 8.67 (d, *J* = 6.3 Hz, 1H), 2.93 (s, 3H), 2.89 (dd, *J* = 6.4, 2.0 Hz, 1H), 2.82 (dd, *J* = 6.4, 2.0 Hz, 1H), 2.60 (dt, *J* = 7.2, 4.7 Hz, 1H), 1.30 (m, 2H), 1.15 (dqd, *J* = 14.6, 7.4, 5.3 Hz, 1H), 0.75 (d, *J* = 7.0 Hz, 3H), 0.67 (t, *J* = 7.4 Hz, 3H); ^{13}C NMR (125 MHz, C_6D_6) δ 198.0, 84.2, 58.4, 58.4, 57.3, 37.6, 23.6, 11.4, 10.2; FTIR (film) ν_{max} 2972, 2930, 2879, 2828, 1732, 1468, 1103 cm^{-1}; HR-ESI-MS *m/z* calcd. for $C_9H_{16}O_3$ $[M+H]^+$: 173.1172, found 173.1174; $[\alpha]^{25}_D$ = +36.1 ° (c = 1.0, CH_2Cl_2).

Marshall addition of allenylstannane 16 to aldehyde 15

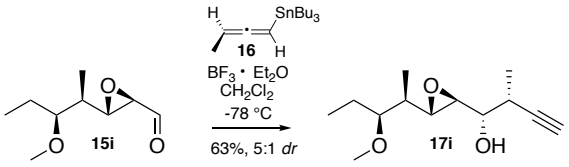

Reagents:

BF_3•Et_2O, 46.5% BF_3 (Alfa Aesar): used without further purification

(1*R*,2*R*)-1-((2*S*,3*S*)-3-((2*R*,3*S*)-3-methoxypentan-2-yl)oxiran-2-yl)-2-methylbut-3-yn-1-ol (17i). Aldehyde **15i** (70.1 mg, 0.408 mmol) and allenylstannane **16** (0.210 g, 0.610 mmol) in a 50 mL flask were dissolved in anhydrous CH_2Cl_2 (10.0 mL) and purged with an Ar atmosphere. The mixture was cooled to -78 °C and BF_3•Et_2O (75.3 μL, 0.610 mmol) was added dropwise over 5 min. The reaction was stirred for 1 h at -78 °C. A mixture of MeOH (5 mL) and satd. $NaHCO_3$ (1 mL) was added, and the solution was warmed to rt. The phases were separated, and the aqueous phases were extracted with Et_2O (3 × 50 mL). The organic phases were combined, dried with Na_2SO_4 and concentrated on a rotary evaporator. Alkyne **17i** (69.2 mg, 63%) was obtained in a 5:1 mixture of diastereomers (by NMR) as a colorless oil by flash chromatography, eluting with a gradient of hexanes to 1:3 Et_2O/hexanes.

Alkyne **17i**: TLC (2:1 hexanes/EtOAc): R_f = 0.40; ^{1}H NMR (500 MHz, C_6D_6,) δ 3.55 (td, *J* = 8.3, 7.6, 4.4 Hz, 1H), 3.18 (q, *J* = 2.7 Hz, 1H), 3.14 (s, 3H), 3.03 (ddd, *J* = 6.8, 4.6, 2.3 Hz, 1H), 2.92 (dt, *J* = 7.5, 4.8 Hz, 1H), 2.55 (dqd, *J* = 10.0, 7.1, 3.4 Hz, 1H), 1.86 (m, 1H), 1.54 (m, 2H),

1.39 (m, 1H), 1.30 (d, J = 7.1 Hz, 3H), 1.06 (d, J = 6.8 Hz, 3H), 0.83 (t, J = 7.3 Hz, 3H); ^{13}C NMR (125 MHz, C_6D_6,) δ 85.4, 84.6, 71.9, 71.2, 59.0, 58.9, 57.4, 57.3 38.4, 31.0, 23.7, 17.4, 12.2, 10.3; ESI–MS m/z 249.14 $[M+Na]^+$; FTIR (film) νmax 3430, 3310, 2967, 2935, 2878, 1457, 1379, 1260, 1093 cm^{-1}; HR– ESI–MS m/z calcd. for $C_{13}H_{22}O_3Na$ $[M+Na]^+$: 249.1461, found 249.1462. $[\alpha]^{25}_D$ = +24.2 ° (c = 1.0, CH_2Cl_2).

Hydrostannylation of alkyne 17i

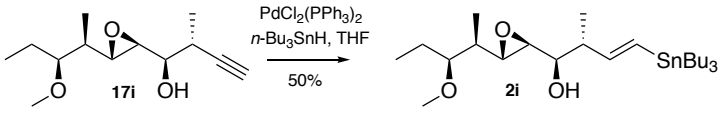

Reagents:

n-Bu_3SnH, 97% contains 0.05% BHT as stabilizer (Acros Organics): used without further purification

$PdCl_2(PPh_3)_2$ (Oakwood Chemical): dried *via* azeotropic distillation of benzene

(1*R*,2*R*,*E*)-1-((2*R*,3*R*)-3-((2*R*,3*S*)-3-Methoxypentan-2-yl)oxiran-2-yl)-2-methyl-4-(tributylstannyl)but-3-en-1-ol (2). $PdCl_2(PPh_3)_2$ (15.5 mg, 0.0221 mmol) was added to a solution of alkyne **17i** (50.1 mg, 0.221 mmol) in a 10 mL flask in anhydrous THF (5 mL). The mixture was cooled to 0 °C and *n*-Bu_3SnH (0.179 mL, 0.663 mmol) was added dropwise. The mixture was stirred for 45 min at 0 °C, at which point the resulting mixture was concentrated to yield a black crude oil. The material was extracted into hexanes, filtered through a pad of Celite and was eluted with hexanes. The elutant was concentrated on a rotary evaporator, and this process was repeated twice until a clear black solution was achieved. Pure vinylstannane **2** (22.0 mg, 50%) was obtained as a mixture of 1:5 α:β regioisomers by flash chromatography, eluting with a gradient of hexanes to CH_2Cl_2 to 1:20 Et_2O/CH_2Cl_2. The desired regioisomer and diastereomer can be obtained in 95+% purity by additional flash chromatography, eluting with a gradient of hexanes to CH_2Cl_2 to 1:20 Et_2O/CH_2Cl_2.

Vinylstannane **2i**: TLC (10:1 hexanes/Et_2O): R_f= 0.25 (CAM stain); ^1H NMR (C_6D_6, 500 MHz) δ 6.16 (m, 2H), 3.54 (m, 1H), 3.16 (s, 3H), 3.07 (d, *J* = 7.2, Hz, 1H), 2.93 (m, 2H), 2.49 (m, 2H),

1.98 (s, 1H), 1.60 (m, 9H), 1.39 (dt, J = 15.5, 8.5 Hz, 6H), 1.28 (d, J = 7.0 Hz, 3H), 1.07 (d, J = 6.9 Hz, 3H), 0.96 (m, 12H), 0.87 (t, J = 7.4 Hz, 3H); ^{13}C NMR (C_6D_6, 500 MHz) δ 151.5, 84.8, 72.7, 59.4, 57.4, 46.5, 38.4, 29.6, 27.7, 23.8, 16.2, 14.0, 12.2, 10.5, 9.8; HR–ESI–MS m/z calcd. for $C_9H_{17}O_3$ $[M+H]^+$ 519.2843, found 519.2839; $[\alpha]^{25}_D$ = +10.1° (c = 1.0, CH_2Cl_2).

Stille coupling of stannane 2i and core 3 to afford 17*S*,18*S*,19*S*-FD-895 (1i).

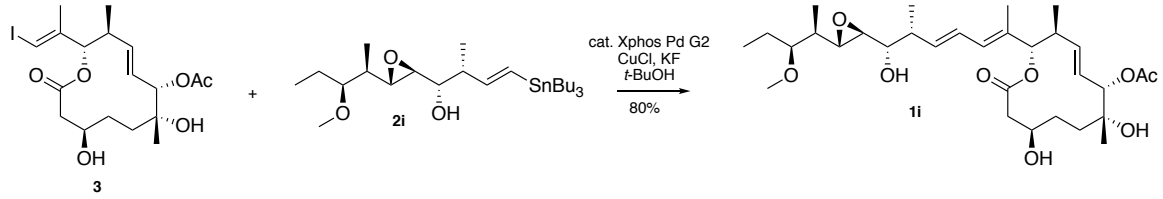

17*S*,18*S*,19*S*-FD-895 (**1i**): Yield: 80%, 7.24 mg; TLC (1:3 acetone/CH_2Cl_2): R_f = 0.28 (CAM stain); NMR data provided in Table S10; FTIR (film) ν_{max} 3447, 2963, 2930, 2875, 1739, 1457, 1374, 1239, 1176, 1089, 1021 cm^{-1}; HR-ESI-MS *m/z* calcd. for $C_{31}H_{50}IO_9Na$ $[M+Na]^+$: 589.3345, found 589.3347; $[\alpha]^{25}_D$ = +4.2 ° (c = 1.0, CH_2Cl_2).

Table S3.11 NMR data for 17*S*,18*S*,19*S*-FD-895 (**1i**) in C_6D_6

Position	δ_H, mult (*J* in Hz)	δ_C	^{1}H, ^{1}H-COSY	^{1}H, ^{1}H-NOESY	^{1}H, ^{13}C-HMBC
1		172.1			
2’	2.31, dd (14.8,	38.5	2’, 3	3w	1, 3, 4
2’’	2.22, dd (14.8,		2’’, 3	3w, 4’/5’	1
3	3.52, m	69.3	2’, 2’’, 4’w,	2’’, 4’/5’w, 5’’	
3-OH			3	3, 24, 30	
4’	1.58, m	30.2	4’’, 5’, 5’’	2’’, 5’’, 24	3w, 4w, 6, 24
4’’	1.33, m		3, 4’	4’, 5’	3, 5
5’	1.55, m	35.8	4’w, 4’’, 5’’	2’’, 4’, 8w	4, 6, 24w
5’’	1.27, m		4’	7	4, 6, 7, 24w
6		73.3			
6-OH				3OH, 24	
7	5.25, d (10.6)	79.2	8	4’/5’, 5’’, 8w, 9, 24	8, 9, 24, 29
8	5.83, dd (15.2,	126.5	7, 9	4’/5’, 7, 9, 10	6w, 10
9	5.64, (15.2, 10.0)	140.6	8, 10	5’’, 8, 10, 11, 25	7, 10, 11w, 25w
10	2.41, m	41.0	9, 11, 25	7w, 8, 25, 26	8, 9, 11, 25
11	5.27, d (11.1)	82.6	10	10, 13, 25	1, 9, 10, 12/13,
12		131.7			
13	6.17, d (10.9)	131.3	14, 26w	11, 14, 15, 25	11, 14, 15, 26
14	6.32, dd (15.1,	126.1	13, 15	13, 15, 16, 26, 27	12, 13, 16
15	5.75, dd (15.1,	138.4	14, 16	13, 14, 16, 17w,	12, z13, 16, 17,
16	2.44, m	41.8	15, 17, 27	14, 15, 17, 27	14, 15, 17, 18,
17	3.48, dd (6.6, 3.6)	72.6	16, 18	15, 16, 18, 19w, 27	15w, 16w, 19,
17-OH					
18	2.78, dd (3.6, 2.3)	59.2	17	15w, 16, 17, 20, 27,	17
19	3.01, dd (7.4, 2.2)	57.3	20	17, 20, 28	18w, 20, 28
20	1.52, m	38.0	19, 28	18, 19w, 21, 28	19, 28
21	2.83, dt (7.5, 4.6)	84.7	20w, 22’	20, 22’, 22’’w, 23,	23, 31
22’	1.49, m	23.5	21, 22’’, 23	21w, 23w	20, 21, 23
22’’	1.38, m		23	21w, 23w	20w, 21w, 23
23	0.83, t (7.4)	10.6	22’, 22’’	21, 22’w, 22’’	21, 22
24	1.02, s	24.7		4’/ 5’, 7	5, 6, 7
25	0.72, d (6.8)	16.4	10	9, 10, 11, 26w	9, 10, 11
26	1.61, d (1.3)	11.8	13	10, 11w, 14	11, 12, 13, 15
27	1.20, d (6.9)	16.3	16	14, 15, 16, 17, 18w	15, 16, 17
28	1.02, d (6.9)	12.4	20	20, 21	19, 20, 21
29		169.1			
30	1.63, s	20.8			29
31	3.11, s	57.1		20, 21	21

Procedures for the synthesis of 17*S*,20*S*,21*S*-FD-895 (1j).

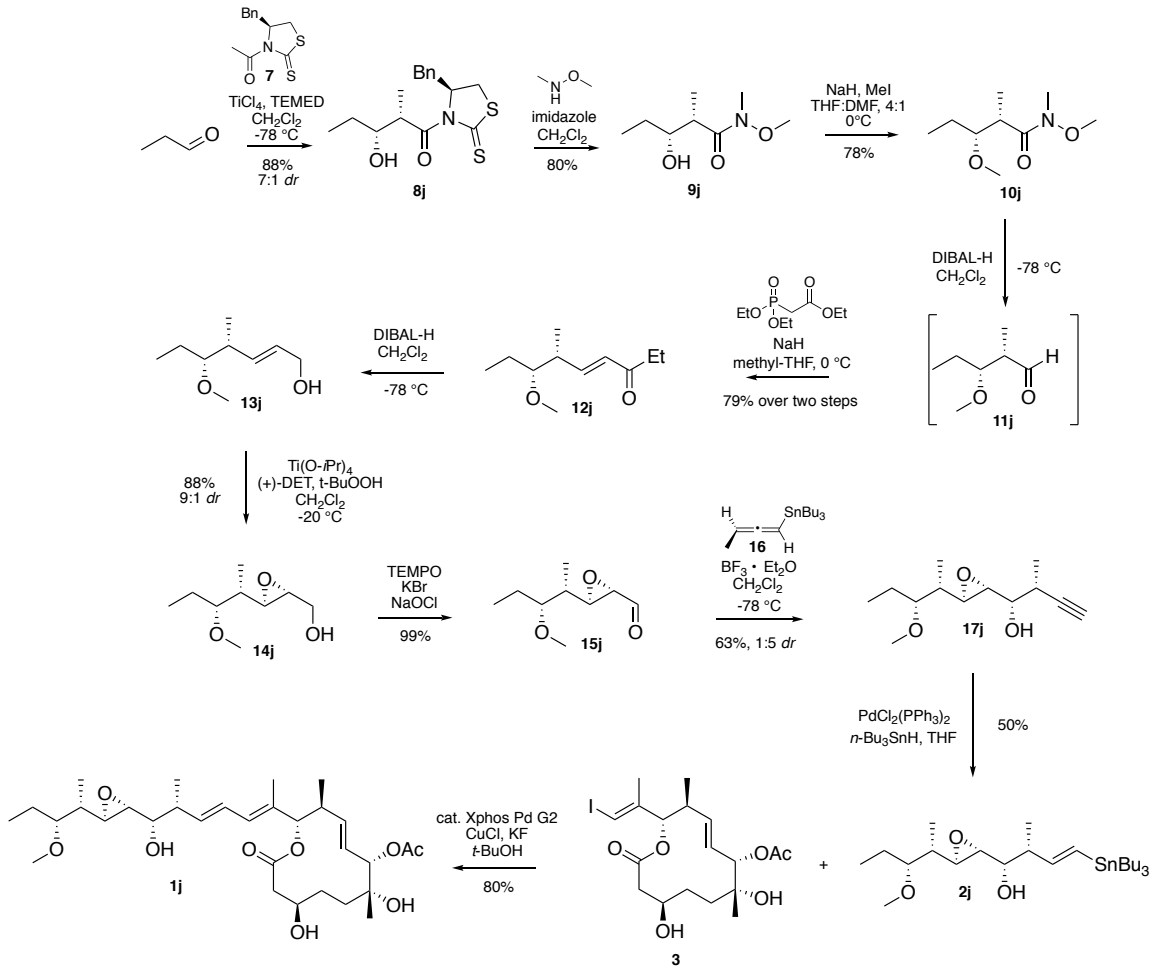

Synthesis of adduct 8j

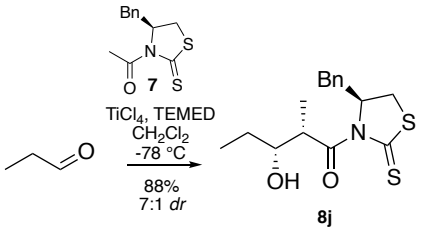

Reagents:

Propionaldehyde, 98% (Alfa Aesar): redistilled before use

EtN(*i*-Pr)$_2$, 97% (Fisher Scientific): redistilled before use

$TiCl_4$, 98% (Alfa Aesar): used without further purification

(2*S*,3*R*)-1-((*S*)-4-Benzyl-2-thioxothiazolidin-3-yl)-3-hydroxy-2-methylpentan-1-one (8j). (*S*)-1-(4-Benzyl-2-thioxothiazolidin-3-yl)propan-1-one (**7**) (23.5 g, 88.7 mmol) was added to a 2 L reaction flask and dissolved in CH_2Cl_2 (700 mL) with mechanical stirring. The mixture was cooled below 0 °C. $TiCl_4$ (10.1 mL, 92.2 mmol) was added dropwise over 1 h, while maintaining the temperature below 0 °C, at which point the mixture turned orange. EtN(*i*-Pr)$_2$ (13.9 mL, 92.2 mmol) was added dropwise over 30 min, at which point the resulting black mixture was stirred at 0 °C for 15 min. After cooling the reaction to -94 °C, a solution of propionaldehyde (7.10 mL, 98.4 mmol) in anhydrous CH_2Cl_2 (50 mL) was added dropwise over 1 h. The mixture was stirred at -94 °C for 30 min before being slowly warmed to rt overnight. The mixture was cooled to 0 °C and satd. $NaHCO_3$ (200 mL) was slowly added. The phases were separated, and the aqueous phase was extracted with CH_2Cl_2 (3 × 300 mL). The combined organic phases were washed with brine (300 mL), dried over Na_2SO_4, filtered and concentrated on a rotary evaporator. Pure adduct **8j** (25.0 g, 88%) was obtained in a 9.5:1 *dr* by flash chromatography, eluting with a gradient of hexanes to 1:3 EtOAc/hexanes.

Adduct **8j**: TLC (1:3 EtOAc/heptane): R_f = 0.63 (CAM stain); ^{1}H-NMR (500 MHz, $CDCl_3$) δ 7.35 (m, 2H), 7.30 (m , 3H), 5.36 (ddd, J = 4.0, 7.0, 10.5 Hz, 1H), 4.52 (dq, J = 3.0, 7.0 Hz, 1H), 3.86 (m, 1H), 3.41 (dd, J = 7.0, 11.5 Hz, 1H), 3.24 (dd, J = 4.0, 13.5 Hz, 1H), 3.06 (dd, J = 10.5, 13.5 Hz, 1H), 2.91 (d, J = 11.5 Hz, 1H), 2.64 (d, J = 3.0 Hz, 1H), 1.57 (m, 1H), 1.45 (m, 1H), 1.25 (d, J = 7.0 Hz, 3H), 0.97 (t, J = 7.5 Hz, 3H). ^{13}C-NMR (125 MHz, $CDCl_3$) δ 201.6, 178.7, 136.6, 129.7, 129.2, 127.5, 73.9, 69.1, 43.1, 37.0, 32.3, 27.5, 10.6, 10.5. FTIR (film) ν_{max} 3444, 3027, 2964, 2937, 2876, 1689, 1455, 1352, 1258, 1191, 1164, 1041, 1029, 960 cm^{-1}; LCMS (ES-API) *m/z* calcd. for $C_{15}H_{19}NO_2S_2$ $[M+1]^+$: 324.40; $[\alpha]^{25}_D$ = 36.2 ° (c = 1.0 CH_2Cl_2).

Synthesis of Weinreb's amide 9j

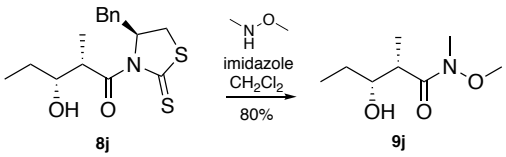

Reagents:

N,*O*-Dimethylhydroxylamine hydrochloride, 99% (Alfa Aesar): used without further purification

Imidazole, 99% (Sigma-Aldrich): used without further purification

(2*S*,3*R*)-3-Hydroxy-*N*-methoxy-*N*,2-dimethylpentanamide (9j). *N*,*O*-Dimethylhydroxylamine hydrochloride (8.70 g, 44.5 mmol) and imidazole (9.1 g, 134 mmol) were added in succession to a solution of **8j** (14.4 g, 44.5 mmol) in CH_2Cl_2 (500 mL) in a 2 L reaction vessel at rt. The mixture was stirred at rt for an additional 16 h. H_2O (300 mL) was added, and the mixture was separated followed by extraction of the aqueous phase with CH_2Cl_2 (3 × 500 mL). The combined organic phases were washed with brine (500 mL), dried over Na_2SO_4, filtered and concentrated on a rotary evaporator to afford a yellow oil. Pure amide **9j** (6.60 g, 80%) was obtained by flash chromatography, eluting with a gradient of hexanes to 3:1 EtOAc/hexanes.

Amide **9j**: TLC (3:1 EtOAc/heptane): R_f = 0.17 ($KMnO_4$); ^{1}H NMR (500 MHz, $CDCl_3$) δ 3.79 (bs, 1H), 3.76 (td, *J* = 5.4, 2.6 Hz, 1H), 3.69 (s, 3H), 3.17 (s, 3H), 2.90 (bs, 1H), 1.77 (bs, 1H), 1.57 (m, 1H), 1.39 (m, 1H), 1.15 (d, *J* = 7.1 Hz, 3H), 0.95 (t, *J* = 7.4 Hz, 3H); ^{13}C NMR (125

MHz, $CDCl_3$) δ 178.5, 73.1, 61.7, 38.1, 32.0, 26.8, 10.5, 10.1; FTIR (film) ν_{max} 2969, 2917, 2855, 1719, 1449, 1265, 1178, 1108, 1020, 715 cm^{-1}; LCMS (ES-API) *m/z* calcd. for $C_8H_{17}NO_3$ $[M+1]^+$: 176.40; $[\alpha]^{25}_D$ = +7.3 ° (c = 1.0, CH_2Cl_2).

Methylation of amide 9j to 10j

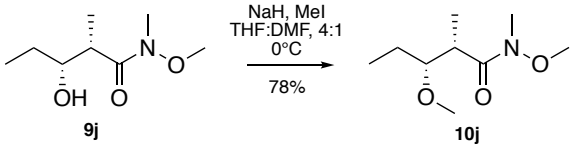

Reagents:

NaH, 60% in mineral oil (Alfa Aesar): used without further purification

MeI, 98% (Sigma-Aldrich): used without further purification

(2*S*,3*R*)-*N*,3-Dimethoxy-*N*,2-dimethylpentanamide (10j). MeI (35.8 mL, 576 mmol) was added at rt to a solution of amide **9j** (5.00 g, 28.4 mmol) in a mixture of anhydrous THF (200 mL) and anhydrous DMF (50 mL) in a 1 L reaction vessel. The mixture was cooled to 0 °C and NaH (60% in mineral oil, 2.83 mg, 70.7 mmol) was added in portions ensuring the mixture remained at 0 °C. The mixture was slowly warmed to rt and stirred for 16 h. After cooling the mixture to 0 °C, a solution of phosphate buffered saline pH 7 (200 mL) was added dropwise. The volatiles were concentrated on a rotary evaporator. H_2O (100 mL) was added to the residue, and the obtained mixture was extracted with *t*-butyl methyl ether (3 × 300 mL). The combined organic phases were washed with brine (300 mL), dried over Na_2SO_4, filtered and concentrated on a rotary evaporator. Pure amide **10j** (4.13 g, 77%) was obtained as a colorless oil by flash chromatography, eluting with a gradient of hexanes to 1:1 EtOAc/hexanes.

Amide **10j**: TLC (3:1 EtOAc/heptane): R_f = 0.27 ($KMnO_4$); ^1H NMR (500 MHz, $CDCl_3$) δ 3.68 (s, 3H), 3.41 (s, 3H), 3.30 (tdd, *J* = 7.0, 4.0, 1.0 Hz, 1H), 3.18 (s, 3H), 3.03 (bs, 1H), 1.58 (dqd, *J* = 14.9, 7.5, 3.9 Hz, 1H), 1.42 (dt, *J* = 14.4, 7.2 Hz, 1H), 1.21 (d, *J* = 6.9 Hz, 3H), 0.93 (t, *J* = 7.4 Hz, 3H); ^{13}C NMR (125 MHz, $CDCl_3$) δ 176.5, 83.9, 61.6, 58.7, 39.6, 32.2, 25.3, 14.5, 9.6; FTIR (film) ν_{max} 3581, 3502, 2969, 2934, 2882, 2820, 1658, 1457, 1379 cm^{-1}; LCMS (ES-API) *m/z* calcd. for $C_9H_{19}NO_3$ $[M+1]^+$: 190.40; $[\alpha]^{25}_D$ = +16.1 ° (c = 1.0 $CHCl_3$).

Conversion of 10 to ester 12

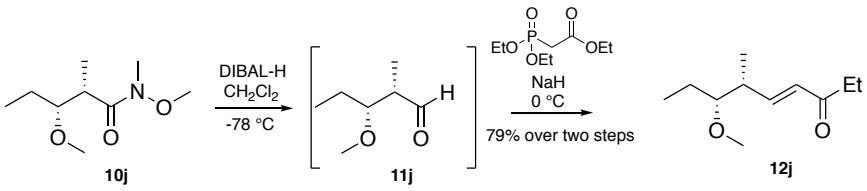

Reagents:

DIBAL-H, 1.0 M in hexanes (Sigma-Aldrich): used without further purification

NaH, 60% in mineral oil, (Alfa Aesar): used without further purification

Triethyl phosphonoacetate, 99% (Oakwood Chemical): used without further purification

Ethyl (4*R*,5*R*,*E*)-5-methoxy-4-methylhept-2-enoate (12j) Amide **10j** (4.00 g, 21.1 mmol) was dissolved in anhydrous CH_2Cl_2 (100 mL) in a 500 mL flask. The mixture was cooled to -78 °C. DIBAL-H (1.0 M, 32.8 mL, 32.8 mol) was added dropwise over 45 min at -78 °C and stirred for 1 hr. Acetone (10 mL) was added dropwise over 10 min, and the mixture was warmed to 0 °C. Satd. Rochelle's salt (100 mL) was added over 30 min, and the mixture was stirred at rt for 1.5 h. The phases were separated, and the aqueous phase was extracted with CH_2Cl_2 (3 × 150 mL). The combined organic phases were dried over Na_2SO_4, filtered and concentrated on a rotary evaporator. The residue was then dried *via* azeotropic removal of toluene to deliver aldehyde **11j**, which was used immediately after preparation. A solution of triethyl phosphonoacetate (21.2 mL, 107 mmol) in anhydrous 2-methyltetrahydrofuran (40 mL) was

added dropwise over 30 min to a 500 mL reaction flask containing a suspension of NaH (60% in mineral oil, 3.6 g, 90.3 mol) in anhydrous 2-methyltetrahydrofuran (150 mL) cooled to 0 °C. The mixture was stirred at 0 °C for 15 min and a solution of **11j** in anhydrous 2-methyltetrahydrofuran (100 mL) was added dropwise over 30 min. The mixture was stirred at rt for 16 h, cooled to 0 °C and quenched with satd. NH_4Cl (250 mL). The organics were concentrated on a rotary evaporator. The mixture was extracted with EtOAc (2 × 300 mL), and the combined organic phases were dried over Na_2SO_4, filtered and concentrated on a rotary evaporator. Pure ester **12j** (3.27 g, 78% over two steps) was obtained as a colorless oil by flash chromatography, eluting with a gradient of CH_2Cl_2 to 1:10 EtOAc/CH_2Cl_2.

Ester **12j**: TLC (CH_2Cl_2): R_f = 0.14 (CAM stain); ^{1}H NMR (500 MHz, $CDCl_3$) δ 6.95 (dd, *J* = 15.8, 7.7 Hz, 1H), 5.82 (dd, *J* = 15.8, 1.3 Hz, 1H), 4.18 (q, *J* = 7.1 Hz, 2H), 3.36 (s, 3H), 3.00 (ddd, *J* = 7.4, 5.6, 4.4 Hz, 1H), 2.57 (m, 1H), 1.51 (m, 1H), 1.41 (m, 1H), 1.28 (t, *J* = 7.1 Hz, 3H), 1.07 (d, *J* = 6.8 Hz, 3H), 0.90 (t, *J* = 7.4 Hz, 3H); ^{13}C NMR (125 MHz, $CDCl_3$) δ 166.8, 151.3, 121.1, 85.6, 60.4, 58.0, 39.3, 20.0, 14.9, 14.4, 10.0; FTIR (film) ν_{max} 2978, 2934, 2882, 2820, 1719, 1650, 1466 cm^{-1}; LCMS (ES-API) *m/z* calcd. for $C_{11}H_{20}O_3$ $[M+NH_4]^+$: 218.6; $[\alpha]^{25}_D$ = +44.9 ° (c = 1.0, CH_2Cl_2).

Reduction of ester 12j to alcohol 13j

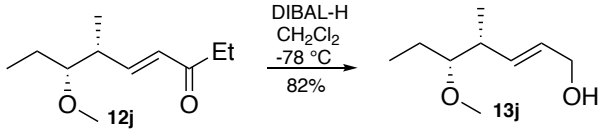

Reagents:

DIBAL-H, 1.0 M in hexanes (Sigma-Aldrich): used without further purification

(4*R*,5*R*,*E*)-5-Methoxy-4-methylhept-2-en-1-ol (13j). DIBAL-H (1.0 M, 37.1 mL, 45.0 mmol) was added dropwise over 60 min to a 5 L reaction flask containing a solution of ester **12j** (3.00 g, 14.9 mmol) in anhydrous CH_2Cl_2 (150 mL) cooled to -78 °C. The mixture was stirred for 1 h at -78 °C. Acetone (30 mL) was then added dropwise. The mixture was warmed to 0 °C, satd. Rochelle's salt (50 mL) was added, and the mixture was stirred at rt for 2 h. The phases were separated, and the aqueous phase was extracted with CH_2Cl_2 (3 × 100 mL). The combined organic phases were washed with brine (100 mL), dried over Na_2SO_4, filtered and concentrated on a rotary evaporator. Pure alcohol **13j** (1.93 g, 82%) was obtained by flash chromatography, eluting with a gradient of heptane to 1:1 EtOAc/heptane.

Alcohol **13j**: TLC (1:3 EtOAc/heptane): R_f = 0.26 (CAM stain); ^{1}H NMR (500 MHz, $CDCl_3$) δ 5.65 (m, 2H), 4.10 (bs, 2H), 3.36 (s, 3H), 2.92 (ddd, *J* = 7.5, 5.7, 4.2 Hz, 1H), 2.44 (m, 1H), 1.52 (m, 1H), 1.40 (m, 1H), 1.01 (d, *J* = 6.9 Hz, 3H), 0.90 (t, *J* = 7.4 Hz, 3H); ^{13}C NMR (125 MHz, $CDCl_3$) δ 135.2, 129.0, 86.4, 64.0, 57.7, 38.9, 23.5, 16.0, 10.0; FTIR (film) ν_{max} 3388, 2968,

2932, 2876, 2826, 1460, 1375 cm^{-1}; LCMS (ES-API) *m/z* calcd. for $C_9H_{18}O_2$ $[M+1]^+$: 158.20; $[\alpha]^{25}_D$ = -33.1 ° (c = 0.2, $CHCl_3$).

Epoxidation of alcohol 13j

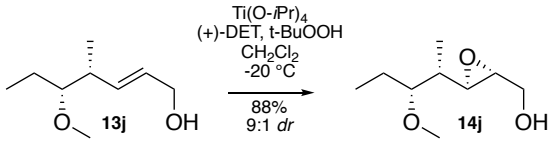

Reagents:

Ti(O*i*-Pr)$_4$, 97% (Sigma-Aldrich): vacuum distilled at 90 °C, 5 mbar

(+)-Diethyltartrate, 99% (Alfa Aesar): used without further purification

t-Butylhydroperoxide, 3.3 M in toluene: dried from a 70% solution in water according to methods developed by the Sharpless laboratory

((2S,3S)-3-((2R,3S)-3-Methoxypentan-2-yl)oxiran-2-yl)methanol (14j). *t*-Butylhydroperoxide (3.3 M, 4.80 mL, 16.3 mmol) was added to a 100 mL flask containing a stirring solution of Ti(O*i*-Pr)$_4$ (0.163 mL, 0.788 mmol), (+)-diethyl tartrate (0.550 mL, 3.15 mmol) and powdered 4Å molecular sieves (1 g) in anhydrous CH_2Cl_2 (100 mL). The mixture was cooled to -20 °C and stirred for 30 min. A solution of alcohol **13j** (1.25 g, 7.98 mmol) in CH_2Cl_2 (25 mL) was added dropwise. The reaction was stirred at -20 °C for 4 h. The reaction was quenched *via* addition of 10% NaOH (10 mL). The mixture was then extracted into CH_2Cl_2 and concentrated on a rotary evaporator. Pure epoxyalcohol **14j** (1.38 g, 88%) was obtained as a 6:1 mixture of diastereomers by flash chromatography, eluting with a gradient of hexanes to 1:1 EtOAc/hexanes.

Oxidation of epoxyalcohol 14j

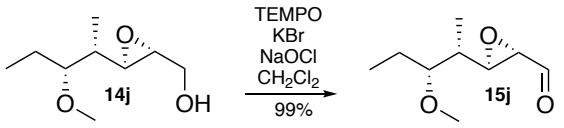

Reagents:

TEMPO, 99% (Oakwood Chemical): used without further purification

KBr, (Spectrum Chemical Mfg. Corp.): used without further purification

NaOCl, 2 M, 10-15% active chlorine (Spectrum Chemical Mfg. Corp.): used without further purification

(2*S*,3*R*)-3-((2*R*,3*S*)-3-Methoxypentan-2-yl)oxirane-2-carbaldehyde (15j). A solution of KBr (60.5 mg, 0.51 mmol) in H_2O (3 mL), satd. $NaHCO_3$ (5 mL) and TEMPO (66.5 mg, 0.425 mmol) were added sequentially to a 125 mL flask containing a solution of epoxyalcohol **14j** (1.11 g, 6.35 mmol) in CH_2Cl_2 (50 mL). The mixture was cooled to 0 °C and a solution of NaOCl (2 M, 4.25 mL, 8.50 mmol) and satd. $NaHCO_3$ (5 mL) were added dropwise *via* an addition funnel. The mixture was allowed to warm to rt and stirred for 2 h. The phases were separated, and the aqueous phase was extracted with CH_2Cl_2 (3 × 50 mL). The combined organic phases were washed with brine (30 mL), dried over Na_2SO_4, filtered and concentrated on a rotary

evaporator. Aldehyde **15j** (1.10 g, 99%) was obtained without further purification and was carried on directly to the next step.

Marshall addition of epoxyaldehyde 15j

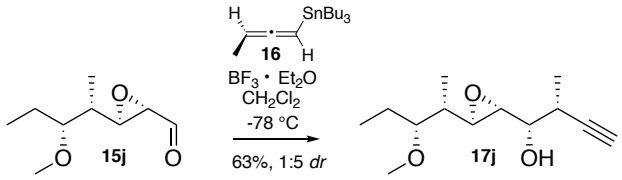

Reagents:

BF_3•Et_2O, 46.5% BF_3 (Alfa Aesar): used without further purification

(1*R*,2*R*)-1-((2*S*,3*S*)-3-((2*S*,3*R*)-3-methoxypentan-2-yl)oxiran-2-yl)-2-methylbut-3-yn-1-ol (17j). Aldehyde **15j** (70.1 mg, 0.408 mmol) and allenylstannane **16** (0.210 g, 0.610 mmol) in a 50 mL flask were dissolved in anhydrous CH_2Cl_2 (10.0 mL) and purged with an Ar atmosphere. The mixture was cooled to -78 °C and BF_3•Et_2O (75.3 μL, 0.610 mmol) was added dropwise over 5 min. The reaction was stirred for 1 h at -78 °C. A mixture of MeOH (5 mL) and satd. $NaHCO_3$ (1 mL) was added, and the solution was warmed to rt. The phases were separated, and the aqueous phases were extracted with Et_2O (3 × 50 mL). The organic phases were combined, dried with Na_2SO_4 and concentrated on a rotary evaporator. Alkyne **17j** (69.2 mg, 63%) was obtained in a 5:1 mixture of diastereomers (by NMR) as a colorless oil by flash chromatography, eluting with a gradient of hexanes to 1:3 Et_2O/hexanes.

Hydrostannylation of alkyne 17i

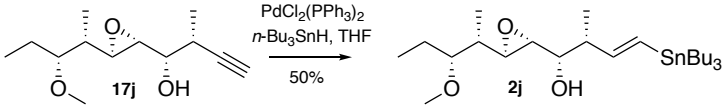

Reagents:

n-Bu_3SnH, 97% contains 0.05% BHT as stabilizer (Acros Organics): used without further purification

$PdCl_2(PPh_3)_2$ (Oakwood Chemical): dried *via* azeotropic distillation of benzene

(1*R*,2*R*,*E*)-1-((2*R*,3*R*)-3-((2*R*,3*S*)-3-Methoxypentan-2-yl)oxiran-2-yl)-2-methyl-4-(tributylstannyl)but-3-en-1-ol (2). $PdCl_2(PPh_3)_2$ (15.5 mg, 0.0221 mmol) was added to a solution of alkyne **17j** (50.1 mg, 0.221 mmol) in a 10 mL flask in anhydrous THF (5 mL). The mixture was cooled to 0 °C and *n*-Bu_3SnH (0.179 mL, 0.663 mmol) was added dropwise. The mixture was stirred for 45 min at 0 °C, at which point the resulting mixture was concentrated to yield a black crude oil. The material was extracted into hexanes, filtered through a pad of Celite and was eluted with hexanes. The elutant was concentrated on a rotary evaporator, and this process was repeated twice until a clear black solution was achieved. Pure vinylstannane **2j** (22.0 mg, 50%) was obtained as a mixture of 1:5 α:β regioisomers by flash chromatography, eluting with a gradient of hexanes to CH_2Cl_2 to 1:20 Et_2O/CH_2Cl_2. The desired regioisomer and diastereomer can be obtained in 95+% purity by additional flash chromatography, eluting with a gradient of hexanes to CH_2Cl_2 to 1:20 Et_2O/CH_2Cl_2.

Stille coupling of vinylstannane 2j and core 3 to afford 17*S*,18*S*,19*S*-FD-895 (1i).

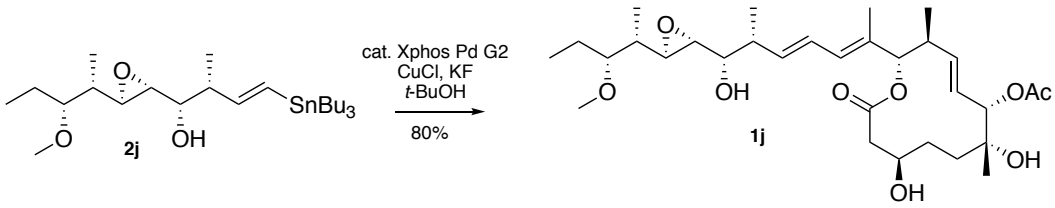

17*S*,18*S*,19*S*-FD-895 (1i): Yield: 80%, 3.45 mg; TLC (1:3 acetone/CH_2Cl_2): R_f = 0.28 (CAM stain); NMR data provided in Table S11; FTIR (film) ν_{max} 3447, 2963, 2930, 2875, 1739, 1457, 1374, 1239, 1176, 1089, 1021 cm^{-1}; HR-ESI-MS *m/z* calcd. for $C_{31}H_{50}IO_9Na$ $[M+Na]^+$: 589.3345, found 589.3347; $[\alpha]^{25}_D$ = -2.3 ° (c = 1.0, CH_2Cl_2).

Table S3.12 NMR data for 17*S*,20*S*,21*R*-FD-895 (1j) in C_6D_6

Position	δ_H, mult (*J* in	δ_C	^{1}H, ^{1}H-COSY	^{1}H, ^{1}H-NOESY	^{1}H, ^{13}C-HMBC
1		172.1			
2’	2.29, dd (14.8,	38.2	3	3w	1, 3, 4
2’’	2.19, dd (14.8,		3	3, 4’/5’	1
3	3.50, m	69.0	3OH, 4’’	2’, 4’/5’, 5’’	
3-OH	3.62, bs		3w, 4’’	3	
4’	1.56, m	30.0	3, 4’’, 5’	2’’, 8w, 24	3w, 6, 24w
4’’	1.25, m		3, 4’, 5’’	5’, 7, 9, 24w	5
5’	1.54, m	35.6	4’, 4’’, 5’’	2’’, 4’’, 8w	3w, 4, 6, 24w
5’’	1.20, m		4’, 4’’, 5’	3, 4’, 7, 24w	4, 6w, 7w
6		73.4			
6-OH					
7	5.24, d (6.6)	78.9	8	4’, 4’’, 8w, 9, 24	8, 9, 24w, 29
8	5.82, dd (15.2,	126.2	7, 9	4’/5’, 7w, 9, 10	6w, 10
9	5.62, dd (15.2,	140.5	8, 10	4’’, 8, 10, 11, 25	7, 10w, 25
10	2.38, m	41.0	9, 11, 25	8, 25, 26	11w, 25
11	5.26, d (7.5)	82.4	10	9, 10, 13, 25	1, 12, 26
12		131.4			
13	6.17, d (10.8)	131.4	14, 26	10w, 11, 14, 15, 25,	11, 14, 15, 26
14	6.32 dd (15.2,	126.2	13, 15	13, 15, 16, 26, 27	13, 16
15	5.83, dd (15.2,	137.9	14, 16	13, 14, 16, 17w,	13, 16, 27w
16	2.44, tq (6.6, 6.3)	41.4	15, 17, 27	17w, 27	14, 15, 17, 18w,
17	3.36, t (4.9)	73.4	16, 18	15w, 16, 18, 19, 27	15w, 18
17-OH					
18	2.74, dd (4.5,	58.6	17, 19	16, 17, 20, 27, 28	17
19	2.95, dd (7.0,	57.4	18, 20	17, 20, 28	20
20	1.55, m	37.8	19, 21, 28	18, 21, 28	19
21	2.84, dt (7.4, 4.7)	84.4	20, 22’, 22’’	20, 22’, 22’’, 23,	19
22’	1.52, m	23.4	20, 21, 23	23w	23
22’’	1.38, m		20, 21, 23	20, 21w, 28	23
23	0.85, t (7.4)	10.2	22’, 22’’	21w, 22’, 22’’	21, 22
24	1.00, s	24.5		4’/5’, 7	5, 6, 7
25	0.70, d (6.7)	16.2	10	9, 10, 11, 13w	9, 10, 11
26	1.58, d (1.2)	11.6	13	10, 11, 14, 15, 25	11, 12, 13
27	1.14, d (6.9)	16.3	16	14, 15, 16, 17, 18w	15, 16, 17
28	1.02, d (7.5)	12.0	20	18w, 20, 21w	19, 20, 21
29		169.0			
30	1.61, s	20.4			29

31	3.11, s	56.9		20w, 21	21

Section 3.6 References

(1) Bonnal SC, Lopex-Oreja I, Valcarcel J. Roles and mechanisms of alternative splicing in cancer- implications for care. *Nat Rev Clin Oncol* **17,** 457–474 (2020).

(2) Wang J, Liu T, Wang M, Lv W, Wang Y, Jia Y, Zhang R, Liu L. SRSF1-dependent alternative splicing attenuates BIN1 expression in non-small cell lung cancer. *J Cell Biochem*. **2019**, 38, 113-126.

(3) Will CL, Lührmann R. Spliceosome Structure and Function. *Cold Spring Harb. Perspect. Biol*. **2011**, 3 (7).

(4) Leon, B., Kashyap, M. K., Chan, W. C., Krug, K. A., Castro, J. E., La Clair, J. J., and Burkart, M. D. (2017) A challenging pie to splice: Drugging the spliceosome. *Angew. Chem., Int. Ed*. 56, 12052−12063.

(5) Cretu, C.; Agrawal, A. A.; Cook, A.; Will, C. L.; Fekkes, P.; Smith, P. G.; Lührmann, R.; Larsen, N.; Buonamici, S.; Pena, V. Structural Basis of Splicing Modulation by Antitumor Macrolide Compounds. *Mol. Cell* **2018**, *70*, 265– 273.

(6) Mandel AL, Jones BD, La Clair JJ, Burkart MD. A synthetic entry to pladienolie B and FD-895. *Bioorg. Med. Chem. Lett.***2007**, 17(18), 5159-5164.

(7) Villa, R., Mandel, A. L., Jones, B. D., La Clair, J. J. La, and Burkart, M. D. (2012) Structure of FD-895 revealed through total synthesis. Org. Lett. 14, 5396−5399.

(8) Villa, R., Kashyap, M. K., Kumar, D., Kipps, T. J., Castro, J. E., La Clair, J. J., & Burkart, M. D. Stabilized cyclopropane analogs of the splicing inhibitor FD-895. *J. Med. Chem.* **2013** *56*(17), 6576-6582.